Journal of Experimental Botany, Vol. 63, No. 13, pp. 4671–4712, 2012
doi:10.1093/jxb/ers165

Journal of Experimental Botany
www.jxb.oxfordjournals.org

DARWIN REVIEW

Estimating evapotranspiration and drought stress with ground-based thermal remote sensing in agriculture: a review

W. H. Maes* and K. Steppe

Ghent University, Department of Applied Ecology and Environmental Biology, Laboratory of Plant Ecology, Coupure Links 653, BE-9000 Ghent, Belgium

* To whom correspondence should be addressed: E-mail: wh.maes@ugent.be

Received 28 November 2011; Revised 6 April 2012; Accepted 14 May 2012

Abstract

As evaporation of water is an energy-demanding process, increasing evapotranspiration rates decrease the surface temperature (T_s) of leaves and plants. Based on this principle, ground-based thermal remote sensing has become one of the most important methods for estimating evapotranspiration and drought stress and for irrigation. This paper reviews its application in agriculture. The review consists of four parts. First, the basics of thermal remote sensing are briefly reviewed. Second, the theoretical relation between T_s and the sensible and latent heat flux is elaborated. A modelling approach was used to evaluate the effect of weather conditions and leaf or vegetation properties on leaf and canopy temperature. T_s increases with increasing air temperature and incoming radiation and with decreasing wind speed and relative humidity. At the leaf level, the leaf angle and leaf dimension have a large influence on T_s; at the vegetation level, T_s is strongly impacted by the roughness length; hence, by canopy height and structure. In the third part, an overview of the different ground-based thermal remote sensing techniques and approaches used to estimate drought stress or evapotranspiration in agriculture is provided. Among other methods, stress time, stress degree day, crop water stress index (CWSI), and stomatal conductance index are discussed. The theoretical models are used to evaluate the performance and sensitivity of the most important methods, corroborating the literature data. In the fourth and final part, a critical view on the future and remaining challenges of ground-based thermal remote sensing is presented.

Key words: Canopy temperature, corn, grapevine, infrared thermography, leaf temperature, non-contact thermocouple, thermal camera, wheat.

1 Introduction

Evapotranspiration is the process in which water stored in the soil or vegetation is converted from the liquid into the vapour phase and is transferred to the atmosphere. Because the energy required to break the hydrogen bonds in this phase transition is withdrawn from the soil or vegetation, evapotranspiration decreases the ecosystem's surface temperature (T_s) (Jones, 1992, 1999b).

Therefore, since the 1960s, researchers tried to apply canopy surface temperature for assessing plant-water and plant-health status (see Fuchs and Tanner, 1966, for an early overview). This pioneering research revealed the extreme difficulties in using surface temperature measurements, caused by the large influence of meteorological conditions and crop characteristics on T_s (Idso, 1982). It wasn't until measurement instruments became cheaper and new methods were developed to correct T_s for meteorological conditions that thermal remote sensing techniques could be applied in irrigation management and planning. The availability of thermal cameras led to a new boom in methods and applications of thermal remote sensing in the 2000s, an evolution that is still ongoing.

In this article, the application of ground-based thermal remote sensing in agriculture is reviewed. First, the basic principles and measurement techniques are introduced (section 2). Next, the theoretical relation between surface temperature and the evapotranspiration/

energy balance is elaborated at leaf and crop scale (section 3), after which the most important application methods are discussed (section 4). Finally, remaining knowledge gaps and future challenges for ground-based thermal remote sensing in agriculture are briefly discussed in section 5. A list of all abbreviations is given in Table 1.

This review focuses on ground-based thermal remote sensing and does not consider satellite or (high-altitude) airborne remote sensing techniques, as these are covered by several recent review papers (e.g. Gowda *et al.*, 2008; Kalma *et al.*, 2008; Li *et al.*, 2009).

Table 1. Abbreviation list

Symbol	Meaning	Unity
α	Albedo	[–]
α_{aero}	Aerodynamic adjustment parameter	[–]
α_l	Albedo of lower leaf side	[–]
α_{PT}	Priestley-Taylor coefficient	[–]
α_u	Albedo of upper leaf side	[–]
a_H	Parameter in equation 34	[–]
a_{pot}	Parameter (intercept) of non-water stressed baseline (equations 45, 47)	[–]
β_{aero}	Aerodynamic adjustment parameter (equation 38)	[–]
B	Sublayer-Stanton number (equation 35)	[–]
BIOTIC	Biologically Identified Optimal Temperature Interactive Console (ST)	[min or hours]
b_{pot}	Parameter (slope) of non-water stressed baseline (equations 45, 48)	[–]
B_r	Sublayer-Stanton number adjusted for radiometric roughness length (equation 37)	[–]
c_p	The heat or thermal capacity of the air	[J kg^{-1} K^{-1}]
CTD	Canopy Temperature Depression ($T_c - T_a$)	[K or °C]
CTV	Critical Temperature Variability ($T_{c,max} - T_{c,min}$)	[K or °C]
CWSI	Crop Water Stress Index (equation 41)	[–]
$CWSI_a$	CWSI obtained with analytical approach	[–]
$CWSI_d$	CWSI obtained with direct approach (equation 49)	[–]
$CWSI_{d,high}$	$CWSI_d$ estimated from T_l, $T_{dry,high}$ and $T_{wet,high}$	[–]
$CWSI_{d,low}$	$CWSI_d$ estimated from T_l, $T_{dry,low}$ and $T_{wet,low}$	[–]
$CWSI_e$	CWSI obtained with empirical approach	[–]
δe	Vapour pressure deficit	[Pa or kPa]
$\triangle T$	Difference between canopy and air temperature ($T_c - T_a$)	[K or °C]
$\triangle T_{dry}$	$\triangle T$ of a non-transpiring crop	[K or °C]
$\triangle T_{pot}$	$\triangle T$ of a potential crop (crop not experiencing drought stress)	[K or °C]
d	Zero displacement height	[m]
D	Characteristic leaf dimension	[m]
Di	Proportion of diffuse light	[–]
ε	Overall emissivity	[–]
ε_{app}	Apparent emissivity (equation 8)	[–]
ε_c	Canopy (or crop) emissivity	[–]
ε_{clr}	Clear-sky emissivity (equation 6)	[–]
ε_{eff}	Effective emissivity of the sky (equation 6)	[–]
ε_l	Leaf emissivity	[–]
ε_{soil}	Soil emissivity	[–]
e_a	Vapour pressure in the air	[Pa or kPa]
$e^*_s(T_0)$	Saturated vapour pressure at temperature T_0	[Pa or kPa]
ϕ	Viewing angle	[°]
F	Factor (≥1) accounting for sky cloudiness (equation 6)	[–]
$f_c(\phi)$	Fractional vegetation cover (equation 9)	[–]
γ	Psychrometric constant	[kPa K^{-1}]
Γ_i	$G_i R_n^{-1}$ (equation 31)	[–]
G	Factor relating g_s and l_g (equation 58)	[mmol s^{-1} m^{-2} or mm s^{-1}]
G_i	Soil heat flux	[W m^{-2}]
g_c	Crop stomatal conductance	[mmol s^{-1} m^{-2} or mm s^{-1}]
g_s	Leaf stomatal conductance	[mmol s^{-1} m^{-2} or mm s^{-1}]
$g_{s,l}$	Stomatal conductance on lower leaf side	[mmol s^{-1} m^{-2} or mm s^{-1}]
$g_{s,u}$	Stomatal conductance on upper leaf side	[mmol s^{-1} m^{-2} or mm s^{-1}]
H	Sensible heat flux (equation 14)	[W m^{-2}]
h_{at}	Indicator of drought stress derived from 3T method (equation 62)	[–]
h_c	Vegetation (canopy) height	[m]

Table 1. *continued*

Symbol	Meaning	Unity
H_{dry}	H of a completely dry leaf	[W m^{-2}]
H_r	Relative humidity	[%]
H_{soil}	H of soil layer in TSM	
I_g	Stomatal conductance index (equation 57)	[–]
IRT	Infrared Thermometer: general name for non-imaging thermal infrared devices (temperature guns or stand-alone sensors)	
K_{in}	Incoming shortwave radiance	[W m^{-2}]
$K_{in,l}$	K_{in} at lower leaf side	[W m^{-2}]
$K_{in,u}$	K_{in} at upper leaf side	[W m^{-2}]
K_{out}	Outgoing shortwave radiance	[W m^{-2}]
k	von Karman constant for momentum (0.41)	[–]
λE	Latent heat flux (evapotranspiration flux density)	[W m^{-2}]
λE_c	λE of canopy layer in TSM	[W m^{-2}]
λE_{pot}	λE of potential crop (crop not experiencing drought stress)	[W m^{-2}]
λE_{soil}	λE of soil layer in TSM	[W m^{-2}]
L	Leaf length	[m]
$L_{emitted}$	Longwave radiation emitted by a system	[W m^{-2}]
L_{in}	Incoming longwave radiance	[W m^{-2}]
$L_{reflected}$	Reflected longwave radiation	[W m^{-2}]
L_{out}	Outgoing longwave radiance (equation 3)	[W m^{-2}]
LAI	Leaf area index	[m^2 m^{-2}]
LAI_{shade}	LAI of shaded canopy	[m^2 m^{-2}]
LAI_{sun}	LAI of sunlit canopy	[m^2 m^{-2}]
NDVI	Normalized difference vegetation index	[–]
OSM	One-source model	
ψ_H	Monin-Obukhov stability function for heat flux	[–]
ψ_M	Monin-Obukhov stability function for momentum	[–]
ρ_a	Air density	[kg m^{-3}]
r_{ae}	Effective aerodynamic resistance (equation 36)	[s m^{-1} or s mm^{-1}]
r_{aH}	Leaf or canopy resistance to sensible heat transport	[s m^{-1} or s mm^{-1}]
$r_{aH,l}$	Resistance to sensible heat transport on lower leaf side	[s m^{-1} or s mm^{-1}]
$r_{aH,u}$	Resistance to sensible heat transport on upper leaf side	[s m^{-1} or s mm^{-1}]
$r_{aH,u}$(free)	Leaf resistance to free convection of H on upper leaf side	[s m^{-1} or s mm^{-1}]
$r_{aH,u}$(forced)	Leaf resistance to forced convection of H on upper leaf side	[s m^{-1} or s mm^{-1}]
r_{aM}	Canopy resistance to momentum exchange	[s m^{-1} or s mm^{-1}]
r_{aV}	Resistance to vapour transport in the boundary layer/air	[s m^{-1} or s mm^{-1}]
r_c	Crop stomatal resistance	[s m^{-1} or s mm^{-1}]
$r_{c,pot}$	r_c of potential crop (crop not experiencing drought stress)	[s m^{-1} or s mm^{-1}]
r_{HR}	Leaf resistance to sensible heat transport and radiative heat loss	[s m^{-1} or s mm^{-1}]
r_l	Total resistance of leaves to vapour losses	[s m^{-1} or s mm^{-1}]
r_R	(Virtual) leaf resistance to radiative transfer (equation 53)	[s m^{-1} or s mm^{-1}]
r_s	Leaf stomatal resistance	[s m^{-1} or s mm^{-1}]
r_{soil}	Resistance to heat flow between the soil layer and the canopy layer in TSM	[s m^{-1} or s mm^{-1}]
r_v	Total resistance to vapour transport	[s m^{-1} or s mm^{-1}]
R_n	Net radioation	[W m^{-2}]
R_{ni}	Isothermal net radiation	[W m^{-2}]
$R_{n,c}$	R_n of the canopy layer	[W m^{-2}]
$R_{n,dry}$	R_n of a completely dry leaf	[W m^{-2}]
$R_{n,soil}$	R_n of the soil layer	[W m^{-2}]
σ	Stefan-Boltzmann constant (5.675 10^{-8} W m^{-2} K^{-4})	[W m^{-2} K^{-4}]
$\sigma(\varepsilon)$	Standard deviation of ε between leaves	[–]
$\sigma(T_c)$	Canopy temperature variability	[K or °C]
$\sigma(T_l)$	Standard deviation on T_l measurement	[K or °C]
s	Slope of the curve relating T with e^*_s(T) (equation 17)	[Pa K^{-1}]
S	Total aboveground energy storage	[W m^{-2}]
SAVI	Soil-adjusted vegetation index	[–]
SDD	Stress degree day (equation 40)	[K or °C]
ST	Stress time index	[min or hours]

Table 1. *continued*

Symbol	Meaning	Unity
θ	Leaf inclination angle	[°]
T_0	Aerodynamic temperature	[K or °C]
T_a	Air temperature	[K or °C]
T_{bb}	Blackbody temperature (equation 1)	[K or °C]
T_{bg}	Background temperature (equation 6)	[K or °C]
T_{br}	Brightness temperature (equation 4)	[K or °C]
T_c	Canopy surface temperature	[K or °C]
T_{dry}	Surface temperature of dry reference surface	[K or °C]
$T_{dry,high}$	Higher estimate of T_{dry} due to difference between reference and measured leaves in weather conditions or leaf characteristics	[K or °C]
$T_{dry,low}$	Lower estimate of T_{dry} due to difference between reference and measured leaves in weather conditions or leaf characteristics	[K or °C]
T_l	Leaf surface temperature	[K or °C]
T_{pot}	Surface temperature of the potential crop	[K or °C]
T_s	(Radiometric) Surface temperature (equation 5)	[K or °C]
TSD	Temperature stress day	[K or °C]
TSM	Two-source model	
T_{soil}	Soil surface temperature	[K or °C]
T_{wet}	Surface temperature of wet reference surface	[K or °C]
$T_{wet,high}$	Higher estimate of T_{wet} due to difference between reference and measured leaves in weather conditions or leaf characteristics	[K or °C]
$T_{wet,low}$	Lower estimate of T_{wet} due to difference between reference and measured leaves in weather conditions or leaf characteristics	[K or °C]
TTT	Temperature-time threshold (= ST)	[min or hours]
u	Wind speed	[m s^{-1}]
u_c	Wind speed at the top of the canopy	[m s^{-1}]
u_{soil}	Wind speed just above the soil layer	[m s^{-1}]
W	Leaf width	[m]
WDI	Water deficit index	[–]
z_{0H}	Roughness length for sensible heat exchange	[m]
$z_{0H,r}$	Radiometric thermal roughness length	[m]
z_{0M}	Roughness length for momentum exchange	[m]
z_u	Height of wind speed measurement	[m]
z_T	Height of air temperature measurement	[m]

2 Basics of thermal remote sensing

2.1 Basic principles and terminology of thermal remote sensing

According to Planck's Fundamental Radiation law and Wien's Displacement law, every system with a temperature above 0 K emits radiation, of which the intensity and the spectral distribution are determined by the temperature of the system (Fuchs, 1990). The energy flux density of all ecosystems peaks at ~10 μm and can be detected optimally in the thermal infrared optical window between 7 and 14 μm (Fuchs and Tanner, 1966; Fuchs, 1990).

The total amount of radiation energy flux density emitted by a system [$L_{emitted}$, W m^{-2})] is a function of its temperature (in K), according to the Stefan-Boltzmann law:

$$L_{emitted} = \sigma T_{bb}^4 = \varepsilon\sigma T_s^4 \quad (1)$$

with T_{bb} the blackbody temperature (K), T_s the surface radiometric temperature (K), σ the Stefan-Boltzmann constant (5.67 10^{-8} W m^{-2} K^{-4}), and ε the overall emissivity (–) of the system.

A blackbody is an idealized object that is a perfect absorber of all incoming radiative energy and a perfect emitter of radiation. The *blackbody temperature* corresponds with the temperature that a blackbody would have if it emits the same radiation energy flux density as the system (Norman and Becker, 1995). In reality, however, systems are not perfect emitters or absorbers of radiation. The *overall emissivity* ε is a dimensionless variable between 0 and 1 that indicates how well a system resembles a blackbody in emitting radiation. Although ε is wavelength specific and depends on the viewing angle (Fuchs, 1990; Norman and Becker, 1995; Jones *et al.*, 2003), a constant overall emissivity can be assumed in agricultural research (Fuchs, 1990) with negligible error (see Norman and Becker, 1995, for a discussion).

(Eco)systems are not perfect absorbers of radiation (i.e. they are not blackbodies), which implies that they reflect some of the incoming longwave radiation L_{in} (W m^{-2}). According to Kirchhoff's law of thermal radiation, the absorption in the thermal wavelengths is equal to the emissivity and the reflected longwave radiation ($L_{reflected}$) is:

$$L_{reflected} = (1 - \varepsilon) L_{in} \quad (2)$$

The total outgoing longwave radiation (L_{out}, (W m^{-2})] from a system, i.e. the radiation measured by the thermal sensor, is:

$$L_{out} = L_{emitted} + L_{reflected} = \varepsilon\ \sigma\ T_s^4 + (1 - \varepsilon)\ L_{in} \quad (3)$$

Equation 3 can be rewritten in terms of temperature by analogy with the Stefan-Boltzmann law ($L = \sigma\ T^4$, see equation 1):

$$T_{br}^4 = \varepsilon\ T_s^4 + (1 - \varepsilon)\ T_{bg}^4 \quad (4)$$

In equation 4, T_{bg} is the *background temperature*, defined as $T_{bg} = \sqrt[4]{\frac{L_{in}}{\sigma}}$, and T_{br} the *brightness temperature* (both in K). T_{br} is not the same as T_{bb}: T_{bb} is the temperature of a blackbody that emits the same amount of radiation as the actual system emits; T_{br} is the temperature of a blackbody emitting the same amount of radiation as what the actual system emits and reflects (Norman and Becker, 1995; Jones *et al.*, 2003), or, from equations 1 and 4, $T_{br}^4 = (1 - \varepsilon)\ T_{bg}^4 + T_{bb}^4$. T_{br} is the 'temperature' actually measured by the infrared radiometer. T_{bb}, on the other hand, is a purely theoretical concept that is not measured directly.

In thermal remote sensing, one is not interested in the brightness temperature but in the *surface radiometric temperature* or *surface temperature* T_s, because it is T_s that reflects the internal energy status of the system. From equation 4, it follows that:

$$T_s = \sqrt[4]{\frac{T_{br}^4 - (1 - \varepsilon)T_{bg}^4}{\varepsilon}} \quad (5)$$

2.2 Measuring surface temperature

T_s can be measured with non-imaging and with imaging devices. Non-imaging devices or infrared thermometers (IRTs) make use of non-contact thermocouples and can be either portable, hand-held 'temperature guns', or continuously monitoring cylindrical stand-alone sensors, which have to be connected to a data logger. They measure the average T_{br} within the field of view of the sensor. They are fast, cheap, do not require an external power resource, and can be installed permanently in the field. On the other hand, the measured T_{br} is often a composite of vegetation and background (soil/sky) temperatures, which makes the interpretation difficult and can cause large estimation errors (Jackson *et al.*, 1981; Gardner *et al.*, 1992b; Moran *et al.*, 1994).

Imaging devices or thermal cameras predominantly use microbolometer sensors. They are more delicate, can often not be installed permanently on the field (because of price considerations, and because they are often not waterproof) and are much more expensive than IRTs, although prices have decreased in recent years. On the other hand, they provide images, are very precise and often give T_s rather than T_{br} as direct output (although T_{bg} and ε must still be supplied by the user).

Indeed, equation 5 shows that background temperature T_{bg} and ε are required to calculate T_s. T_{bg} can be assessed in several ways:

Directly: by measurement of T_{br} of overhead sky, without including the sun in the field of view (Loheide and Gorelick, 2005), with an infrared thermometer, sensitive in the same wavelengths as the thermometer used to measure T_s (Blonquist *et al.*, 2009).

Indirectly: measurement of T_{br} of blotted aluminum foil: as aluminium foil has an emissivity of 0.03, close to 0, T_{br} will be almost equal to T_{bg} (see equation 4) (Jones *et al.*, 2002, 2003).

By estimation: T_{bg} can be estimated from the air temperature T_a (K) as (Flerchinger *et al.*, 2009; Sedlar and Hock, 2009):

$$T_{bg}^4 = \varepsilon_{eff}\ T_S^4 = \varepsilon_{clr}\ F\ T_S^4 \quad (6)$$

with ε_{eff} the effective sky emissivity, ε_{clr} the sky emissivity at clear sky, and F a unitless factor ($\geq$1) accounting for the cloudiness of the sky. Methods to estimate ε_{clr} and F are reviewed and evaluated by Flerchinger *et al.* (2009) and Sedlar and Hock (2009). As a rule of thumb, ε_{clr} is close to 0.7. Hence, at T_a = 20 °C and for clear skies (F = 1), T_{bg} will be around 268 K or –5 °C. T_{bg} is close to T_a in greenhouses and with fully overcast skies and is lowest with clear skies.

2.2.1 Measuring leaf emissivity and leaf surface temperature

Values of leaf emissivity (ε_l) are available for a large number of plant species (see Gates *et al.*, 1965 and Salisbury and D'Aria, 1992, for an overview) and are generally 0.95 or higher (Fuchs, 1990); 0.97 is a good approximation (Kustas *et al.*, 2004).

Leaf emissivity can be estimated if T_l, T_{br}, and T_{bg} are known:

$$\varepsilon_l = \frac{\left(T_{br}^4 - T_{bg}^4\right)}{\left(T_l^4 - T_{bg}^4\right)} \quad (7)$$

For the most precise measurements, leaves can best be put in well-stirred water baths with controlled temperatures; T_l can then be assumed to be equal to the temperature of the water, and T_{br} and T_{bg} can be measured.

Very often, T_{bg} is not measured or known and T_l is calculated as $T_l = T_{br}$ or $T_l = \sqrt[4]{\varepsilon_l T_{br}^4}$ with ε_l taken from literature. However, both methods introduce significant error, as shown in Fig. 1a. When T_l is assumed equal to T_{br}, T_l is underestimated by 0.6–0.8 °C in clear-sky conditions; in cloudy conditions or inside greenhouses, errors are negligible. Applying ε_l without incorporating T_{bg} leads to a significant overestimation of T_l, which will be larger in cloudy conditions or inside greenhouses (Fig. 1a).

An alternative method in case T_{bg} cannot be measured uses an *apparent emissivity* (ε_{app}). ε_{app} is estimated from T_l (measured in a stirred bath or directly with contact thermocouples) and T_{br} only, as $\varepsilon_{app} = T_{br}^4\ T_l^{-4}$ (Jones *et al.*, 2003; Blonquist *et al.*, 2009). Combining equation 4 with $T_{br}^4 = \varepsilon_{app}\ T_l^4$ gives:

$$\varepsilon_{app} = \varepsilon_l + (1 - \varepsilon_l)\frac{T_{bg}^4}{T_l^4} \quad (8)$$

Hence, ε_{app} is higher than ε_l and ($\varepsilon_{app} - \varepsilon_l$) is larger when T_{bg} is high and when ε_l and T_l are low. T_l estimated with ε_{app} gives only an unbiased estimate of T_l when T_l and T_{bg} are the same as they were when ε_{app} was estimated. The error for deviating T_l

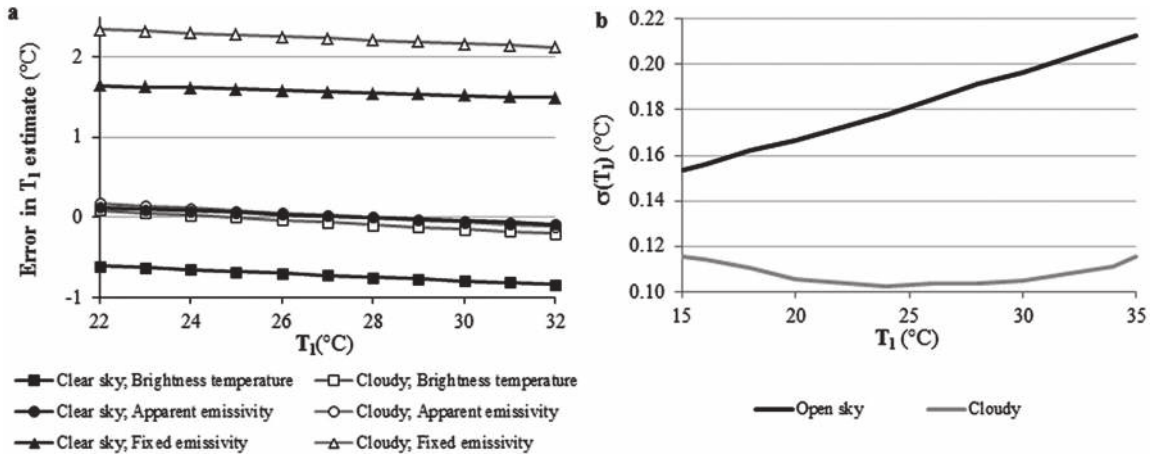

Fig. 1. (a) The error in the estimation of T_l when background temperature (T_{bg}) is not measured and T_l is estimated (i) as brightness temperatures, (ii) by using of the literature value of **ε** from literature, and (iii) by using ε_{app} (apparent emissivity). The error is calculated for open-sky and cloudy/greenhouse conditions and expressed as a function of T_l. (b) The precision of the T_l estimate, expressed as standard deviation of the T_l measurement ($\sigma(T_l)$), when ε and T_{bg} are known for open-sky and cloudy/greenhouse conditions. See text for details. In both parts, T_a = 25 °C and $T_{bg} = (0.7\ T_a^4)^{0.25}$ (equation 6) for clear-sky conditions and $T_{bg} = T_a$ for clouded/greenhouse conditions. In part a, it was assumed that ε = 0.97, T_a = 25 °C, and T_l = 28 °C; from equation 8, ε_{app} = 0.9910 in clear sky and ε_{app} = 0.9988 in greenhouse/cloudy conditions.

values is up to ~0.2 °C and is larger in cloudy conditions or inside greenhouses (Fig. 1a). Still, it is lower than the error introduced when either only T_{br} or only T_{br} and ε_l are used. Deviating T_{bg} values will not lead to significant errors (not shown). Overall, if T_{bg} cannot be assessed, the ε_{app}-method is recommended.

Apart from avoiding measurement bias, it is important to know the measurement precision (or standard deviation, $\sigma(T_l)$) of T_l measurements. This depends on the measurement precision of T_{br} and T_{bg} and on the standard deviation of ε_l between the leaves [$\sigma(\varepsilon_l)$]. The measurement precision is sensor specific; precise sensors have a standard deviation of about 0.1 °C. σ(ε) is species specific and ranges from 0.004 to 0.010 (e.g. Rubio *et al.*, 1997; López *et al.*, 2012), although these estimates might also include measurement errors rather than true differences in ε between leaves.

$\sigma(T_l)$ was calculated with a Monte Carlo approach from 5000 random values of ε_l, T_{bg}, and T_{br}, each having a normal distribution with a standard deviation of 0.1 °C (for T_{bg} and T_{br}) and 0.005 (for ε). In open-sky conditions, $\sigma(T_l)$ increases with T_l and is between 0.15 and 0.21 °C; the average $\sigma(T_l)$ is 0.18 °C (Fig. 1b). $\sigma(T_l)$ is lower (0.11 °C on average) in cloudy conditions or inside greenhouses and reaches a minimum of 0.10 °C when $T_l = T_{bg}$.

A linear regression analysis, fitted through the $T_l - \varepsilon_l$, T_{bg}, and T_{br} scatterplot, indicates that, with open-sky conditions, small deviations in ε_l have a relatively large impact on T_l: a decrease as small as 0.0035 in ε_l causes a 0.1 °C error in T_l; in cloudy conditions, this is a decrease of 0.0191. T_l is much less influenced by T_{bg}; in fact, only an error in T_{bg} of above 5.6 °C (open sky) or 9.8 °C (cloudy/greenhouse) causes an error in T_l of 0.1 °C (Table 2).

2.2.2 Measuring canopy surface temperature

T_l can vary with several degrees within and between plants as a consequence of differences in leaf angle, dimension, and radiation (see section 3.2.2). It is therefore often preferable to measure the canopy surface temperature (T_c) as an aggregate of all leaf temperatures (Jones *et al.*, 2009). Measurements of T_c differ in several ways from those of single leaves. First, canopy emissivity (ε_c) is larger than ε_l, because of the partial cavities in the foliage, entrapping the radiation (Fuchs, 1990; Jones *et al.*, 2003). Estimating ε_c is more difficult than in the case of ε_l and requires night measurements; see Fuchs and Tanner (1966) or Huband and Monteith (1986) for a description of the methodology. Fortunately, because ε_c of dense canopies is very high (0.98–0.99; Huband and Monteith, 1986; Sobrino *et al.*, 2001, 2002), measurement of T_{br} or precise knowledge of ε_c are of lesser importance; estimating T_s by either assuming $T_s = T_{br}$ or by assuming ε_{app} = 0.99 will normally cause negligible error, in particular in cloudy conditions.

A second difference with leaf temperature measurements is the fact that the measured signal is a composite of surface temperatures of several objects, including leaves and branches,

Table 2. Correlation (R^2) between the measurement error in T_l and ε, T_{bg} and T_{br}, and the increase in ε, T_{bg}, and T_{br} that causes an increase in T_l of 0.1 °C, in open sky and cloudy conditions.

Calculated using a Monte Carlo approach for ε = 0.970 ± 0.005, T_{br} = 21.18 ± 0.1, and T_{bg} = −10 ± 0.1 °C in open-sky conditions and T_{br} = 22.09 ± 0.1 and T_{bg} = 25 ± 0.1 °C in cloudy conditions (in both cases, T_l = 22 °C),

	Open sky		Cloudy	
	R^2	△x causing a △T_l of 0.1 °C	R^2	△x causing a △T_l of 0.1 °C
ε	0.66	-0.0035	0.032	–0.0191
T_{bg}	2 10^{-4}	5.6	4 10^{-4}	–9.8
T_{br}	0.32	0.1	0.96	0.1

which make up the canopy, and soil (Kustas and Daughtry, 1990; Sánchez *et al.*, 2008):

$$\varepsilon T_s^4 = f_c(\phi)\,\varepsilon_c T_c^4 + (1 - f_c(\phi))\,\varepsilon_{soil}\,T_{soil}^4 \quad (9)$$

with ε and ε_{soil} the overall and soil emissivity, T_{soil} the soil surface temperature, and $f_c(\phi)$ the portion of the field of view occupied by the vegetation as influenced by viewing angle ϕ. In general, T_{soil} is higher than T_c (Kustas and Daughtry, 1990); the difference can be up to 30 °C in very sunny conditions and for dry, bare soils (Jackson, 1985). Hence, T_s is usually higher than T_c. Particularly in orchards or in croplands at the beginning of the growing season, when the canopy cover is low, this can make T_s measurements unreliable.

Several ways exist to estimate T_c instead of T_s. The first way is to simply delay the measurements until the canopy is fully closed and $f_c(\phi)$ is (close to) 1. Obviously, delaying the measurements is not always an option.

Second, the viewing angle ϕ can be adjusted to increase $f_c(\phi)$. $f_c(\phi)$ is in general smallest for nadir measurements (when the sensor is looking straight down) (Jones *et al.*, 2003; Luquet *et al.*, 2004) and highest for oblique views (Chehbouni *et al.*, 2001; Koksal, 2008). However, increasing ϕ is often not feasible and holds the risk of including air.

A third approach uses the angle-dependence of $f_c(\phi)$ to estimate T_{soil} and T_c separately. Under the assumption $\varepsilon_{soil} = \varepsilon_c = \varepsilon$, T_{soil} and T_c can be estimated separately from two simultaneous T_s measurements made under different viewing angles (Sánchez *et al.*, 2008).

A fourth way to reduce the influence of T_{soil} is by using a thermal camera and by separating canopy from soil pixels combining visual and thermal images (e.g. Leinonen and Jones, 2004; Möller *et al.*, 2007; Wang *et al.*, 2010a).

3 Relation between surface temperature and sensible and latent heat flux

3.1 General relations between surface temperature and sensible and latent heat flux

The energy balance of a leaf or vegetation is given by:

$$R_n = H + \lambda E + G_i + S \quad (10)$$

with R_n the net radiation, λE the latent heat flux, G_i the soil heat flux, and S the total aboveground energy storage (all in W m^{-2}).

The *net radiation* R_n is the sum of incoming (positive) and outgoing (negative) shortwave (0.3–3 μm) and longwave (3–50 μm) radiation, or:

$$R_n = K_{in} - K_{out} + L_{in} - L_{out} \quad (11)$$

with K_{in} the incoming and K_{out} the outgoing shortwave radiation. For vegetations, R_n is given by:

$$R_n = K_{in}\,(1 - \alpha) + \varepsilon\,L_{in} - \varepsilon\,\sigma\,T_s^4 \quad (12)$$

where α is the albedo (the fraction of incoming radiation that is reflected or reradiated). For leaves, R_n is still expressed per unit area (i.e. the leaf area on one side of the leaf), but the two leaf sides must be taken into account (Guilioni *et al.*, 2008); in addition, R_n is influenced by the transmittance (the fraction of incoming radiation that passes through the leaves) of the leaf:

$$R_n = K_{in,u}\,(1 - \alpha_u - \tau) + K_{in,l}\,(1 - \alpha_l - \tau) + \varepsilon_u\,L_{in,u} - \varepsilon_u\,\sigma\,T_l^4 + \varepsilon_l\,L_{in,l} - \varepsilon_l\,\sigma\,T_l^4 \quad (13)$$

where the subscript u refers to the upper side and the subscript l to the lower side of the leaf.

The *sensible heat flux H* (W m^{-2}) from a surface to the air is given by (see derivation in Supplementary Data S1.1, available in *JXB* online):

$$H = \rho_a c_p \frac{(T_0 - T_a)}{r_{aH}} \quad (14)$$

with ρ_a the air density (kg m^{-3}), c_p the specific heat of the air (J kg^{-1} K^{-1}), T_0 the aerodynamic temperature, T_a the air temperature, and r_{aH} the resistance of diffusive heat transfer to air (s m^{-1}). ρ_a and c_p can be considered constants. T_0, the aerodynamic temperature, is defined by equation 14. For leaves, $T_0 = T_l$ (Huband and Monteith, 1986). In vegetations, T_0 is not a directly measurable variable. Although T_s is also commonly used as a surrogate for T_0 in vegetations (Colaizzi *et al.*, 2004), the relationship between T_0 and T_s is a complex function of viewing angle, atmospheric stability and vegetation structure. This will be discussed in section 3.3.4.

The *latent heat flux* (λE; (W m^{-2}) describes the energy transfer related to transpiration/evapo transpiration of water from a leaf/vegetation to the air. It is given by (see Supplementary Data S1.2 for derivation):

$$\lambda E = \frac{\rho_a c_p}{\gamma} \frac{(e_s^*(T_0) - e_a)}{r_v} \quad (15)$$

where γ is the psychrometric constant (kPa K^{-1}), which is a function of T_a, e_a the vapour pressure in the air (kPa), r_v the total resistance to vapour transport (s m^{-1}), and $e_s^*(T_0)$ the saturated vapour pressure (indicated by *) at the surface (indicated by subscript s) (kPa).

The *total aboveground energy storage* S covers the physical storage (the energy for heating/cooling the biomass and the air in the canopy) and the energy stored in photosynthesis. At leaf scale, the storage term simplifies to the sum of the energy stored in photosynthesis and the physical (heat) storage of the leaves. Compared with the other terms in equation 10, this term is generally small and is most often ignored in leaf energy balance calculations, as is the *soil heat flux* G_i (Jones, 1992). In vegetations, however, S and G_i can make up a significant part of the energy budget (see section 3.3.4 for a discussion).

T_0 can be expressed as a function of the energy flux terms by combining equations 10 and 14:

$$T_0 = \frac{r_{aH}}{\rho_a c_p}(R_n - \lambda E - G_1 - S) + T_a \quad (16)$$

It follows that T_0 decreases linearly with increasing evapotranspiration. The relation between T_0 and λE is not as straightforward as it appears from equation 16. First of all, from equation 12, it follows that T_s and R_n (thus, also T_0 and R_n) are interrelated. Second, the resistance of the air to heat transfer, r_{aH}, is a complex function of leaf/vegetation characteristics and meteorological conditions. This issue will be discussed in more detail in sections 3.2 and 3.3.

It is often more convenient to express T_0 as a function of r_V rather than λE. This can be done by applying the Penman transformation:

$$(e_s^*(T_0) - e_a) = s(T_0 - T_a) + \delta e \quad (17)$$

in which s is the slope of the curve relating T with the saturated vapour pressure $e^*(T)$. δe is the *vapour pressure deficit* (Pa or kPa) or the difference between the maximal possible amount and the actual amount of water vapour in an air volume at temperature T_a. δe can be calculated from relative humidity (H_r; %) and T_a as:

$$\delta e = \left(1 - \frac{H_r}{100}\right) a \exp\left(\frac{b T_a}{c + T_2}\right) \quad (18)$$

with T_a in °C and $e^*_s(T_a)$ in Pa and, under normal atmospheric pressure, $a = 613.75$, $b = 17.502$, and $c = 240.97$.

Combining equations 10, 14, 15 and 17 gives:

$$(T_0 - T_a) = \frac{r_{aH} r_v \gamma (R_n - G_i - S) - r_{aH} \rho_a c_p \delta e}{\rho_a c_p (\gamma\, r_v + s\, r_{aH})} \quad (19)$$

It follows that if $(R_n - G_i - S)$ increases or δe decreases, $(T_0 - T_a)$ increases linearly. The relation between $(T_0 - T_a)$ and r_{aH} and r_V is less straightforward.

3.2 The relations between T_s, stomatal conductance, and weather at leaf scale

3.2.1 Resistances associated with energy processes at leaf scale

The resistance terms r_{aH} and r_V can be estimated by applying the electric circuit theory to transfer processes in leaves (Jones, 1992). The resistance terms are schematized in Fig. 2. r_{aH} is the parallel sum of $r_{aH,u}$ and $r_{aH,l}$. As $r_{aH,u} = r_{aH,l}$ (Guilioni *et al.*, 2008), r_{aH} is:

$$r_{aH} = \left(r_{aH,u}^{-1} + r_{aH,l}^{-1}\right)^{-1} = 0.5\ r_{aH,u} \quad (20)$$

Sensible heat exchange can occur either through free or through forced convection, which are also parallel processes. Forced air convection, with resistance $r_{aH,u}$(forced), is caused by wind flowing over the leaves altering the boundary layer; free air convection, giving rise to $r_{aH,u}$(free), occurs when air above a heated surface expands and rises. $r_{aH,u}$ is then given by:

$$r_{aH,u} = \left(r_{aH,u}(\text{forced})^{-1} + r_{aH,u}(\text{free})^{-1}\right)^{-1} \quad (21)$$

The stomatal resistance at each leaf side ($r_{s,u}$ and $r_{s,l}$) expresses the degree of stomatal closing (Jones, 1992); the reciprocal of the stomatal resistance is stomatal conductance ($g_{s,u}$ and $g_{s,l}$). It can be assumed that the resistance of the leaf to water vapour losses on each side is equal to its stomatal resistance (Jones, 1992). However, after the water has left the leaf, it still has to pass through the boundary layer of the air before it reaches the free-flowing air. This boundary layer is characterized by a resistance to vapour transport ($r_{aV,l}$ and $r_{aV,u}$; subscript a stands for air). It can also be assumed that $r_{aV,l} = r_{aV,u}$. Consequently, the total roughness length for water vapour transport of leaves, r_V, is a parallel sum of two serial sums (Fig. 2), or (Guilioni *et al.*, 2008):

$$r_V = \left(\frac{1}{r_{s,u} + r_{aV,u}} + \frac{1}{r_{s,l} + r_{aV,u}}\right)^{-1} = \frac{(r_{s,u} + r_{aV,u})(r_{s,l} + r_{aV,u})}{2\, r_{2V,u} + r_{s,l} + r_{s,u}} \quad (22)$$

For isolateral leaves (leaves with $r_{s,l} = r_{s,u}$), equation 22 becomes:

$$r_V = \frac{r_{s,l} + r_{aV,l}}{2} \quad (23)$$

In hypostomatous leaves (leaves with stomata only on the lower leaf side), $r_{s,u} = \infty$ and r_v is:

$$r_V = r_{s,l} + r_{aV,l} \quad (24)$$

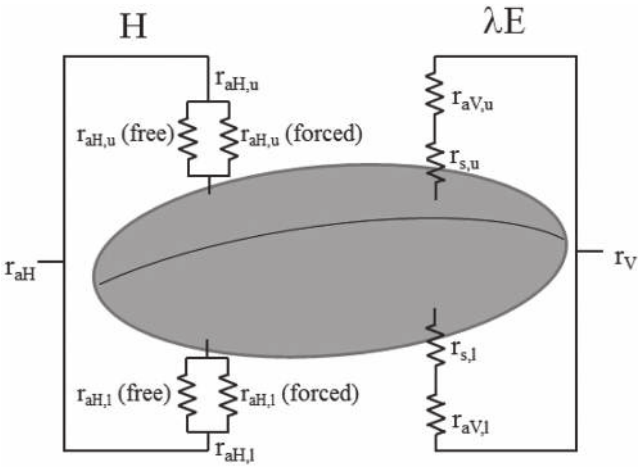

Fig. 2. Schematic overview of the resistances associated with sensible and latent heat transfer and radiation at leaf scale (this figure is available in colour at *JXB* online).

3.2.2 Modelling the influence of leaf characteristics and weather on T_l

Model description T_l was estimated from equation 19, with $T_l = T_0$, $G_i = 0$, and $S = 0$. Equations from Jones (1992) were used to calculate ρ_a, γ, and s as a function of T_a. $r_{aH,u}$(free) and $r_{aH,u}$(forced) were calculated from empirical relations of Monteith (1973) and Jones (1999a), respectively:

$$r_{aH,u}(\text{free}) = \frac{400}{|T_l - T_2|^0}.33 \quad (25)$$

$$r_{aH,u}(\text{forced}) = 100\left(\frac{D}{u}\right)^0.5 \quad (26)$$

In equation 26, D is the characteristic leaf dimension (m) and u the wind speed (m s^{-1}). The model assumes ellipsoid shape with leaf length L and width W. Based on $D = \sqrt{(L^2 + W^2)}$ (Dauzat *et al.*, 2001), D was calculated from leaf size (A_l) and W/L as:

$$D = \sqrt{\frac{A_l}{\pi}\left(\frac{1}{W/L} + W/L\right)} \quad (27)$$

$r_{aH,u}$ was calculated from equations 22, 25, and 26, r_{aH} from equation 20. The model assumes hypostomatous leaves; $r_{s,l}$ and $g_{s,l}$ will further be denoted simply as r_s and g_s. r_V was calculated from equation 24, with $r_{aV,l} = 0.92\ r_{aH,l}$ (Jones, 1992). Conductances in mmol m^{-2} s^{-1} were converted to resistances in s m^{-1} as a function of T_a with equations from Jones (1992).

R_n was calculated from equation 13, with the following assumptions:

$K_{in,u}$ is a function of K_{in} on a horizontal plane ($K_{in,hor}$; W m^{-2}), as would be measured by a pyranometer, the angle between the leaf and the horizontal plane (θ; °) and the proportion of diffuse light (Di; –) (Maes *et al.*, 2011):

$$K_{in,u} = K_{in,hor}((1 - Di)\cos\vartheta + Di) \quad (28)$$

Di was estimated as 0.15, typical for open-sky conditions (Gates, 2003; Jones *et al.*, 2009).

$K_{in,l}$ was modelled as $K_{in,l} = \alpha\ K_{in,hor}$. This equation is obtained by assuming that the modelled leaf is a top leaf: hence, $K_{in,l}$ is the reflected radiation by the lower canopy. This reflected radiation is assumed to be perfectly diffuse (hence, not a function of θ).

$$\alpha_u = \alpha_l = \alpha.$$

α and τ are not influenced by θ. Standard values for α and τ were 0.25 and 0.28, respectively, derived from the LOPEX93 library as the average α and τ of 10 crop species (Hosgood *et al.*, 1994).

$$\varepsilon_u = \varepsilon_l = \varepsilon = 0.97 \text{ (Kustas } et\ al.\text{, 2004)}.$$

$L_{in,u} = 0.7\ \sigma\ T_S^4$ (equation 6), also corresponding to open sky.

It was assumed that $L_{in,l}$ is the radiation coming from the canopy below, which had the same T_l as the actual leaf, or $L_{in,l} = \varepsilon\ \sigma\ T_l^4$. Note that in this (common) case, $L_{in,l} = L_{out,l}$.

R_n was estimated as:

$$R_n = K_{in,hor}(1 - \alpha - \tau)((1 - Di)\cos\vartheta + Di + \alpha) + 0.7\sigma T_2^4 - \varepsilon\sigma T_l^4 \quad (29)$$

The mutual dependency of T_l and R_n (equations 19 and 29) required an iterative procedure, in which R_n, r_{ah}(free) (and r_{aH}, r_{aV}, and r_V), and T_l were iteratively calculated, after a first assumption of $(T_l - T_a) = 2$, until the difference in subsequent estimates of $(T_l - T_a)$ was less than 0.001 °C.

The influence of T_a on $(T_l - T_a)$ was modelled for different levels of g_s by calculating $(T_l - T_a)$ for varying T_a, while assuming constant standard values for all other factors. The influence on $(T_l - T_a)$ of K_{in}, u, and δe and of the leaf properties θ, A_l, W/L, and α was simulated similarly. The 95% confidence intervals for measurement of $(T_l - T_a)$ are indicated by the colour bars, with a width of 2 $\sigma(T_l - T_a)$ on each side. $\sigma(T_l - T_a)$ was 0.206 °C, obtained from $\sigma^2(T_l - T_a) = \sigma^2(T_l) + \sigma^2(T_a) = 0.18^2 + 0.1^2$ (see section 2.2.1).

Results

The influence of weather conditions on $(T_l - T_a)$ is shown in Fig. 3. $(T_l - T_a)$ decreases non-linearly with increasing g_s; the rate of decrease depends on the weather conditions.

T_a and δe influence $(T_l - T_a)$ in an analogous way (Fig. 3a, 3g); at low g_s, $(T_l - T_a)$ does not depend on T_a or δe. The relationship between $(T_l - T_a)$ and δe when g_s is not zero, is linear (see also equation 19), an important characteristic first described by Ehrler (1973) and used as a basis for the calculation of the empirical crop water stress index ($CWSI_e$; see section 4.3.3). $(T_l - T_a)$ rises linearly with increasing K_{in} with larger slopes for leaves with low g_s (Fig. 3c).

At high T_a, K_{in}, and δe and low u, differences in $(T_l - T_a)$ between leaves with different g_s are large; hence these are ideal conditions for thermal remote sensing. Overall, even modest changes in K_{in}, T_a, u, and δe can have a profound impact on $(T_l - T_a)$.

With the exception of θ, leaf characteristics have a much smaller impact on $(T_l - T_a)$ than weather conditions (Fig. 4). There is little difference in $(T_l - T_a)$ between 'horizontal' leaves (with $\theta = 0$) and leaves with angles up to 30%. At higher θ, however, $(T_l - T_a)$ can decrease with several degrees and the influence of g_s on $(T_l - T_a)$ becomes less explicit (Fig. 4a, 4b).

$(T_l - T_a)$ increases slightly with increasing leaf size. $(T_l - T_a)$ of very small leaves tends to zero, regardless g_s (Fig. 4c, 4d). Similarly, for a constant A_l, leaf shape (W/L) has a rather limited influence on $(T_l - T_a)$, except for very thin, needle-like leaves. $(T_l - T_a)$ decreases slightly and steadily with increasing α (Fig. 4g, 4h). ε, finally, has very limited impact on $(T_l - T_a)$ (not shown).

Even if all leaves within the canopy have the same g_s, $(T_l - T_a)$ can be very heterogeneous because θ and A_l tend to vary within the canopy and because shaded leaves, which receive lower K_{in} and experience lower T_a and δe, have a lower $(T_l - T_a)$. As a consequence, it is often preferred to measure the temperature of (parts of) the entire canopy, rather than that of single leaves.

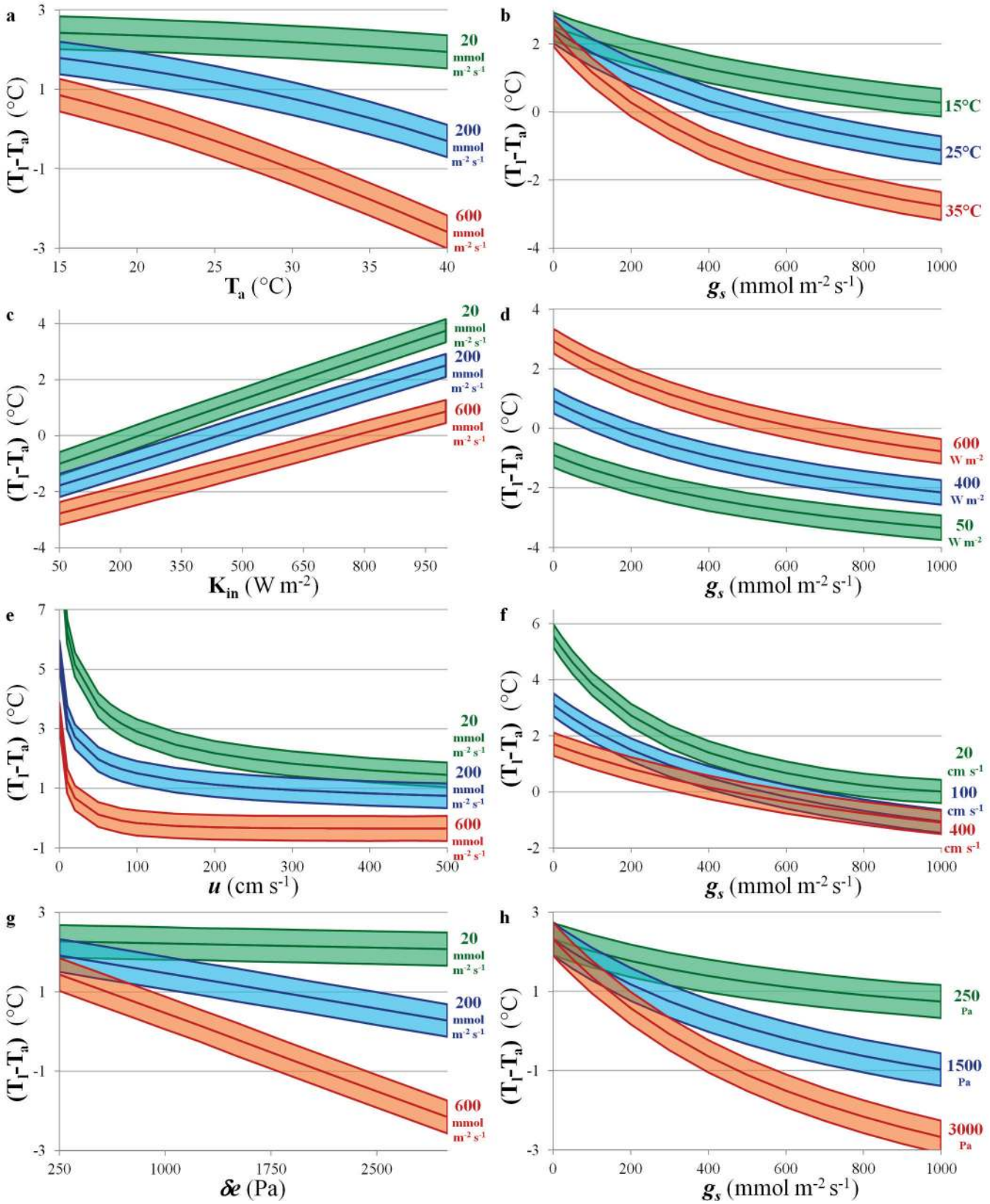

Fig. 3. Influence on the mean and 95% confidence interval of (T_l – T_a) of weather conditions air temperature (T_a), incoming shortwave radiation (K_{in},), wind speed (u), and vapour pressure deficit (δe) for a low, medium, and high level of g_s (left column) and of g_s for a low, medium, and high level of T_a, K_{in}, u, and δe (right column). See section 3.2.2 for model description. Standard conditions included T_a = 25 °C, K_{in} = 700 W m^{-2}, u = 2 m s^{-1}, and δe = 1590 Pa (H_r = 50%). Standard leaf characteristics were θ = 0 °, ε = 0.97; τ = 28%, α = 25%, A_l = 39.3 cm^2 (L = 10 cm), and W/L = 50%.

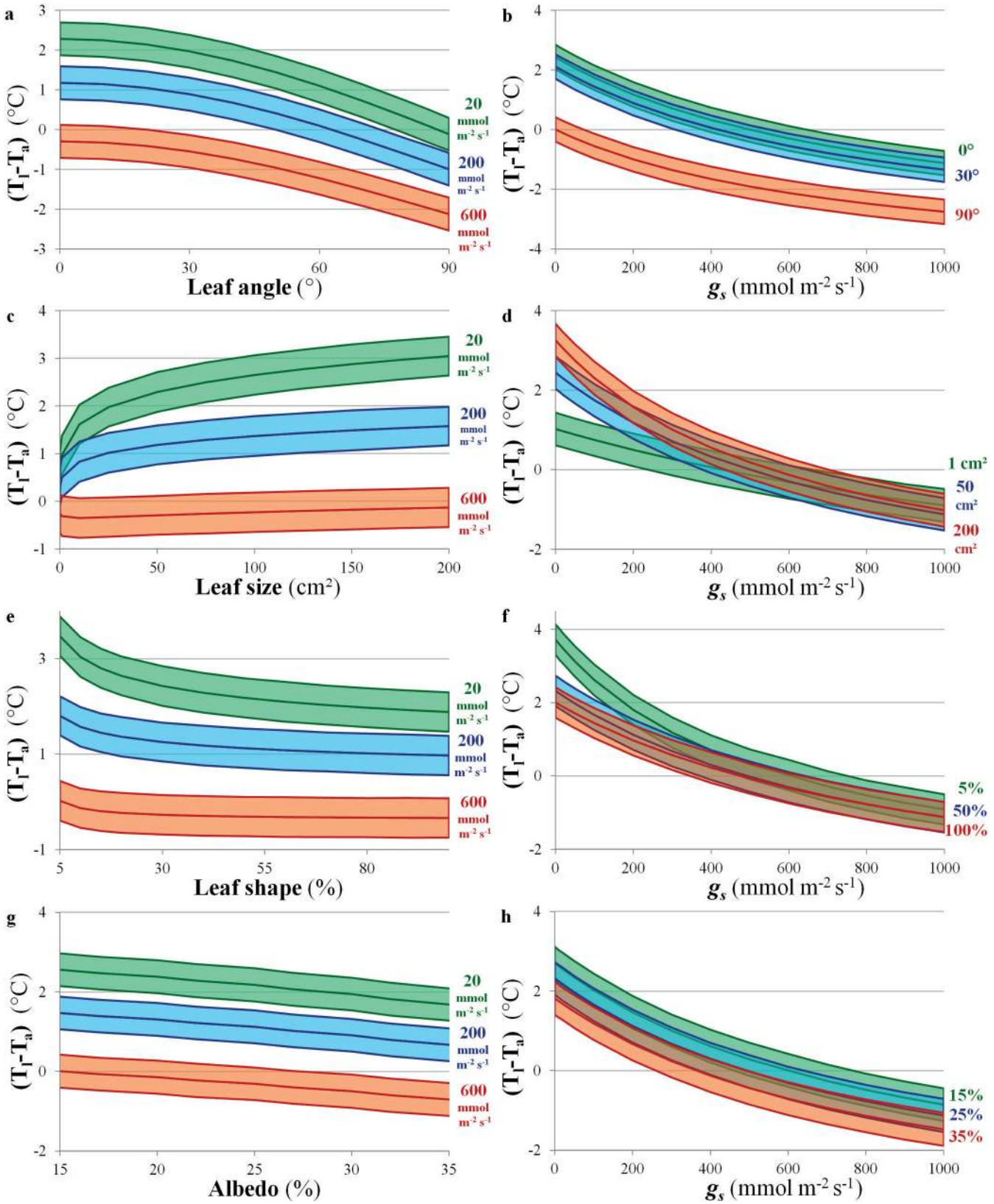

Fig. 4. Influence on the mean and 95% confidence interval of (T_l – T_a) of leaf characteristics (leaf angle, size, shape, and albedo) for a low, medium, and high level of g_s (left column) and of g_s on for a low, medium, and high level of leaf angle, size, shape, and albedo (right column). See Fig. 3 for model descriptions and standard conditions. Leaf shape = 100 leaf width/leaf length.

3.3 Relation between T_s and evapotranspiration at canopy level

Equation 19 can be applied to estimate T_0 at field scale. In that case, the canopy (and soil) are represented as one single layer with one side (the 'upper' side), so $r_{aH} = r_{aH,u}$ and $r_V = r_c + r_{aV} = r_c + r_{aH}$, with r_c the canopy stomatal resistance:

$$T_0 - T_a = \frac{r_{aH}(r_c + r_{aH})\gamma(R_n - G_i - S) - r_{aH}\rho_a c_p \delta e}{\rho_a c_p(\gamma[(r_c + r]_{aH}) + s\, r_{aH})} \quad (30)$$

3.3.1 Soil heat flux (G_i) and aboveground energy storage (S)

The *soil heat flux* (G_i) follows a daily trend that lags several hours behind R_n (Jarvis *et al.*, 1976; Samson and Lemeur, 2001). G_i is most often calculated as a fraction of R_n and is then denoted as Γ_i:

$$\Gamma_i = G_i\, R_n^{-1} \quad (31)$$

Whereas Γ_i is usually small (~0.05) and is in practice often ignored in ecosystems with dense canopies (Clothier *et al.*, 1986), it is significantly larger in ecosystems with sparse canopies (Norman *et al.*, 1995; Su, 2002) or with very wet or permafrost soils (Chapin *et al.*, 2002) Often, a value of 0.1 is often used for Γ_i (Choudhury *et al.*, 1986; Jackson *et al.*, 1988).

When thermal measurements are performed around and short after solar noon, the aboveground energy storage term S can be ignored (Meesters and Vugts, 1996; Samson and Lemeur, 2001), except in very dense woody vegetation (McCaughey, 1985; Samson and Lemeur, 2001; Lindroth *et al.*, 2010).

3.3.2 Canopy stomatal resistance r_c and conductance g_c

The canopy stomatal conductance (g_c) can be interpreted as the stomatal conductance of the 'big leaf' that represents the canopy and is composed of the stomatal conductances of all individual leaves. The most practical way to calculate g_c is by discerning a sunlit and a shaded layer (Blonquist *et al.*, 2009):

$$g_c = g_{s,sun}\, LAI_{sun} + g_{s,shade}\, LAI_{shade} \quad (32)$$

where LAI_{sun} and LAI_{shade} are the leaf area index of the sunlit and the shaded canopy, respectively ($LAI_{sun} + LAI_{shade} = LAI$). LAI_{sun} can be calculated, provided data of the solar zenith angle and canopy structure are available (Lemeur, 1973); else, g_c can be roughly estimated for crops as (Allen *et al.*, 1998):

$$g_c = 0.5\, g_s\, LAI \quad (33)$$

with g_s measured on sunlit leaves.

3.3.3 Resistance to sensible and latent heat transport in air (r_{aH} and r_{aV})

Based on the calculation of momentum flux and the observed logarithmic profile of wind speed close to surfaces, r_{aH} of ecosystems is given by (see Supplementary Data S2.3, equation S34):

$$r_{aH} = \frac{\left[\ln\left(\frac{z_u - d}{z_{0M}}\right) - \Psi_M\right]\left[\ln\left(\frac{z_T - d}{z_{0H}}\right) - \Psi_H\right]}{a_H\, k^2\, u} \quad (34)$$

where z_u and z_T are the heights at which u and T_a were measured, d is the zero displacement height, z_{0M} the roughness length of momentum, z_{0H} the roughness length of sensible heat exchange, k the dimensionless von Karman constant ($k = 0.41$), ψ_M and ψ_H the Monin-Obukhov stability functions for momentum and latent heat exchange, and a_H a parameter.

The *displacement height d* and *roughness length* z_{0M} are complex functions of the vegetation height and architecture. They can be estimated precisely with drag partition models, taking canopy height (h_c; m), width, and element spacing into account (Raupach, 1992, 1994). Other methods estimate d and z_{0M} as a function of h_c and leaf area index (LAI) (e.g. Pereira *et al.*, 1999; Colaizzi *et al.*, 2004) or of h_c alone. Estimates of d/h_c and z_{0M}/h_c can be found for a wide variety of vegetations (e.g. Stanhill, 1969; Jarvis *et al.*, 1976; Dolman, 1986). For dense crops, the values $d = 0.64\ h_c$ and $z_{0M} = 0.13\ h_c$ (Stanhill, 1969) are universally used.

The *roughness length for sensible heat* z_{0H} is usually expressed as a function of z_{0M} as (Owen and Thomson, 1963; Chamberlain, 1968; Colaizzi *et al.*, 2004):

$$\ln(z_{0M}\, z_{0H}^{-1}) = k\, B^{-1} \quad (35)$$

with B the dimensionless sublayer-Stanton number. Although $k\, B^{-1}$ is a complex function of the time of day, weather, and the vegetation type (Garrath and Hicks, 1973; Mölder and Lindroth, 2001), constant values for z_{0H}/z_{0M} of 0.0907 or 0.1 for dense crops and 0.2 for sparse crops are often used (Monteith, 1973; Campbell, 1977; Allen *et al.*, 1989; Mölder and Lindroth, 2001).

ψ_M and ψ_H, the Monin-Obukhov stability functions for momentum and latent heat exchange, can be estimated as a function of one of two variables, the Richardson number or the Monin-Obukhov length (see Supplementary Data S2.3, equations S35 and S36). This requires detailed meteorological measurements at several heights. Hence, it is often not feasible to estimate ψ_M or ψ_H in agricultural applications. Omitting ψ_M and ψ_H from equation 34 gives unrealistic results at low wind speeds (at $u = 0$, r_{aH} would become $+\infty$, and so would $(T_0 - T_a)$ (see equation 34 below; also Jackson *et al.*, 1988). This can be overcome by using r_{ae} instead of r_{aH}. r_{ae} is the *effective aerodynamic resistance*. This semi-empirical equation includes the influence of buoyancy on aerodynamic resistance (Thom and Oliver, 1977):

$$r_{ae} = 4.72\frac{\left[\ln\left(\frac{z_u - d}{z_{0M}}\right)\right]^2}{(1 + 0.54u)} \quad (36)$$

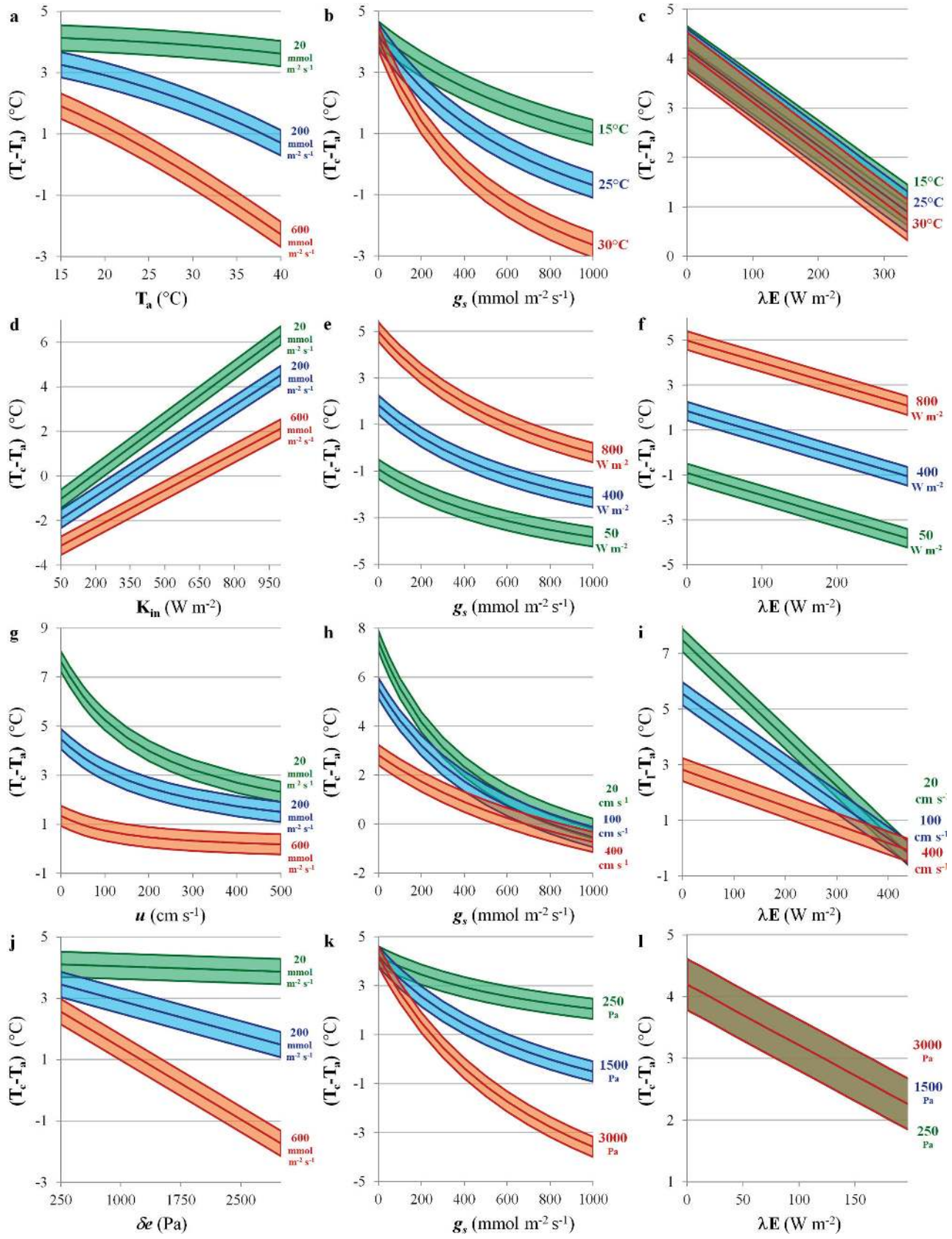

Fig. 5. Influence on the mean and 95% confidence interval of (T_l – T_a) of weather conditions air temperature (T_a), incoming shortwave radiation (K_{in}), wind speed (u), and vapour pressure deficit (δe) for a low, medium, and high level of g_s (left column) and of g_s (middle column) and λE (right column) for a low, medium, and high level of T_a, Kin, u and δe. See section 3.3.5 for a model description. Standard meteorological conditions were T_a = 25 °C, K_{in} = 700 W m^{-2}, z_u = 3 m, u = 2 m s^{-1}, and δe = 1590 Pa (H_r = 50%). Standard crop properties were α = 0.20, h_c = 1m, LAI = 2 m^2 m^{-2}, ε = 0.98, z_0 = 0.13 h_c, and d = 0.64 h_c.

3.3.4 Surface temperature versus aerodynamic temperature

As mentioned, T_0 is not equal to T_s at canopy level. T_0 is not a directly measurable variable but is defined by equation 14 and represents the temperature of the apparent source/sink of sensible heat flux (Blonquist *et al.*, 2009). From independent measurements of H and of T_s, it is known that T_s is usually 2–3 °C higher than T_0 for uniform canopy covers and up to 10 or 15 °C higher for incomplete canopy covers (Chavez *et al.*, 2010), due to the influence of the high T_{soil} on T_s.

T_0 is not always equal to T_c either. First, $(T_c - T_0)$ tends to be larger in stable than in unstable conditions (see Supplementary Data S2.3 for a discussion on atmospheric stability) (Choudhury *et al.*, 1986; Colaizzi *et al.*, 2004). Second, T_c is influenced by the viewing angle ϕ. The place of the virtual 'big leaf' of T_0 does not coincide with the canopy viewed when taking (near-)nadir T_c measurements. Because all canopy layers in which transpiration occurs contribute to T_0, the virtual big leaf is located somewhere in the middle of the actual canopy (Blonquist *et al.*, 2009). If T_c is measured from a (near-)nadir position, it is the temperature of the outer canopy layer, which tends to be larger than T_0 because of the direct sunlight received (Chehbouni *et al.*, 2001; Jones *et al.*, 2003; Colaizzi *et al.*, 2004; Matsushima, 2005). At larger ϕ, the measured T_c incorporates the temperature of deeper canopy layers and is closer to T_0. In theory, an optimum ϕ, usually between 50 and 70 ° from nadir, exists at which T_s coincides with T_0 (Huband and Monteith, 1986; Matsushima and Kondo, 1997). Unfortunately, defining the optimum ϕ is difficult, for it is influenced by canopy structure, sensor characteristics, and measurement conditions (Hall *et al.*, 1992; Matsushima, 2005).

Several other approaches have therefore been developed for acquiring correct T_0 estimates. A first approach consists in replacing z_{0H} in equation 34 with $z_{0H,r}$, the so-called radiometric roughness length, usually expressed as a function of z_{0M}, similar to equation 35 (Colaizzi *et al.*, 2004; Mahrt and Vickers, 2004):

$$\ln(z_{0M}\, z_{0H,r}^{-1}) = k\, B_r^{-1} \tag{37}$$

in which B_r is the sublayer-Stanton number, modified to radiometric roughness length. The determination of B_r and $z_{0H,r}$ has been the subject of intense research, which showed that B_r is a complex function of weather conditions, vegetation characteristics, and viewing angle (Blyth and Dolman, 1995; Matsushima and Kondo, 1997; Kustas *et al.*, 2007). The application of $z_{0H,r}$ proved particularly difficult for partial canopies and has been largely abandoned (Kustas *et al.*, 2007) in favour of approaches in which T_0 is estimated as a function of T_s and weather and canopy variables (e.g. Su *et al.*, 2001; Mahrt and Vickers, 2004; Chavez *et al.*, 2010).

One such approach, introduced by Chehbouni *et al.* (1997), uses an adjustment parameter β_{aero}:

$$\beta_{aero} = \frac{(T_0 - T_a)}{(T_s - T_a)} \tag{38}$$

As $(T_0 - T_a) = \frac{(T_0 - T_a)}{(T_s - T_a)}(T_s - T_a) = \beta_{aero}(T_s - T_a)$, equation 14 becomes:

$$H = \rho_a\, c_p\, \beta_{aero} \frac{(T_s - T_a)}{r_{aH}} \tag{39}$$

Matsushima (2005) proposed the adjustment parameter α_{aero}, defined as $\alpha_{aero} = \frac{(T_s - T_0)}{(T_s - T_2)}$; this is essentially the same approach. These adjustment parameters were estimated from independent measurements of T_s and H and were found to be closely related to LAI and hardly influenced by the viewing angle (Chehbouni *et al.*, 1997; Matsushima, 2005). This approach is more reliable and robust than the $z_{0H,r}$ approach but has its limitations when $|T_s - T_0|$ is very large, due to more extreme weather conditions or vegetation characteristics (Kustas *et al.*, 2007; Kustas and Anderson, 2009).

Finally, two-source models estimate the aerodynamic temperature of the soil and the canopy compartment separately (Kustas and Anderson, 2009). They will be discussed in section 4.6.

3.3.5 Modelling the influence of weather conditions and vegetation characteristics on (T_c– T_a)

Model description T_c will be simulated in order to illustrate the effect of ecosystem/canopy properties and weather conditions. The model is based on equation 19 and assumes that $r_{aH} = r_{aV}$, $S = 0$, $G_i = 0$ (simulation of T_c, not T_s), and $T_c = T_0$. g_c was calculated with equation 33, r_{aH} with equation 36, and L_{in} with equation 6, with $\varepsilon_{eff} = 0.7$. A value of 0.98 was used for emissivity. For all vegetations, it was assumed that $d = 0.64\, h_c$ and $z_{0M} = 0.13\, h_c$ (Stanhill, 1969). λE (Fig. 5f) was calculated from the estimated T_c and from equation 10. Like for the $(T_l - T_a)$ measurements, the 95% confidence intervals have a width of 0.206 °C and are indicated.

Results

The simulations show that the influence of weather conditions on $(T_c - T_a)$ (Fig. 5) is similar to the influence on $(T_l - T_a)$ (Fig. 3). $(T_c - T_a)$ decreases non-linearly with increasing T_a and u and linearly with increasing δe; this decrease is largest when stomata are wide open in the case of T_a and δe, but opposite in the case of increasing u; $(T_c - T_a)$ increases linearly with increasing K_{in}, with the largest increase observed in drought-stressed vegetations. $(T_c - T_a)$ also decreases non-linearly with increasing g_s; all weather conditions have an impact on the relation between g_s and $(T_c - T_a)$ (Fig. 5, middle column). $(T_c - T_a)$ decreases linearly with increasing λE. The validity of this linear relationship has been confirmed in several studies (Vidal and Perrier, 1989; Loheide and Gorelick, 2005; Jones and Vaughan, 2010) and forms the basis of several thermal remote sensing applications (e.g. water deficit index, WDI, section 4.3.5). T_a and δe hardly influence this linear relation, whereas K_{in} influences the intercept and u the slope and intercept (Fig. 5, right column).

$(T_c - T_a)$ decreases with increasing canopy height, leaf area index, and albedo, but the relations are very different (Fig. 6,

left column). Canopy height has a particularly large influence on $(T_c - T_a)$, with $(T_c - T_a)$ becoming very high in drought-stressed very low vegetations. However, in taller vegetations, differences in g_s are much more difficult to detect with $(T_c - T_a)$ (Fig. 6a). The influence of LAI on $(T_c - T_a)$ is largest for fully transpiring vegetations; the crop albedo has little effect on the potential to detect differences in $(T_c - T_a)$ between vegetations of different g_s. The three vegetation characteristics also influence the relation between g_s and $(T_c - T_a)$, although the impact of albedo is limited. Differences in LAI do not influence the relation between λE and $(T_c - T_a)$; differences in albedo influence the intercept of this relation, whereas differences in h_c have a severe impact on both slope and intercept (Fig. 6, right column).

3.3.6 *Thermal remote sensing in croplands versus orchards*

The large difference in vegetation characteristics between croplands and orchards has a large influence on the

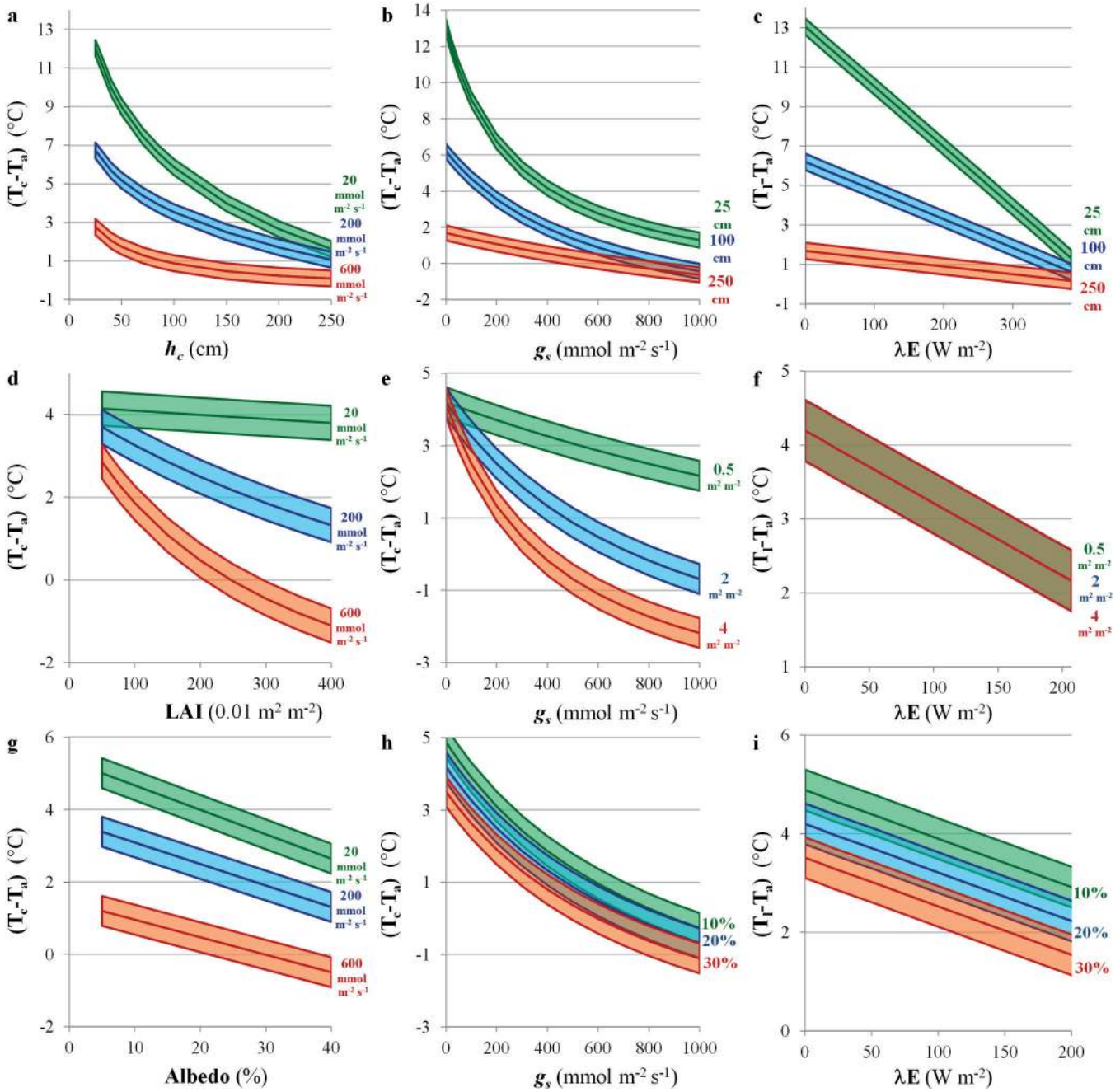

Fig. 6. Influence on the mean and 95% confidence interval of $(T_l - T_a)$ of vegetation characteristics canopy height (h_c), leaf area index (LAI), and albedo for a low, medium, and high level of g_s (left column), and the influence on $(T_l - T_a)$ of g_s (middle column), and λE (right column) for a low, medium, and high level of h_c, LAI, and albedo. See section 3.3.5 for a model description. See Fig. 5 for standard meteorological conditions and crop properties.

applicability of thermal remote sensing. In croplands, during most of the growing season, the vegetation is homogeneous and the canopy very dense, ideal characteristics for thermal remote sensing. The characteristics of orchards, on the other hand, are more challenging for thermal remote sensing: the structure is heterogeneous, often with tall vegetation (trees) planted in rows with zones of bare soil or very low vegetation in between.

This heterogeneous canopy structure in orchards makes it difficult to estimate G_i, which is a function of the net radiation of the soil compartment ($R_{n,soil}$) (Norman *et al.*, 1995), in its turn a complex function of solar zenith angle and vegetation structure (e.g. Gijzen and Goudriaan, 1989; Kustas and Norman, 1999a).
The uneven leaf distribution makes up scaling from g_s to g_c more difficult (equation 33 is no longer valid).
In this heterogeneous canopy structure, d and z_{0M} can often not be expressed as a simple function of h_c (section 3.3.3).

Furthermore, it is challenging to acquire reliable thermal measurements in orchards:

Due to the sparse canopy, T_s obtained from (near-)nadir viewing is much higher than T_c and T_0, because of the large influence of the higher T_{soil} (section 3.3.4). Hence, sensors must be installed at appropriate viewing angles.
Tall trees can make thermal measurements with IRTs particularly challenging, because of the large noise when open sky is within in the sensor field of view. Thus, handheld measurements must be performed with great care; fixed IRT measurements are preferably installed on high poles.
Moreover, the tree canopy usually has a vertical rather than a horizontal structure. As a consequence, there is a very large difference in $T_c$between the shaded and the sunlit sides, making it much more difficult to obtain a reliable T_c estimate.

Finally, due to the larger h_c (taller canopies), z_{0H}, d, and z_{0M} are relatively high. As a consequence, differences in g_c (and λE) are less reflected in T_c than for lower cropland canopies (Fig. 5a). This, in combination with the higher variability in T_c, makes drought stress detection in orchard trees more difficult than for croplands.

It is therefore not surprising that ground-based thermal remote sensing methods were predominantly developed for application in homogeneous cropland. However, in recent years, the number of ground-based thermal remote sensing studies in orchards has increased significantly and includes applications in grapevine, olive, peach, apple, nectarine, citrus, almond, and pistachio tree orchards. There are two reasons for this increased interest. First, the application of thermal cameras allows more precise assessment of T_c and the removal of noise from the soil and background. Second, two-source models (section 4.6) were developed specifically for sparse canopies such as orchards. However, this does not mean that the classic one-source methods are of no use for orchards: in fact, most of these methods have recently been successfully applied in orchard vegetations as well, although the applications in cropland-like vegetations still outnumber those in orchards.

4 Application of ground-based thermal remote sensing in agriculture

In this section, an overview is given of the most important applications of ground-based thermal remote sensing in agriculture, with a focus on applications related to the assessment of plant-water status, drought stress, or irrigation scheduling.

4.1 Direct use of brightness or surface temperature

4.1.1 Brightness and surface temperature

As discussed in section 3, under the assumption that $T_c = T_0$, T_c is linearly related with λE and can be used as a proxy measure of λE or g_c. Canopy temperature has therefore been widely used in plant breeding studies of (winter) wheat (e.g. Araus *et al.*, 2003; Nautiyal *et al.*, 2008; Reynolds *et al.*, 2009; Gutierrez *et al.*, 2010) and other dense crops (Sanchez *et al.*, 2001; Hamidou *et al.*, 2007; Khan *et al.*, 2007). In most of these studies, T_{br} rather than T_s or T_c is used as the indicator. In general, varieties with a lower brightness temperature are preferred, as it is assumed that these are more successful in avoiding drought stress (Araus *et al.*, 2003).

Similarly, T_c, T_l, or T_{br} have been used as a drought stress index for the evaluation of different irrigation treatments of one (e.g. Singandhupe *et al.*, 2003; Pettigrew, 2004; Yuan *et al.*, 2004; Qiu *et al.*, 2008) or several (e.g. Rashid *et al.*, 1999; Siddique *et al.*, 2000; Ko and Piccinni, 2009) crop varieties and for monitoring the effect of heat stress (Ayeneh *et al.*, 2002; Sadras and Soar, 2009) and CO_2 increases (Yoshimoto *et al.*, 2005) on plant health.

Because of the large influence of meteorological conditions on T_s (Figs. 4 and 6), repeated measurements will give very different T_s, unless meteorological conditions are extremely constant and vegetation structure does not change.

4.1.2 Temperature variability

At very low g_s (i.e. in stressed conditions), the total range in T_l between leaves of different inclinations is larger than in unstressed conditions (Fig. 3.f). Several authors proposed canopy temperature variability as an index of drought stress (Aston and Vanbavel, 1972; Clawson and Blad, 1982; Fuchs, 1990), by either looking at the difference between the minimal and maximal T_c (*Critical Temperature Variability*, CTV (Clawson and Blad, 1982) or at the *standard deviation of* T_c (σ_{Tc}) within the canopy. Gonzalez-Dugo *et al.* found that σ_{Tc} first increased with mild stress and then decreased again under more severely stressed vegetation, in airborne images of cotton (Gonzalez-Dugo *et al.*, 2006) and of almond trees (Gonzalez-Dugo *et al.*, 2012). However, in studies at plant and leaf scale, σ_{Tc} was not correlated with g_s or drought stress level (Grant *et al.*, 2007; Maes *et al.*, 2011).

Infrared thermography can also be used for disease detection. Because local infections within a leaf show up as either warm or cold spots, CTV and (to a lesser extent) σ_{Tl} within the leaf are useful in disease detection (e.g. Vanderstraeten *et al.*, 1995; Chaerle *et al.*, 1999; Lindenthal *et al.*, 2005; Oerke *et al.*, 2006, 2011; Stoll and Jones, 2007).

4.1.3 Stress time (ST)

The *stress time* (ST) concept is the only concept that does not depart from the relation between g_s and λE and T_c. Instead, it is based on the relation between plant temperature and metabolic activity (Upchurch and Mahan, 1988) and is inspired by the positive correlation between plant performance and the period in which plant temperatures remain within a narrow optimal crop temperature window (Burke *et al.*, 1988). Irrigation is started as soon as T_c exceeds a certain crop-specific threshold for a certain length of time.

The simplicity of the algorithm makes it very well suited for automated irrigation (O'Shaughnessy and Evett, 2010) of crops as cotton (Wanjura *et al.*, 1990, 1992, 2002, 2006; Wanjura and Upchurch, 2000), corn (Evett *et al.*, 2000), groundnut (Mahan *et al.*, 2005), and soybean (Peters and Evett, 2007, 2008). ST can also be used to detect and to respond to spatial patterns of drought stress when measured with a large number of IRT sensors mounted on a centre pivot (Peters and Evett, 2007, 2008). Furthermore, ST outperformed the more commonly applied crop water stress index (CWSI, section 4.3) in estimating drought stress and yield (Wanjura *et al.*, 2006; Bajwa and Vories, 2007). However, ST has only been successfully applied in the semi-arid climates of Texas and, recently, Australia (Conaty, 2010). Other limitations are the requirement of continuous measurements, the crop specificity of the temperature thresholds and the sensitivity to T_{soil} measurements (see equation 9), limiting the application to full cover conditions only. ST is also known as the *Temperature–Time Threshold* (TTT) method (Wanjura *et al.*, 1995) or the *BIOTIC* protocol (biologically identified optimal temperature interactive console) (Mahan *et al.*, 2005; Wanjura *et al.*, 2006).

4.2 Difference between canopy and air or reference crop temperature

($T_c - T_a$), sometimes referred to as *canopy temperature depression* (CTD), is the most straightforward normalization of T_c and is used widely as an indicator of plant health, heat stress tolerance or drought stress in crops (e.g. Ehrler, 1973; Sadler *et al.*, 2000; 2002; Patel *et al.*, 2001; Baker *et al.*, 2007), often for studying crops experiencing different irrigation regimes (e.g. Olufayo *et al.*, 1996; Singandhupe *et al.*, 2003; Pettigrew, 2004; Qiu *et al.*, 2008; Garcia-Tejero *et al.*, 2011). ($T_c - T_a$) has also been used intensively for wheat cultivar selection (Amani *et al.*, 1996; Olufayo *et al.*, 1996; Rashid *et al.*, 1999; Balota *et al.*, 2007, 2008; Kumari *et al.*, 2007). ($T_c - T_a$) is widely applied for woody crops as apple (Andrews *et al.*, 1992), olive (Sepulcre-Canto *et al.*, 2006), cherry (Stoimenov *et al.*, 2007), grapevine (Serrano *et al.*, 2010), peach (Massai *et al.*, 2000; Wang and Gartung, 2010), and citrus (Garcia-Tejero *et al.*, 2011; Zarco-Tejada *et al.*, 2012), often showing to be closely related with irrigation treatment, leaf water potential, or g_s.

Irrigation scheduling based on ($T_c - T_a$) has mostly occurred in the form of the *stress degree day* (SDD; °C or K) method, originally proposed by Idso *et al.* (1977) and Jackson *et al.* (1977):

$$SDD = \sum_{i=1}^{n} (T_c - T_a)_i \quad (40)$$

with T_c and T_a measured 1–1.5 hours after solar noon at day i during a n-day period. Irrigation is started as soon as SDD exceeds 0. Although also applied successfully for other crops (Walker and Hatfield, 1979; Idso *et al.*, 1980), SDD worked particularly well for wheat. SDD was the first attempt to schedule irrigation based on T_c and was the most widely used thermal index until $CWSI_e$ (section 4.3.3) was developed (Gardner *et al.*, 1992a). Nowadays, SDD is still occasionally used as a drought stress index or estimator of yield and water use (Olufayo *et al.*, 1996; Collino *et al.*, 2000; Patel *et al.*, 2001; Onyibe *et al.*, 2003; Ajayi and Olufayo, 2004; Zhang *et al.*, 2005; Chakravarti *et al.*, 2010).

In general, because of the large influence of weather conditions on ($T_c - T_a$) (Fig. 5), ($T_c - T_a$) and SDD can only be used in (semi-)arid climates where weather conditions vary little between consecutive days (Keener and Kircher, 1983; Al-Faraj *et al.*, 2001; Moran, 2004). Some authors suggested replacing T_a with T_c of an unstressed crop (T_{pot}) and to use ($T_c - T_{pot}$) as an estimator of drought stress (Fuchs and Tanner, 1966; Clawson and Blad, 1982; Berliner *et al.*, 1984; Sepulcre-Canto *et al.*, 2006). Similarly, Gardner *et al.* (1981a,b) proposed the *temperature stress day* (TSD), a variant of SDD in which T_{pot} replaces T_a. Both indices have been hardly applied because ($T_c - T_{pot}$) also depends on weather conditions and because unstressed reference crops are often not available (Moran, 2004). In addition, TSD was less related with sorghum evapotranspiration and crop yield than SDD and CWSI (Olufayo *et al.*, 1996; Ajayi and Olufayo, 2004).

4.3 Crop water stress index

4.3.1 Background and theory

The *crop water stress index* (CWSI) is a drought stress index that uses the T_s of a potential and dry crop. The *potential crop* is identical to the actual crop but is transpiring at maximal rate (λE_{pot}) with an associated canopy resistance $r_{c,pot}$ and temperature T_{pot}. The *dry crop*, with associated λE_{dry}, $r_{c,dry}$, and T_{dry}, is a crop with identical properties as the actual crop that is not transpiring at all. CWSI is calculated as (see Supplementary Data S3):

$$CWSI = 1 - \frac{\lambda E}{\lambda E_{pot}} = \frac{\gamma \left(\frac{r_c - r_{c,pot}}{r_{aH}} \right)}{s + \gamma \left(1 + \frac{r_c}{r_{aH}} \right)} = \frac{\Delta T_{pot} - \Delta T}{\Delta T_{pot} - \Delta T_{dry}} \quad (41)$$

where $\triangle T_{pot}$, $\triangle T_{dry}$, and $\triangle T_a$ are defined as ($T_{pot} - T_a$), ($T_{dry} - T_a$), and ($T_c - T_a$), respectively. The introduction of CWSI by Jackson *et al.* (1981) and Idso *et al.* (1981a) was an important breakthrough in ground-based thermal remote sensing. Its innovative aspect was the normalization by T_a and, more importantly, by $\triangle T_{pot}$ and $\triangle T_{dry}$, underpinned by a solid theoretical base. This approach of using an upper and lower boundary $\triangle T$ or T_s, was later used in the large majority of ground-based and airborne and satellite thermal remote sensing methods.

Different approaches to calculate CWSI were developed: the analytical ($CWSI_a$), empirical ($CWSI_e$), direct approach ($CWSI_d$),

and the WDI will be discussed in the following sections. As they are all based on equation 41, it is important to know the underlying assumptions of this equation:

It is a one-source model.
$r_{aH} = r_{aV} = r_{aM}$, with raM the roughness lengths for momentum exchange. This corresponds with assuming that the Reynolds analogy holds (see Supplementary Data S2.3 for a discussion).
$r_{aH,dry} = r_{aH,pot} = r_{aH}$.
Differences in R_n between T_{dry}, T_{pot}, and T_c, caused by the differences in outgoing longwave radiation (equation 12) can be ignored.
$S = 0$.
$G_i = 0$. Jackson *et al.* (1988) proposed to replace R_n with 0.9 R_n (i.e. assuming $\Gamma_i = 0.1$; section 3.3.1) to compensate for this in the analytical approach.
$T_s = T_c$. In partially vegetated fields, this assumption is problematic (Moran *et al.*, 1994) and the use of the water deficit index (WDI; section 4.3.5) is recommended.
$T_0 = T_c$ (Boulet *et al.*, 2007, see section 3.3.4 for a discussion). In fact, most studies assume that $T_{br} = T_c$.

4.3.2 Analytical approach ($CWSI_a$)

In the analytical approach, T_c measurements are combined with meteorological data to compute CWSI. Originally, Jackson *et al.* (1981) proposed to calculate $CWSI_a$ from $\mathrm{CWSI} = \dfrac{\gamma\left(\dfrac{r_c - r_{c,pot}}{r_{aH}}\right)}{s+\gamma\left(1+\dfrac{r_c}{r_{aH}}\right)}$. This requires an estimate of r_{aH}, $r_{c,pot}$, and r_c/r_{aH}, estimated as (see Supplementary Data S3, equation S40):

$$\frac{r_c}{r_{aH}} = \frac{\dfrac{\gamma\, r_{aH}}{\rho_a c_p} R_n - \Delta T\,(s+\gamma) - \delta e}{\gamma\left(\Delta T - \dfrac{r_{aH}}{\rho_a c_p} R_n\right)} \quad (42)$$

where s is calculated from the average of the air and surface temperature. Hence, ΔT is used to calculate r_c/r_{aH}. Although this method is still occasionally applied (e.g. da Silva and Rao, 2005; Berni *et al.*, 2009a), most studies using $CWSI_a$ calculate ΔT_{pot} and ΔT_{dry} directly (e.g. Feldhake *et al.*, 1997; Yuan *et al.*, 2004; Gonzalez-Dugo *et al.*, 2006; Gontia and Tiwari, 2008; Ben Gal *et al.*, 2009; Alchanatis *et al.*, 2010; Li *et al.*, 2010) as (see Supplementary Data S3, equations S41 and S43):

$$\Delta T_{pot} = \frac{r_{aH}}{\rho_a c_p} = \frac{\gamma\left(1+\dfrac{r_{c,pot}}{r_{aH}}\right)}{s+\gamma\left(1+\dfrac{r_{c,pot}}{r_{aH}}\right)} R_n - \frac{1}{s+\gamma\left(1+\dfrac{r_{c,pot}}{r_{2H}}\right)} \delta e \quad (43)$$

$$\Delta T_{dry} = \frac{r_{aH}}{\rho_a c_p} R_n \quad (44)$$

Both methods are essentially the same and require, apart from standard meteorological data (T_a, δe, R_n), estimates of u, z_{0M}, d, h_c and possibly z_{0H} to estimate r_{aH} (equations 34 or 36). Furthermore, $r_{c,pot}$ must be estimated (equation 43) from literature or derived from the observed ΔT_{min} (the minimal observed ΔT) during the growth period, as suggested by Jackson *et al.* (1981) and later elaborated by O'Toole and Real (1986).

$CWSI_a$ was developed for and has mostly been applied in dense crops, although it was also successfully applied for orchard trees as apple (Andrews *et al.*, 1992), olive (Ben Gal *et al.*, 2009; Berni *et al.*, 2009a), and peach (Wang and Gartung, 2010).

Still, the large input requirements have hampered a routine use of the analytical approach (Gardner *et al.*, 1992a; Payero *et al.*, 2005). The most important sources of error are incorrect measurements of u, R_n, T_a, and T_c (Jackson *et al.*, 1981). ΔT_{dry} (equation 44) only requires R_n and r_{aH} for its estimation and is often assumed constant (see further; see also Fig. 5j). The estimation of ΔT_{pot} bears more uncertainty (equation 43). Alves and Pereira (2000) suggested replacing T_{pot} by the wet bulb temperature, which can be measured directly without the requirement of wind speed or of crop data. This method is appealing but has the disadvantage that it sets $r_{c,pot} = 0$ (Yuan *et al.*, 2004), making CWSI no longer equal to $1 - \dfrac{\lambda E}{\lambda E_{pot}}$.

4.3.3 Empirical or baseline approach ($CWSI_e$)

Definition and baseline calculation of empirical approach

In the empirical or baseline approach, the data input is limited to T_a, δe, and T_c. The approach was introduced by Idso *et al.* (1981a) and was inspired by the observation that ΔT decreases linearly with δe (Ehrler, 1973, see also Figs. 3d and 5d). This allows expressing ΔT_{pot} as:

$$\Delta T_{pot} = a_{pot} + b_{pot}\, \delta e \quad (45)$$

Equation 45 is the mathematical expression of the lower or *non-water stressed baseline* (*NWSB*). The basic assumption of the method is that a_{pot} and b_{pot} are constant and crop specific, at least for a given location and for a certain growth stage.

These parameters can be derived in two ways. In the diurnal method, ΔT of a fully watered crop is collected from different measurements during one or several days and plotted against δe. As R_n is not constant during the sampling, this usually does not yield reliable estimates of a_{pot} and b_{pot}. In the seasonal method, one ΔT measurement of a fully watered crop is taken every day around solar noon during the entire growing season. Although more demanding, this gives more robust estimates (Gardner *et al.*, 1992a). In Table S1 of Supplementary Data S4, an overview is presented of available non-water-stressed baselines, with data of 39 different crops.

ΔT_{dry} is usually calculated as the average ΔT of a fully stressed canopy (e.g. Lacape *et al.*, 1998; Alderfasi and Nielsen, 2001; Emekli *et al.*, 2007; Kar and Kumar, 2010; Li *et al.*, 2010). Alternatively, ΔT_{dry} can be estimated as (Idso *et al.*, 1981a):

$$\Delta T_{dry} = a_{pot} + b_{pot}\,[e^*(T_a) - e^*(T_a + a_{pot})] \quad (46)$$

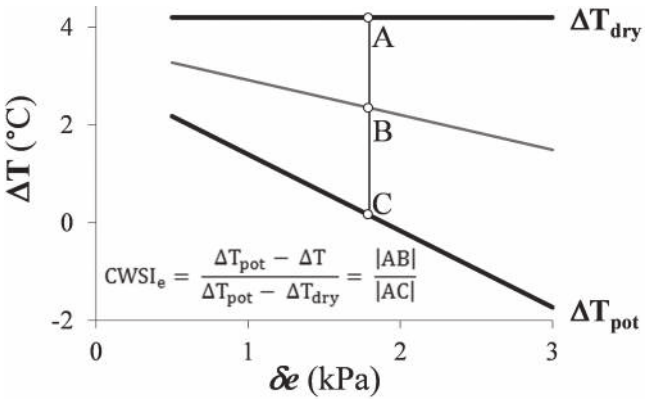

Fig. 7. Illustration of the baseline approach of the crop water stress index.

with $e^*(T_a)$ and $e^*(T_a + a_{pot})$ the saturated vapour pressure at temperature T_a and $(T_a + a_{pot})$, respectively.

The concept is illustrated in Fig. 7. $CWSI_e$ is calculated as BC/AC. Note that if δe changes while r_c remains constant, the ratio of BC/AC, hence $CWSI_e$, will not change. This is illustrated by the thin grey line, which represents $\triangle T$ for g_s= 50 mmol m^{-2} s^{-1}.

Application

$CWSI_e$ was closely correlated with leaf water potential (e.g. Idso *et al.*, 1981bc; Wang *et al.*, 2005; Testi *et al.*, 2008), soil moisture level (Colaizzi *et al.*, 2003a; Chen *et al.*, 2010), and evapotranspiration (Nielsen and Anderson, 1989; Yazar *et al.*, 1999; Lebourgeois *et al.*, 2010) of a variety of crops. The average seasonal $CWSI_e$ was closely related with water use efficiency (Garrot *et al.*, 1993; Yazar *et al.*, 1999; Wang *et al.*, 2005; da Silva *et al.*, 2007; Kirnak and Dogan, 2009) and can be used as precise indicators of crop yield (e. g. Garrot *et al.*, 1994; Orta *et al.*, 2003; Simsek *et al.*, 2005; Emekli *et al.*, 2007; Erdem *et al.*, 2010). Although also developed for dense crops, $CWSI_e$ has also been applied for orchard trees as pistachio trees, citrus, nectarine, and cherry trees (Table 2).

Soon after its introduction, $CWSI_e$ became the most commonly used thermal drought stress index (Jackson *et al.*, 1988; Gardner *et al.*, 1992a), which it has remained ever since. It is one of the common irrigation scheduling methods in regions with stable sunny summer conditions (Gardner *et al.*, 1992a,b, see also Table S1) and proved as reliable in terms of yield and water savings as more expensive soil water-based irrigation techniques (Stegman, 1986; Steele *et al.*, 1994, 2000; Shae *et al.*, 1999).

The main reasons for its success are the limited data requirements and straightforward calculation, which makes $CWSI_e$ easy to apply for non-scientists. In addition, its introduction went hand in hand with a drop in price of portable IRTs, making $CWSI_e$ relatively cheap to measure.

Disadvantages and limitations of the empirical approach

However, $CWSI_e$ has its limitations:

In general, it is less reliable than $CWSI_a$ (e.g. Stockle and Dugas, 1992; Jalalifarahani *et al.*, 1993; Yuan *et al.*, 2004).

$CWSI_e$ is unreliable when the canopy is not fully closed (Moran *et al.*, 1994). This can only be partially overcome by adjusting the viewing angle. However, this does not guarantee reliable results (Koksal, 2008), in particular when the baselines were established for other viewing angles.

The most important limitation, however, is related to the fact that a_{pot} and b_{pot} are not entirely crop specific or weather independent. Theoretically, they are estimated as (equation 43):

$$a_{pot} = \frac{r_{aH}}{\rho_a c_p} \frac{\gamma\left(1+\frac{r_{c,pot}}{r_{aH}}\right)}{s+\gamma\left(1+\frac{r_{c,pot}}{r_{aH}}\right)} R_n \quad (47)$$

$$b_{pot} = \frac{-1}{s+\gamma\left(1+\frac{r_{c,pot}}{r_{aH}}\right)} \quad (48)$$

a_{pot} and b_{pot} change with different T_a and particularly u (e.g. Jensen *et al.*, 1990; Payero and Irmak, 2006; Testi *et al.*, 2008) and K_{in} (e.g. Gardner *et al.*, 1992b; Olufayo *et al.*, 1996; Al-Faraj *et al.*, 2001; Ajayi and Olufayo, 2004). Hence, $CWSI_e$ requires stable weather conditions (preferably hot and dry, with open skies) (Gardner *et al.*, 1992b). Measurements should also be taken only around solar noon (Idso *et al.*, 1981a; Jackson *et al.*, 1981; Testi *et al.*, 2008).

These requirements form an important drawback in humid or temperate regions (Payero *et al.*, 2005; Payero and Irmak, 2006), where $CWSI_e$ is only reliable when the weather is as described above (Keener and Kircher, 1983; Anda, 2009; Lebourgeois *et al.*, 2010).Therefore, rather than as a stand-alone technique for irrigation monitoring, $CWSI_e$ is often complemented with soil moisture measurements or used to assist decision making for irrigation scheduling (e.g. Steele *et al.*, 1997; Yazar *et al.*, 1999; Al-Faraj *et al.*, 2001; Chen *et al.*, 2010).

Another major drawback is the fact that a_{pot} and b_{pot} are not crop specific, but are influenced by crop characteristics as crop height and leaf area (Alves and Pereira, 2000; Payero and Irmak, 2006), so that the NWSB changes within the season and between seasons (e.g. Kirkham *et al.*, 1983; Yuan *et al.*, 2004; Simsek *et al.*, 2005; Payero and Irmak, 2006; Erdem *et al.*, 2010).

Adaptations and improvements of the empirical approach

Two methods were proposed to correct $CWSI_e$ for non-constant meteorological conditions. In a first method, different classes of R_n and/or u are considered and a separate NWSB is built for each class (e.g. Jensen *et al.*, 1990; Olufayo *et al.*, 1996). In the second method, u, R_n or T_a are included in the regression model of the NWSB. Although more robust (e.g. Keener and Kircher, 1983; Jalalifarahani *et al.*, 1993; Payero and Irmak, 2006), these methods require more input data and can be interpreted as intermediate between the empirical and analytical methods. A common adaptation to correct for crop growth is the definition of different NWSBs per growth stage, such as the pre-heading and post-heading phase in

wheat crops (e.g. Idso, 1982; Howell *et al.*, 1986; Gontia and Tiwari, 2008).

4.3.4 Direct approach ($CWSI_d$)

In the direct approach, T_{pot} and/or T_{dry} are measured directly along with T_c. The original method, in which T_{pot} was measured as T_c of a fully transpiring crop, was applied in a limited number of studies (e.g. Katerji *et al.*, 1988; Olufayo *et al.*, 1996; Wanjura and Upchurch, 2000; Bajwa and Vories, 2007). A more practical method uses the temperature of dry or wet artificial reference surfaces.

At single plant level, dry reference surfaces, with corresponding temperature (T_{dry}) are created by covering leaves with a layer of petroleum jelly, blocking all transpiration flows. Wet leaves, with temperature Twet, are leaves sprayed with a thin layer of water on one or both leaf sides.

$CWSI_d$ is then calculated as:

$$CWSI_d = \frac{T_{wet} - T_l}{T_{wet} - T_{dry}} \quad (49)$$

When thermal cameras are used, the reference leaves can be physically embedded in the scene and T_l, T_{wet}, and T_{dry} are measured within the same image. As such, no additional meteorological measurements are required. This makes the method very appealing, all the more because it allows for fully automated image analysis and $CWSI_d$ assessment (Wang *et al.*, 2010a). In addition, measurement errors of ε_l or L_{in} are reduced because they will cause similar errors for T_{wet}, T_{dry}, and T_l. This makes $CWSI_d$ a very appealing method. Its reliability and sensitivity for weather conditions and leaf characteristics are modelled in the next section.

Obtaining the sensitivity of $CWSI_d$ at leaf level to weather conditions and leaf characteristics

Model description T_l, T_{dry}, and T_{wet} were calculated with the model described in section 3.2 for the same range of weather conditions and leaf characteristics as in Figs. 3 and 4.

T_{dry} is calculated as (equation 19 and assuming $r_s = \infty$):

$$T_{dry} = T_a + \frac{r_{aH} R_n}{\rho_a c_p} \quad (50)$$

T_{wet} of leaves sprayed on one side ($r_V = r_{aV}$, see equation 24) is:

$$T_{wet} = T_a + \frac{r_{aH}\gamma\, r_{aV}\, R_n - r_{aH}\, \rho_a\, c_p \delta e}{\rho_a\, c_p (\gamma\, r_{aV} + s r_{aH})} \quad (51)$$

Two sets of confidence bands for $CWSI_d$ were calculated. For the first set, it was assumed that the estimation error from each of the three temperature measurements (T_l, T_{dry} and T_{wet}) is the only source of error. The average and standard deviation of $CWSI_d$ ($\overline{CWSI_d}$; $\sigma(CWSI_d)$) were calculated from 5000 random samples of T_l, T_{dry}, and T_{wet}, generated assuming a normal distribution with as average the T_l, T_{dry}, and T_{wet} value from the leaf model and 0.18 °C as standard deviation. Confidence bands were calculated as $\overline{CWSI_d} \pm 2\,\sigma(CWSI_d)$.

In the second set, a small difference in leaf characteristics or weather conditions between the measured and reference leaves was additionally taken into account. Because, in practice, dry and reference leaves are normally selected right next to each other and of two very similar leaves, it was assumed that the two reference leaves experienced identical weather conditions and leaf characteristics. T_{dry} and T_{wet} were estimated when (for instance) u is 10% higher ($T_{dry,high}$ and $T_{wet,high}$) or 10% lower ($T_{dry,low}$ and $T_{wet,low}$) than the wind speed experienced by the measured leaves. $CWSI_d$ was calculated for 5000 randomly generated values of T_l, $T_{dry,high}$, and $T_{wet,high}$ ($CWSI_{d,high}$) or T_l, $T_{dry,low}$, and $T_{wet,low}$ ($CWSI_{d,low}$) and the average and standard deviation of $CWSI_{d,high}$ and $CWSI_{d,low}$ calculated; the confidence bands were calculated as [minimum($\overline{CWSI_{d,low}} - 2\,\sigma(CWSI_{d;low})$, $\overline{CWSI_{d,high}} - 2\,\sigma(CWSI_{d,high})$); maximum ($\overline{CWSI_{d,low}} + 2\,\sigma(CWSI_{d,low})$, $\overline{CWSI_{d,high}} + 2\,\sigma(CWSI_{d,high})$)].

The relation between each variable and $CWSI_d$ is calculated for three levels of g_s (20, 200, and 600 mmol m^{-2} s^{-1}) (Figs. 8 and 9, left column); additionally, the relation between *gs* and CWSId is given for three levels of each variable (Figs. 8 and 9, right column). To further investigate the discriminative power, the $CWSI_d$ values of the confidence bands were reconverted to g_s values using a splining algorithm. For each of the three g_s levels, this gives the lower and higher level of g_s that can be statistically distinguished from this level; the narrower the bands, the higher the discriminative power (Figs. 8 and 9, middle column).

Modelling results

Leaves with lower g_s have higher $CWSI_d$; however, $CWSI_d$ is not linearly related with g_s (Fig. 8). The expected value of $CWSI_d$ is not influenced by K_{in}, δe, θ, or α. Higher T_a and A_l and lower u lead to lower $CWSI_d$ values.

If only measurement errors are considered, the discriminative power (dark confidence band width of graphs in middle column of Fig. 8) increases with increasing T_a, K_{in}, and δe and decreasing u (except for high g_s at very low u, Fig. 8d). The discriminative power is very low when δe is low. Differing conditions between the reference and measured leaves (a 10% difference was assumed, except for T_a, where the difference was fixed at 0.2 °C) further decrease the discriminative power; the discriminative power is even rather constant over K_{in}. The lower discriminative power at g_s = 600 mmol m^{-2} s^{-1} is caused by the non-linear relationship between g_s and T_l; at higher g_s, a further increment in g_s has a lower impact on T_l (or $\Delta T_l/\Delta g_s$ decreases with increasing g_s, Figs. 3 and 4).

As long as the reference and the measured leaves have identical leaf characteristics, the discriminative power of $CWSI_d$ is relatively independent of the leaf characteristics (Fig. 9, middle column). For measured leaves with high θ and (to a much lesser extent) α, deviations in α and θ between the measured and reference leaves reduce the discriminative power significantly (Fig. 9b, 9k).

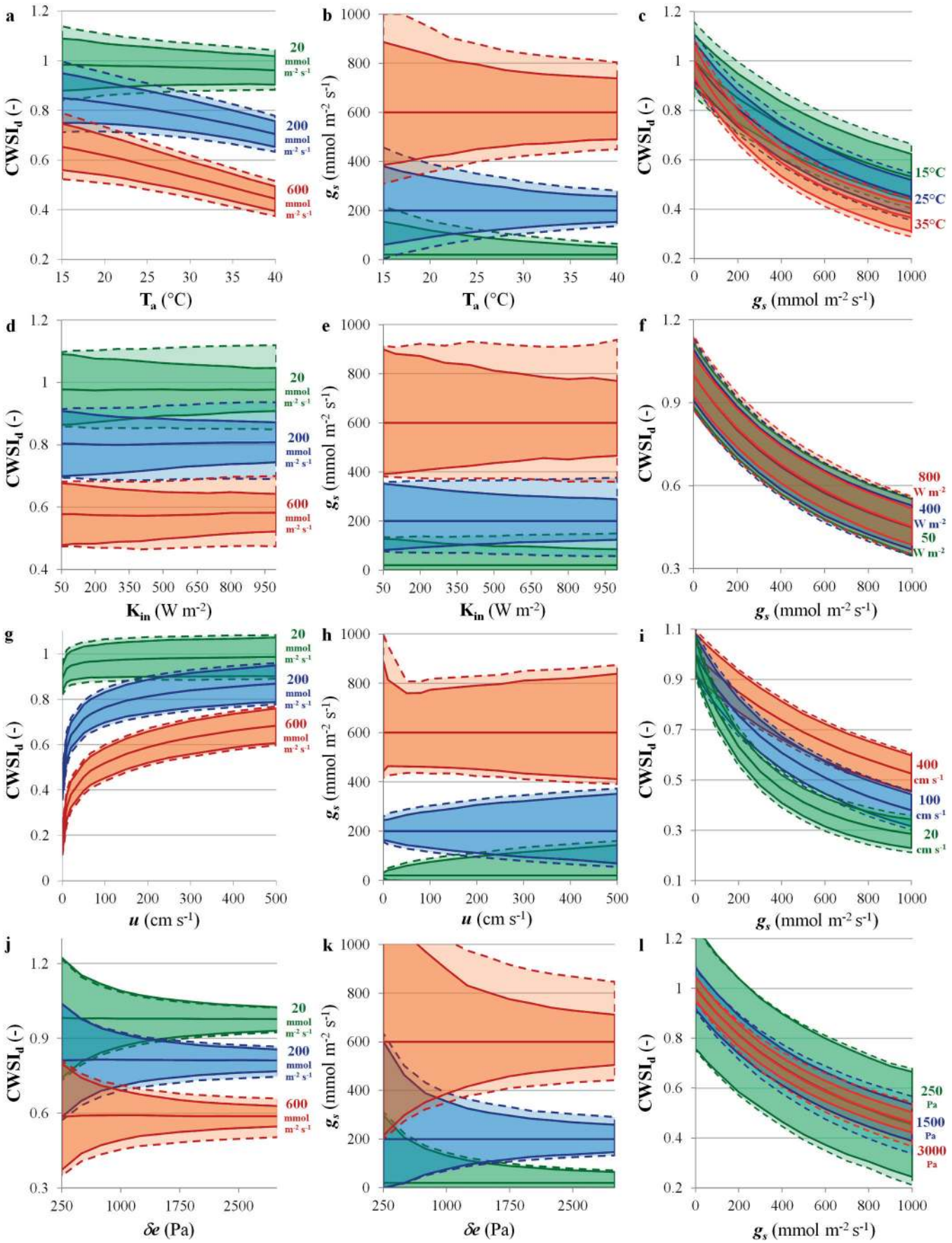

Fig. 8. Influence of weather conditions on $CWSI_d$ at leaf level. In the left column, the influence of the weather conditions air temperature (T_a), incoming shortwave radiation (K_{in}), wind speed (u), and vapour pressure deficit (δe) on the mean and 95% confidence intervals

Application and evaluation of $CWSI_d$

Overall, the simulations showed that $CWSI_d$ can be estimated with relatively low error, even in non-ideal measurement conditions. This has been confirmed experimentally: $CWSI_d$ was measured in several studies and showed good correlations with g_s (Jones, 1999b; Leinonen and Jones, 2004; Grant *et al.*, 2006, 2012; Maes *et al.*, 2011), leaf (Grant *et al.*, 2007) and stem water potential (Wang *et al.*, 2010a).

Unfortunately, the method has a number of drawbacks as well. First of all, $CWSI_d$ is analogous to but not the same as $CWSI_e$ or $CWSI_a$. Even at very high g_s, $CWSI_d$ does not tend to zero (Figs. 8 and 9), because T_{wet}, used to calculate $CWSI_d$, is much lower than T_{pot}. Furthermore, the lower boundary level of $CWSI_d$ (e.g. at g_s = 1000 mmol m^{-2} s^{-1}) depends on T_a, u, A_l, and leaf shape (Figs. 8 and 9), which complicates the interpretation of $CWSI_d$. This is not the case when the same data are used to calculate I_g, as will be discussed in section 4.4.

Another clear disadvantage of the method is related to the scale level, as working with single leaves is not feasible at field scale. To apply $CWSI_d$ to the field, the wet reference leaves are replaced by wet artificial reference surfaces or WARS (Meron *et al.*, 2003). This WARS consists of a plastic tray, filled with water and covered by a polystyrene foam, covered by a water-absorbent cloth (Möller *et al.*, 2007). With the application of WARS, $CWSI_d$ was highly correlated with the leaf water potential of cotton and soybean (e.g. Cohen *et al.*, 2005; Meron *et al.*, 2010; O'Shaughnessy *et al.*, 2011), even higher than $CWSI_a$ (Alchanatis *et al.*, 2010). $CWSI_d$ performs equally well for orchard trees as olive (Ben Gal *et al.*, 2009) and grapevine (Möller *et al.*, 2007). Given the ease of measurement, this currently seems the most promising CWSI technique for field application and is particularly suited for assessing the spatial variability of the crop water status.

However, some issues must be solved before the method can shift from purely scientific studies to application for irrigation steering. It is not clear how the WARS relates to T_{pot} or T_{wet}, how its temperature is influenced by weather conditions, or whether it should be placed at a particular height above the ground. Moreover, the fact that the WARS needs to be visible in every analysed image limits the frequency at which data can be assessed and requires high spatial resolution (Ben Gal *et al.*, 2009).

In addition, there is still no artificial reference surface to measure T_{dry} for canopy scale measurements. Although actually a function of R_n and r_{aH} (equation 44), $\triangle T_{dry}$ is usually set arbitrarily at 5 °C (Ben Gal *et al.*, 2009). Given the sensitivity of $CWSI_d$ to T_{dry}, this issue should be solved, particularly for application in temperate or humid regions. T_{dry} should preferentially be obtained through dry artificial reference surfaces, as this reduces the requirement of meteorological measurements. Finally, obtaining a thermal image that covers a sufficiently large area (if possible, the entire field) at sufficient resolution remains challenging. This issue is not specific for $CWSI_d$ and will be discussed in section 5.1.

4.3.5 The water deficit index

As discussed, the calculation of CWSI assumes that $T_s = T_c$, which requires a fully closed canopy (equation 9). Else, T_s is higher than T_c and CWSI is overestimated. This problem is overcome with the water deficit index (WDI), through relating $\triangle T$ with fractional cover [$f_c(\phi)$] or with a vegetation index (Moran *et al.*, 1994).

If $\triangle T$ is plotted against $f_c(\phi)$, all points fall within a trapezoid-shaped region. The vertices of this trapezoid correspond with well-watered, full cover vegetation, drought-stressed full cover vegetation, saturated bare soil, and dry bare soil, as schematized in Fig. 10. Moran *et al.* (1994) showed that these vertices could be calculated with meteorological and crop data.

Under the assumption that $\triangle T_s$ is a linear function of $f_c(\phi)$ [$\triangle T_s = f_c(\phi)\ \triangle T_s + (1 - f_c(\phi))\ \triangle T_{soil}$], the line between $\triangle T_{WC}$ and $\triangle T_{WS}$ represents the minimum possible temperature as a function of $f_c(\phi)$ ($\triangle T_{pot}[f_c(\phi)]$) and the line between $\triangle T_{DC}$ and $\triangle T_{DS}$ the maximum possible temperature as a function of $f_c(\phi)$ ($\triangle T_{dry}(f_c(\phi))$). If it is further assumed that $\triangle T_c$ and $\triangle T_{soil}$ are linearly related with transpiration and soil evaporation, respectively, for a given R_n, δe, and r_{aH} (Fig. 5f), the WDI can be defined, by analogy with CWSI, as:

$$WDI = 1 - \frac{\lambda E}{\lambda E_{pot}} = \frac{\Delta T_{pot}(f_c(\varphi)) - \Delta T}{\Delta T_{pot}(f_c(\varphi)) - \Delta T_{dry}(f_c(\varphi))} \qquad (52)$$

In Fig. 10, WDI of a crop with $f_c(\phi)$ and $\triangle T$ of point B is calculated as $WDI = \frac{|AB|}{|AC|}$.

In practice, a vegetation index, calculated from the near infrared and red wavelengths of a pixel, is used instead of $f_c(\phi)$. Moran *et al.* (1994) originally proposed to use the soil-adjusted vegetation index (SAVI), but as the normalized difference vegetation index (NDVI) gives more reliable results (Koksal, 2008), it is more commonly used. However, the underlying assumption that $f_c(\phi)$ is linearly related with NDVI or SAVI is not correct (Jones and Vaughan, 2010).

of $CWSI_d$ is given for three levels of g_s; in the middle column, the discriminative power is given, expressed as the lower and higher boundary (i.e., the confidence interval) of g_s that is statistically different from the mean level of g_s; in the right column, the influence of g_s on the mean and 95% confidence intervals of $CWSI_d$ is given for three levels of T_a, K_{in}, u, and δe. Two sets of confidence intervals are given: one set in which the only estimation error was generated from the uncertainty on the temperature measurements (darker colours, full lines) and one set in which small differences in weather conditions between the reference and the measured leaves were additionally simulated (brighter colours, dashed lines). Based on the T_l model of section 3.2.2. See captions of Fig. 3 for standard weather conditions and standard leaf characteristics. The second set of confidence intervals was calculated assuming differences of ± 0.2 °C for T_a and of ± 10% of the measured leaf's K_{in}, u, and δe between measured and reference leaves.

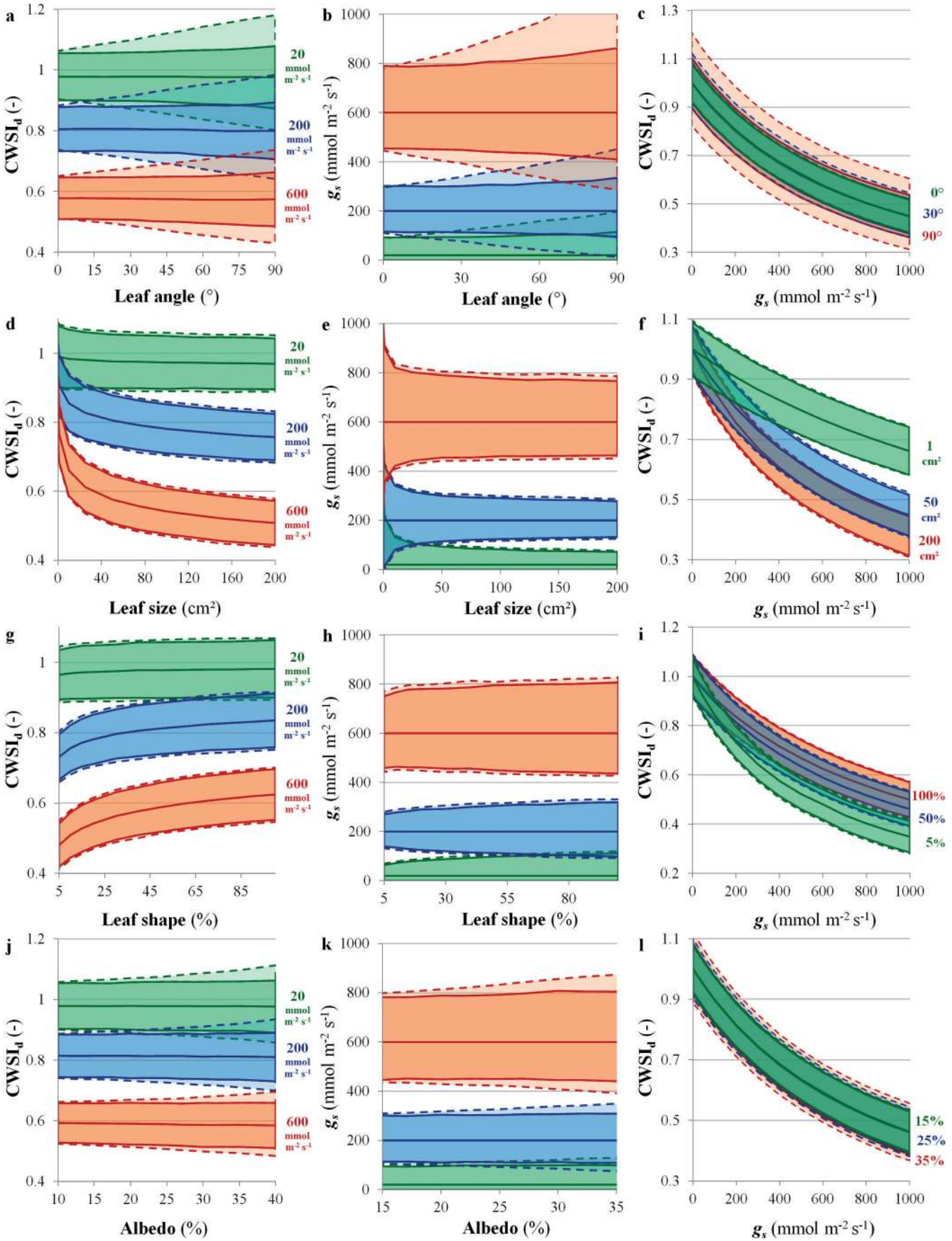

Fig. 9. Influence of leaf characteristics on $CWSI_d$ at leaf level. In the left column, the influence of the leaf angle, size, shape, and albedo on the mean and 95% confidence intervals of $CWSI_d$ is given for three levels of g_s; in the middle column, the discriminative power is

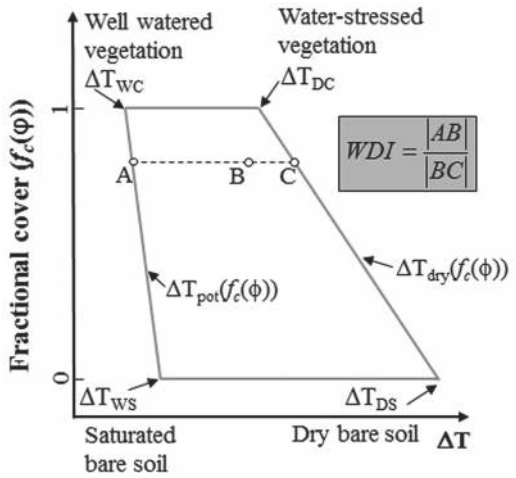

Fig. 10. Illustration of the water deficit index.

Originally, an 'analytical' version of WDI was proposed by Moran *et al.* (1994) and WDI was a ground-based method. However, a huge amount of data was required to estimate WDI analytically: apart from the visual, near infrared, and thermal infrared measurements, the method also required weather data (R_n, δe, u, and T_a) and crop characteristics (LAI, h_c, r_{aH}), additional parameters such as the maximum possible LAI and g_s, r_{aH} of the soil, and the SAVI values corresponding with full cover and completely bare soil. Hence, this analytical version of WDI was applied in a very limited number of studies, although these reported high correlations with irrigation level, $\left(1-\frac{\lambda E}{\lambda E_{pot}}\right)$, g_s, or leaf water potential in cotton (Colaizzi *et al.*, 2003b; Luquet *et al.*, 2004), broccoli (El-Shikha *et al.*, 2007), and dwarf bean (Koksal, 2008).

An empirical version of WDI was developed (Clarke, 1997) in which the boundaries of the trapezoid are derived from the T_s – VI scatterplot, without requiring any ground-based weather measurement. This empirical version is widely applied, but is largely limited to airborne thermal remote sensing; this review will therefore not go deeper into this version. For ground-based measurements, a simplification of WDI was proposed with a method combining T_s and VI data with an empirical baseline approach as in $CWSI_e$ (Barnes *et al.*, 2000), but this approach was not picked up by other researchers (but see Tilling *et al.*, 2007) and will not be further discussed.

4.4 Stomatal conductance index

4.4.1 Calculation and modelling

The stomatal conductance index (I_g) uses the same input data as $CWSI_d$ at leaf scale, but has the advantage over $CWSI_d$ that it is linearly related with g_s (except for anisolateral leaves (amphistomatous leaves with $r_{s,l} \neq r_{s,u}$) (Guilioni *et al.*, 2008)).

For its derivation, Jones (1999a,b) made use of the isothermal net radiation R_{ni}, instead of R_n. R_{ni} is defined as the net radiation of a leaf that would be received by an identical leaf if it were at air temperature (Jones, 1992). R_n can be substituted with R_{ni} in equations 19, 50, and 51 if r_{aH} is replaced by a new resistance term r_{HR}. This is the parallel sum of r_{aH} and r_R (rHR = (raH rR)/(raH + rR)), with r_R the virtual leaf resistance to radiative transfer:

$$r_R = \left(\frac{\rho_a c_p}{4\varepsilon\,\sigma T_2^3}\right) \tag{53}$$

The derivation of R_{ni}, r_R, and r_{HR} is given in Supplementary Data S5. Equations 19, 50, and 51 then become:

$$T_l = T_a + \frac{r_{HR}\gamma\, r_V R_{ni} - r_{HR}\,\rho_a c_p \delta e}{\rho_a c_p(\gamma\, r_V + s\, r_{HR})} \tag{54}$$

$$T_{dry} = T_a + \frac{r_{HR} R_{ni}}{\rho_a c_p} \tag{55}$$

$$T_{wet} = T_a + \frac{r_{HR}\gamma\, r_{aV} R_{ni} - r_{HR}\,\rho_a c_p \delta e}{\rho_a c_p(\gamma\, r_{aV} + s\, r_{HR})} \tag{56}$$

Note that T_{wet} in equation 56 is the T_l of a reference leaf wetted on one side; T_{wet} of leaves wetted on both sides is obtained by replacing r_{aV} with 0.5 r_{aV}.

R_{ni} has the advantage that is independent of T_l; hence, in contrast with R_n in equations 19, 50, and 51, R_{ni} has the same value in equations 54–56, which allows calculating the stomatal conductance index I_g as $\frac{(T_{dry}-T_l)}{(T_l-T_{wet})}$. For hypostomatous leaves, combining equations 24 and 54–56 gives:

$$I_g = \frac{(T_{dry}-T_l)}{(T_l-T_{wet})} = \frac{\gamma\, r_{aV} + s\, r_{HR}}{\gamma\, r_s} \tag{57}$$

given, expressed as the lower and higher boundary of g_s that is statistically different from the mean level of g_s; in the right column, the influence on the mean and 95% confidence intervals of $CWSI_d$ of g_s is given for three levels of leaf angle, size, shape, and albedo. Two sets of confidence intervals are given: one set in which the only estimation error was generated from the uncertainty on the temperature measurements (darker colours, full lines) and one set in which small differences in weather conditions between the reference and the measured leaves were additionally simulated (brighter colours, dashed lines). Based on T_l model of section 3.2.2. See captions of Fig. 3 for standard weather conditions and standard leaf characteristics. The second set of confidence intervals was calculated assuming differences of ± 10% of the measured leaf's leaf angle, shape, size, and albedo between measured and reference leaves. Leaf shape = 100 leaf width/leaf length.

or

$$g_s = I_g \frac{\gamma}{\gamma\ r_{aV} + s\ r_{HR}} = I_g\ G \qquad (58)$$

with $G = \frac{\gamma}{\gamma\ r_{aV} + s\ r_{HR}}$. For isolateral leaves and when a wet reference leaf wetted on both sides is used, the relation is similar, with $G = \frac{\gamma}{\gamma\ r_{aV} + 2s\ r_{HR}}$. In other cases, the relation between I_g and g_s becomes more complex (see Guilioni *et al.* (2008) for an overview). In the case of anisolateral leaves, I_g is a linear function of r_V (equation 22), not of g_s.

For hypostomatous and isolateral leaves, I_g is linearly related with g_s as long as G remains constant (equation 58). The influence of g_s and meteorological conditions on G is given in Fig. 11. G hardly changes with g_s, K_{in}, or δe, but is very much influenced by u and T_a.

Although g_s can be calculated from I_g, I_g is most often used as a stress indicator itself, because of the linear relation with g_s and the fact that no additional microclimatic measurements are needed. The reliability and sensitivity for weather conditions and leaf characteristics was modelled, using the same leaf model and techniques as for $CWSI_d$ (hence, hypostomatous leaves with wet reference leaves wetted on one side, section 4.3.4).

4.4.2 Application of I_g and its sensitivity to weather conditions and deviations in leaf characteristics

I_g is indeed linearly related with g_s (Figs. 12 and 13, but see also Fig. 12i). This agrees with observations in grapevine (Jones *et al.*, 2002; Leinonen and Jones, 2004; Fuentes *et al.*, 2005; Grant *et al.*, 2006, 2007; Leinonen *et al.*, 2006; Loveys *et al.*, 2008), in several varieties of bean (Jones, 1999a,b; Leinonen and Jones, 2004; Grant *et al.*, 2006), in cucumber (Kaukoranta *et al.*, 2005), and in the biodiesel plant *Jatropha curcas* L. (Maes *et al.*, 2011).

A thermal and visual image of this last study is given in Fig. 14. The seedling on the left (drought plant) was not irrigated for about 2 months; the seedling on the right (control plant) was fully irrigated. T_{dry} was 27.3 for both plants and T_{wet} 19.4 and 18.4 for the drought and control plant, respectively. Average T_l of the control plant was 24.8 °C, resulting in $I_g = 0.39$ and $CWSI_d$ of 0.72; and average T_l of the drought plant was 26.7, resulting in $I_g = 0.09$ and $CWSI_d = 0.92$.

Similar to $CWSI_d$, the expected value of I_g is not influenced by K_{in}, δe, θ, or α (Fig. 12), but increases with increasing T_a and A_l, and with decreasing u. Optimal conditions for application of I_g (i.e. higher difference between the lines in left column; lower confidence bandwidths in middle column of Fig. 12) include high T_a, K_{in}, and δe and relatively low u (Fig. 12), which are also the conditions in which most studies were performed; however, I_g has also been successfully applied at low or highly variable incoming radiation (Maes *et al.*, 2011; Grant *et al.*, 2012).

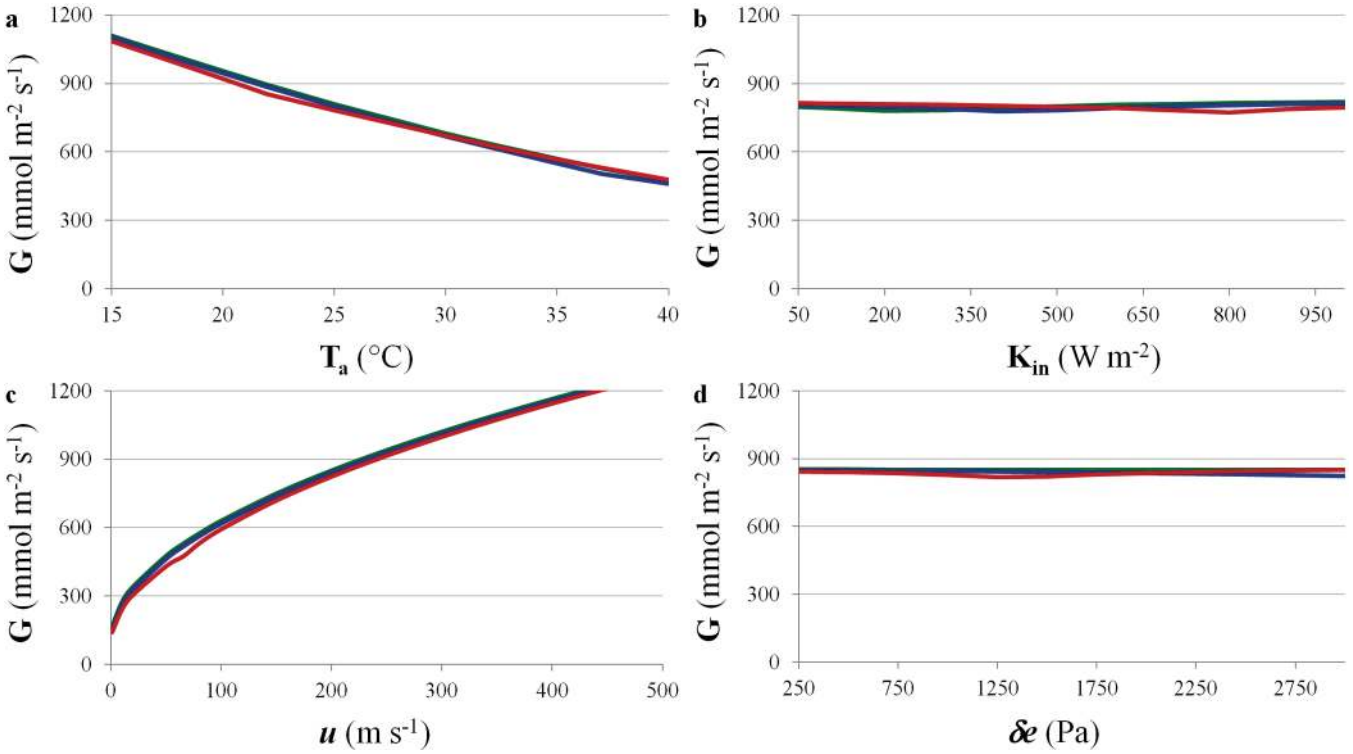

Fig. 11. Influence of weather conditions: (a) air temperature (T_a), (b) incoming shortwave radiation (K_{in}), (c) wind speed (u), and (d) vapour pressure deficit (δe) on G ($G = I_g\ g_s^{-1}$), calculated for hypostomatous leaves, and for three levels of g_s; 20 (green), 200 (blue), and 600 (red) mmol m^{-2} s^{-1}. Based on equation 58 and derived from the leaf model described in section 3.2.2. See Fig. 3 for standard weather conditions and leaf characteristics.

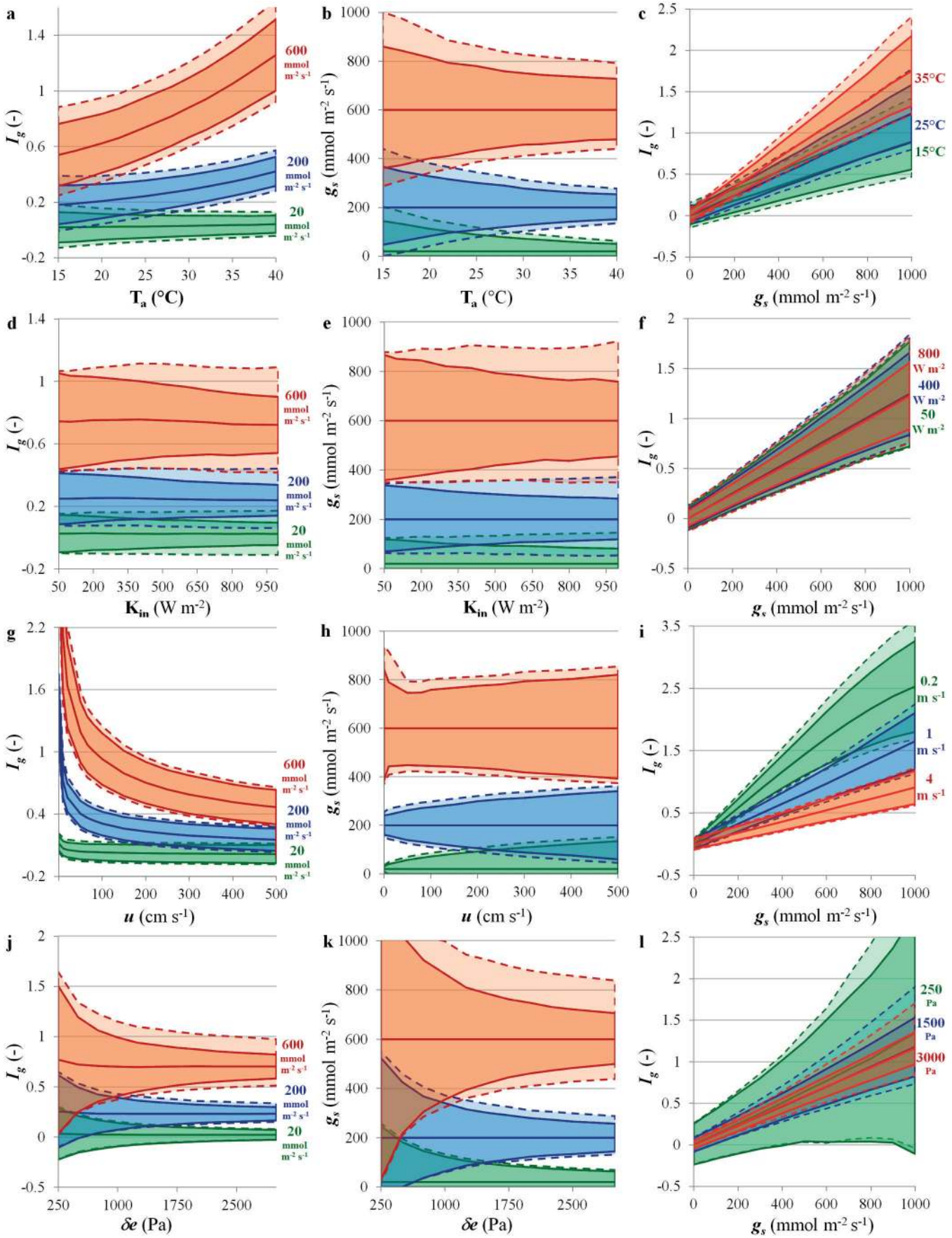

Fig. 12. Influence of weather conditions air temperature (T_a), incoming shortwave radiation (K_{in},), wind speed (u), and vapour pressure deficit (δe) on I_g. See Fig. 8 for a detailed description.

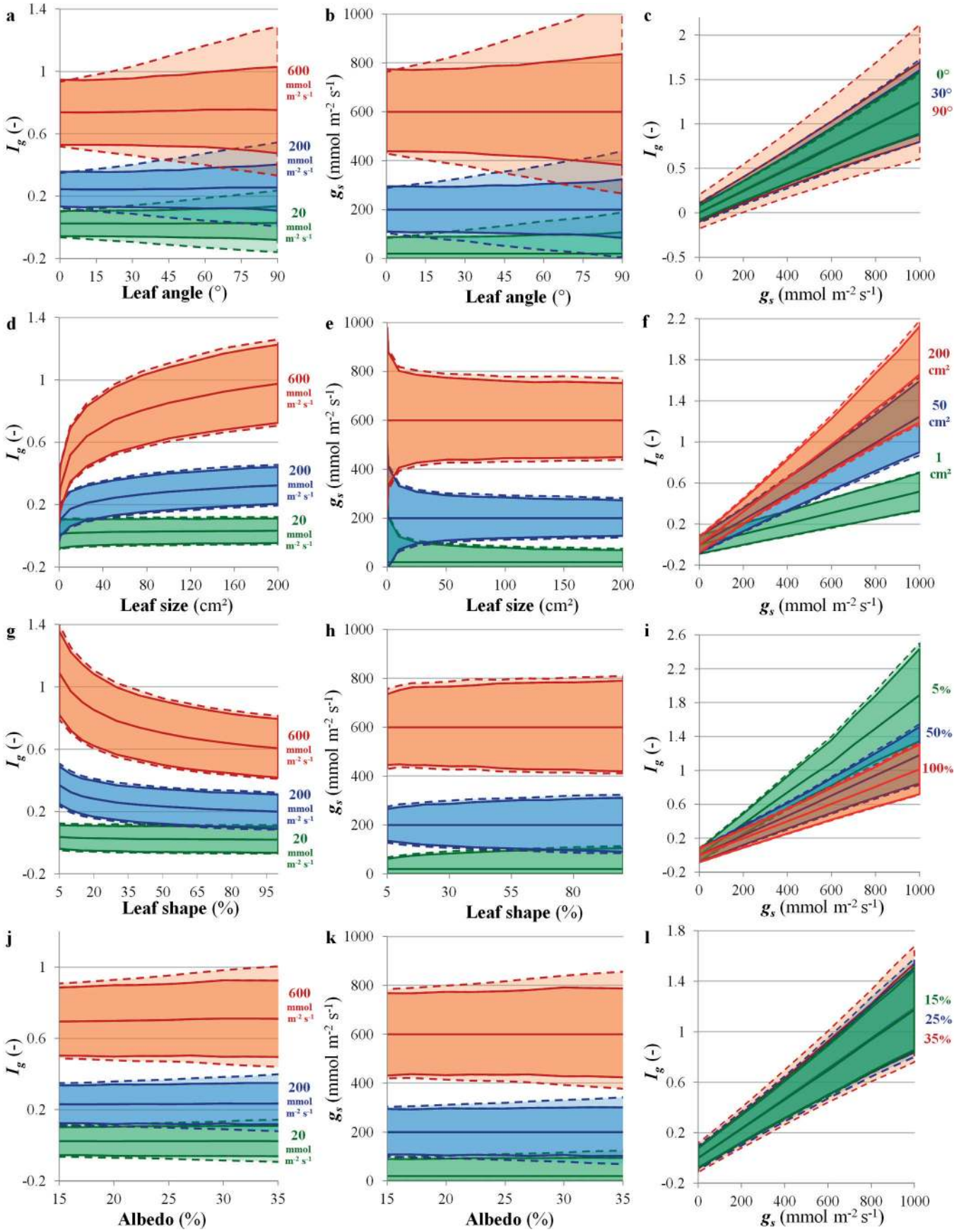

Fig. 13. Influence of leaf characteristics (leaf angle, size, shape, and albedo) on I_g. See Fig. 9 for a detailed description.

Fig. 14. Visible (left) and thermal infrared (right) view from above of seedlings of *Jatropha curcas* L. Wet reference leaves were created by spraying the leaves about 1 minute before image capture and are indicated with the white ellipses; dry reference leaves of both plants were created by covering the leaves with petroleum jelly and are indicated with red ellipses. Image taken in a greenhouse in Heverlee, Belgium on 18 October 2007 with a ThermaCAM SC3000 PAL (FLIR Systems) and a Panasonic Lumix DMC-TZ3. See Maes *et al.* (2011) for more details.

Indeed, if differences between measured and reference leaves are taken into account, the discriminative power roughly does not change with K_{in} (Fig. 12e).

As for $CWSI_d$, leaf characteristics have relatively little influence on the discriminative power, with the exception of θ at more vertical leaf angles. Note that θ, defined as the angle between the leaves and the plane perpendicular to the incoming sunlight, is also influenced by the position of the sun; hence, measurements in early morning and later afternoon or in early spring or late autumn, are prone to significantly larger error.

In field conditions, the large variation in T_l within the canopy, mainly as a consequence of leaf orientation and shading, complicates the use of I_g. Grant *et al.* (2006, 2012) suggested placing leaves in a horizontal grid, but it is not certain that this will not disturb leaf functioning – furthermore, this is often unfeasible. More robust I_g estimates can be obtained by taking the average temperature of several leaves as input for T_l in equation 57 (Maes *et al.*, 2011). In addition, separating canopy from background pixels, based on visual or near-infrared images (e.g. Leinonen and Jones, 2004; Möller *et al.*, 2007; Wang *et al.*, 2010a; see section 5.3.1), makes the estimates more robust.

The large variability of leaf canopy temperature also complicates the assessment of a reliable reference leaf temperature estimate. If different dry reference leaves are spread over the canopy, their T_{dry} can differ with several degrees, due to the impact of θ and K_{in} on T_{dry} (Figs. 3c, d and 4a, b). Grant *et al.* (2006) suggested taking the maximum observed T_{dry} rather than average T_{dry}; Maes *et al.* (2011) pinpointed the need to measure and use a separate T_{dry} per plant, if possible.

T_{wet} is slightly less influenced by K_{in} or θ (Figs. 3d and 4b), but there are practical limitations to its use (Jones *et al.*, 2009). Moreover, different times between wetting and image capture can cause inconsistent T_{wet} estimates and wetting the reference leaves can influence T_l of other leaves, both directly (dripping of the water on other leaves) and indirectly (through changes in microclimate) (Jones *et al.*, 2002; Grant *et al.*, 2007).

This calls for alternatives for the single reference leaves for application of I_g at canopy or field scale. The wet reference leaves could be replaced by the WARS, used in $CWSI_d$ (section 4.3.4); as mentioned, no larger-scale alternative exists at the moment for the dry reference surfaces; as for $CWSI_d$, T_{dry} might be taken as a constant level or can be estimated from equation 44 or 55.

4.4.3 $CWSI_d$ or I_g?

As discussed, the same data are used for the calculation of $CWSI_d$ or I_g; in fact, $CWSI_d = (1 + I_g)^{-1}$ (equations 51 and 57). So, which indicator is to be preferred? Interestingly, the modelling shows that the discriminative power of both methods is very similar (compare middle columns of Figs. 8 and 12 and of Figs. 9 and 13). So far, most scientists have preferred $CWSI_d$ because the CWSI concept is well known. However, $CWSI_d$ is not linearly related with g_s and, due to the use of T_{wet} instead of T_{pot}, there is no firm theoretical relation between $CWSI_d$ and $\left(1-\frac{\lambda E}{\lambda E_{pot}}\right)$. The use of I_g can therefore be recommended, at least at leaf level.

4.4.4 Alternative indices

(T_{dry} − T_l) (T_{dry} − T_l) is a simplified index that avoids the measurement problems related to the wet reference leaf. (T_{dry} − T_l) was closely related with g_s in grapevine and *Jatropha* (Grant *et al.*, 2006; Maes *et al.*, 2011) Model simulations (Supplementary Figs. S1 and S2 in Supplementary Data S6) show that (T_{dry} − T_l) is almost linearly related with g_s and that the influence of weather conditions and leaf characteristics is similar to that of I_g, although the discriminative power is lower, particularly when there is a difference in θ between measured and dry reference leaves at large θ.

Estimating g_s without reference leaves or with only dry reference leaves

As discussed, one of the great advantages of I_g (and $CWSI_d$) is the fact that it can be assessed without requiring additional microclimatic measurements. However, if the aim is to estimate g_s or r_s, precise microclimatic measurements (particularly of T_a and u) are required to estimate r_{HR} and r_{aV} (equations 20, 21, 25, 26, and 53) and to calculate G.

In that case, it would be more practical if the wet and/or dry reference leaves are not needed. For hypostomatous leaves, r_s can be estimated directly as (equation 54):

$$r_s = \frac{-r_{HR}\,\rho_a c_p\left[\, s\,(T_l - T_a) + \delta e \,\right]}{\gamma\left[\,\rho_a c_p\,(T_l - T_a) - r_{HR} R_{ni}\,\right]} - r_{aV} \qquad (59)$$

However, due to its sensitivity to measurement errors (Leinonen *et al.*, 2006), r_s calculated with equation 59 correlated rather poorly with the measured r_s (Leinonen *et al.*, 2006; Grant *et al.*, 2012). A similar approach was used by Blonquist *et al.* (2009) to estimate g_c at canopy scale. A sensitivity analysis showed that errors in g_c were particularly large in cloudy conditions, and that very precise measurements of T_c and T_a are required.

If T_{dry} is additionally measured, r_s can be estimated as (again for hypostomatous leaves, and combining equations 54 and 55) (Leinonen *et al.*, 2006):

$$r_s = \frac{r_{HR}\left[\, s\,(T_l - T_a) + \delta e \,\right]}{\gamma\,(T_{dry} - T_l)} - r_{aV} \qquad (60)$$

Note that no radiation data are required, but that δe, r_{HR}, and r_{aV} have to be determined precisely. Results show that estimations of g_s are comparable or even better than those obtained with I_g (Leinonen *et al.*, 2006; Grant *et al.*, 2011).

4.5 The three-temperature model (3T model)

The three-temperature model (3T model) was developed and tested by Qiu *et al.* (2000, 2002, 2003, 2009). It makes use of a dry reference leaf, with assumed $\lambda E = S = G_i = 0$. From equations 10 and 14, it follows that $R_{n,dry} = H_{dry} = \rho_a c_p \dfrac{(T_{dry} - T_a)}{r_{aH}}$. For normal leaves, this sensible heat is given by $H = \rho_a c_p \dfrac{(T_l - T_a)}{r_{aH}} = R_n - \lambda E$. Assuming an identical r_{aH} for normal and dry reference leaves gives:

$$\lambda E = R_n - R_{n,dry}\frac{(T_l - T_a)}{(T_{dry} - T_a)} \qquad (61)$$

Equation 61 is the basic formula used in the three-temperature model, which owes its name to the three temperatures (T_l, T_a, T_{dry}) needed for its calculation. In addition, R_n and $R_{n,dry}$ must be known; R_n is either measured or can be derived from measurements of K_{in} and T_l, if estimates of α, τ, and ε are available for both leaf sides (equation 13); $R_{n,dry}$ can be calculated from R_n replacing T_l with T_{dry} and assuming that α and ε of the reference leaf are the same as those of the actual leaves.

The ratio of the right-hand side of equation 61, called h_{at}, was proposed as an indicator of drought stress and stomatal conductance (Qiu *et al.*, 2003, 2009):

$$h_{at} = \frac{(T_l - T_a)}{(T_{dry} - T_a)} \qquad (62)$$

The authors claimed that $h_{at} \leq 1$, with lower values indicating higher λE.

The method has been mainly tested for sorghum, but also for melon (Qiu *et al.*, 2000, 2003), tomato (Qiu *et al.*, 2003), and lettuce (Qiu *et al.*, 2009). High correlations were observed between λE obtained from equation 61 and measured λE (Qiu *et al.*, 2000, 2002). In addition, h_{at} was highly correlated (R^2 = 0.97) with $CWSI_e$ of sorghum (but with T_{dry} obtained from the dry reference leaf) and was capable of distinguishing between different drought and temperature treatments of melon and tomato (Qiu *et al.*, 2009).

The method seems very appealing: h_{at} can easily be measured, is linearly related with λE, and can be used to calculate λE without requiring estimates of r_{aH} or r_{aV} (hence, of δe or u). Still, the method has not been picked up by other researchers, so there is still very little experience with this method. We therefore modelled the sensitivity of h_{at} to weather conditions and leaf characteristics, using the same approach as explained in section 4.3.4 for $CWSI_d$. For the T_a measurements, a standard deviation of 0.1 °C was assumed. The results are given in Figs. 15 and 16.

h_{at} decreases non-linearly with increasing g_s. Unlike I_g and $CWSI_d$, the expected h_{at} value is influenced by all weather variables and leaf characteristics. The influence of most variables on the discriminative power of h_{at} is comparable with that of $CWSI_d$ and I_g; differences in δe between the reference and the measured leaves furthermore do not influence h_{at}. However, h_{at} responds strangely to decreasing K_{in} and increasing θ. At low irradiance, due to either low K_{in} or high θ, ($T_l - T_a$) becomes negative, resulting in negative h_{at} values. When the irradiance decreases further, ($T_{dry} - T_a$) first tends to 0, resulting in very negative h_{at} values; with an even further drop in irradiance, ($T_{dry} - T_a$) can become negative (e.g. Figs. 3d and 4b), in which case h_{at} actually attains very high positive values (e.g. Fig. 15f).

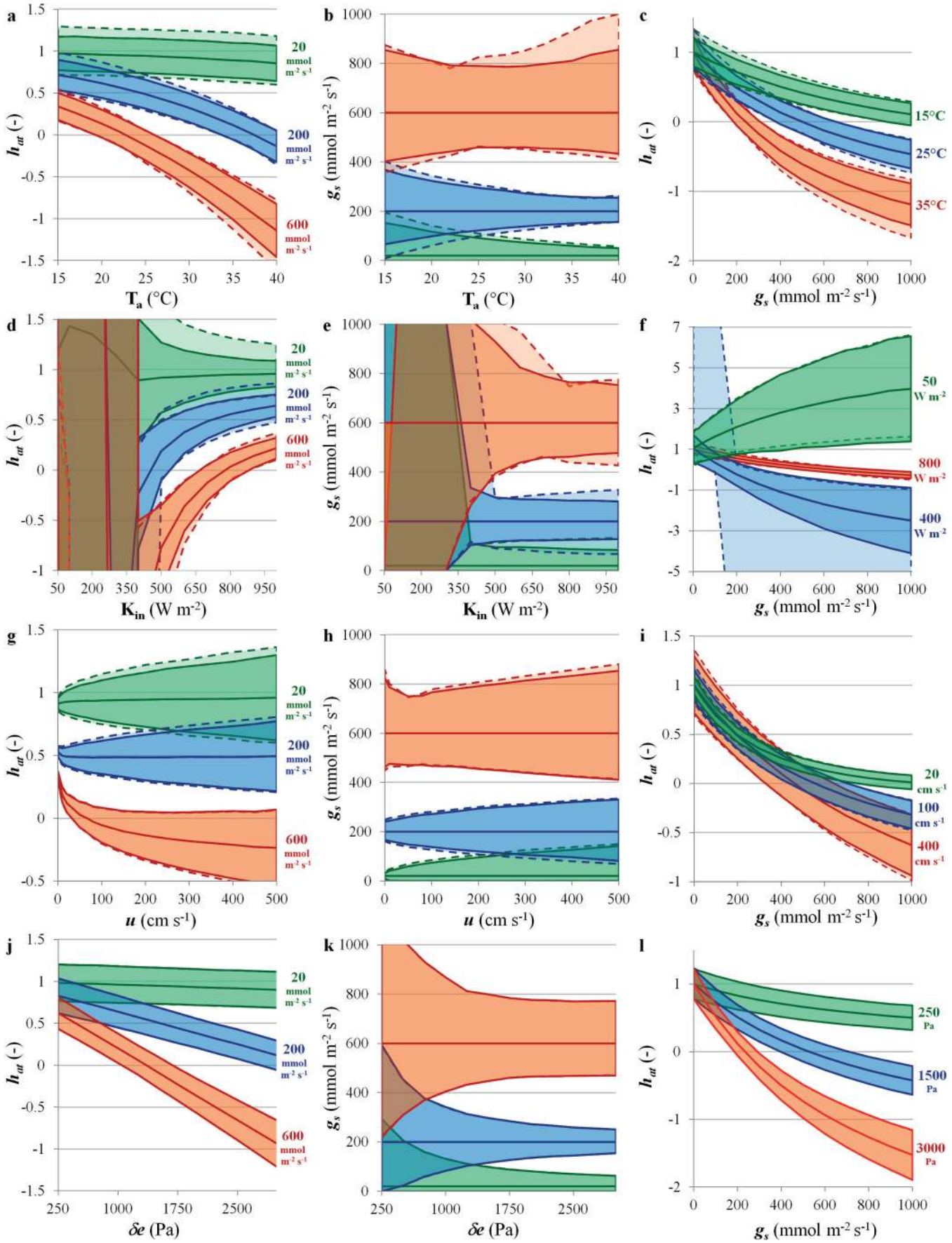

Fig. 15. Influence of weather conditions air temperature (T_a), incoming shortwave radiation (K_{in},), wind speed (u), and vapour pressure deficit (δe) on h_{at}. See Fig. 8 for a detailed description.

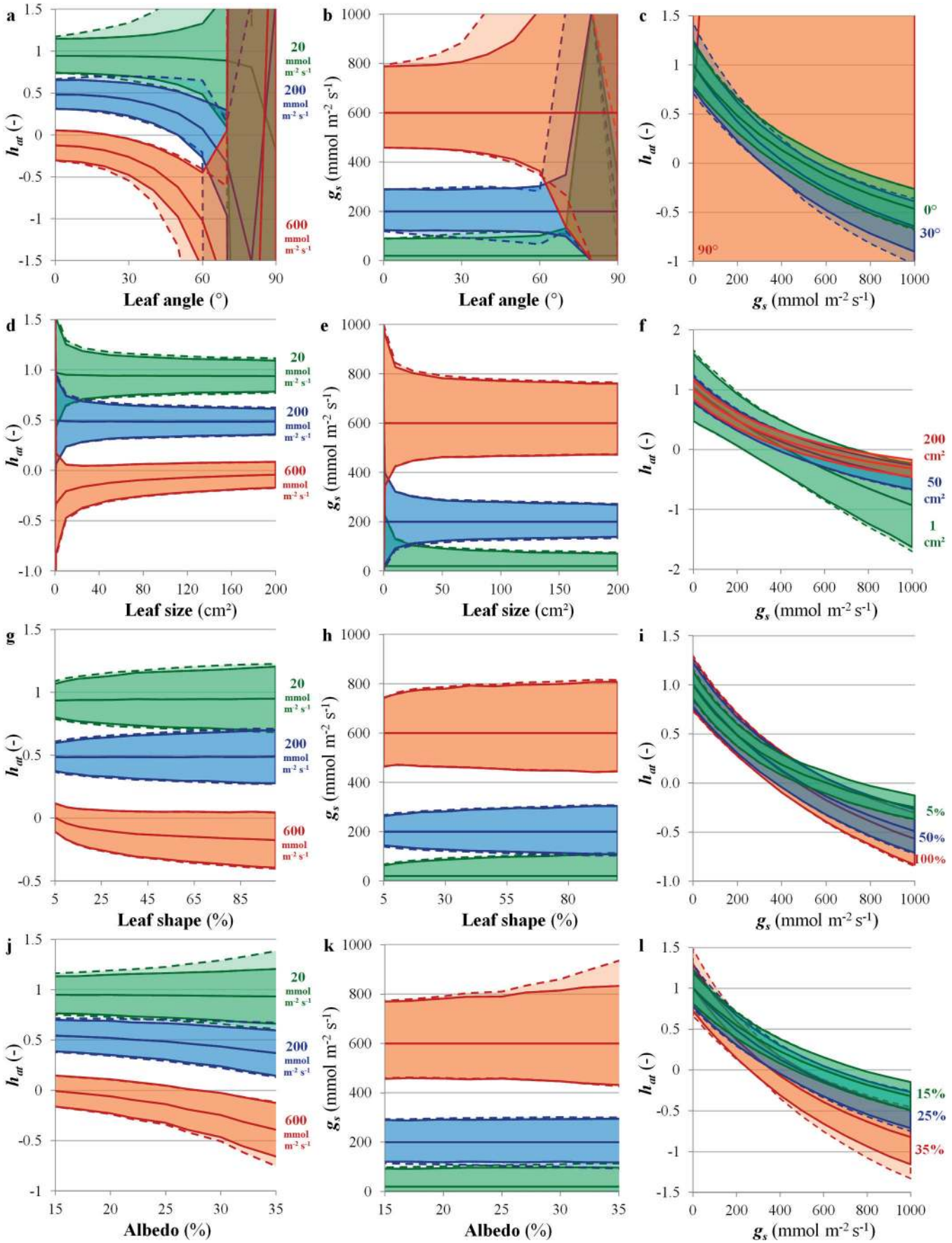

Fig. 16. Influence of leaf characteristics (leaf angle, size, shape, and albedo) on h_{at}. See Fig. 9 for a detailed description.

The unsuitability of h_{at} at low radiation levels was confirmed in a re-analysis of data from Maes *et al.* (2011) on *Jatropha*. Measurements were performed in relatively low-light conditions (max. 130 W m^{-2}) in six measurement runs. In all measurements runs, significant differences between the drought treatments could be distinguished using CWSId, I_g or (T_{dry} – T_l). However, when h_{at} was used, significant differences between the treatments were not found for any measurement run; in addition, in only two of the six measurement runs, h_{at} was significantly correlated with g_s.

All in all, the use of the 3T model or h_{at} can be appealing for its simplicity and its limited data and labour requirements, but is highly restricted due to its sensitivity to low-irradiation conditions.

4.6 Direct estimation of canopy evapotranspiration: one- and two-source models

The methods discussed so far calculated indices from T_s, T_c, or T_l to express drought stress or as an indirect indicator of g_s, g_c, or λE. Although these methods are at least theoretically related with λE, g_s, or g_c, the estimation of λE is normally not the aim. Several thermal remote sensing methods have been developed with the specific aim to estimate λE. As discussed previously, they can be divided into one-source models (OSM) and two-source models (TSM).

In one-source models, the entire ecosystem is represented as one single layer or big leaf. Usually, λE is estimated as the rest fraction of R_n, G_i, and H (equation 10). The methods mainly differ in the way r_{aH} and G_i, and particularly T_0, are calculated. The different approaches were discussed in section 3.3 and will not be repeated here.

In TSMs, the vegetation is divided into a canopy and a soil layer. A TSM was proposed by Norman *et al.* (1995) and was later refined in several follow-up papers (Kustas and Norman, 1999a, b, 2000). The energy balances of the soil and the canopy layer are calculated separately based on one T_s measurement, several vegetation characteristics and weather data. The relation between T_s, T_c, and T_{soil} is given by an adjustment of equation 9, in which it is assumed that $\varepsilon = \varepsilon_{soil} = \varepsilon_c$:

$$T_s^4 = f_c(\varphi)\, T_c^4 + (1 - f_c)(\varphi))\, T_{soil}^4 \tag{63}$$

where $f_c(\phi)$ is calculated as a function of the view zenith angle, LAI, and a clumping factor (see equation 6 of Kustas and Norman, 2000).

The heat fluxes of the soil and vegetation compartments are considered parallel processes. H_c is estimated as (equation 14) $H_c = \rho_a c_p \dfrac{(T_c - T_a)}{r_{aH}}$, with r_{aH} from equation 34. The total resistance to sensible heat flux from the soil compartment is the serial sum of r_{aH} and an additional resistance, r_{soil}, that expresses the resistance to heat flow between the soil layer and the canopy layer. H_{soil}, the sensible heat of the soil compartment is:

$$H_{soil} = \rho_a c_p \frac{(T_{soil} - T_a)}{r_{aH} + r_{soil}} \tag{64}$$

r_{soil} is calculated from the empirical function:

$$r_{soil} = \frac{1}{0.004 + 0.012\, u_{soil}} \tag{65}$$

with u_{soil} the wind speed just above the soil surface, estimated as:

$$u_{soil} = u_c \exp\left(-a \left(1 - \frac{0.05}{h_c} \right) \right) \tag{66}$$

with u_c the wind speed at the top of the canopy (derived from the logarithmic wind speed profile) and a the extinction coefficient, which is a function of LAI, h_c, vegetation width, and a clumping factor that takes vegetation density into account (see equation 8 of Kustas and Norman, 2000).

The total sensible heat flux H is:

$$H = H_c + H_{soil} = \rho_a c_p \left[\frac{(T_c - T_a)}{r_{aH}} + \frac{(T_{soil} - T_a)}{r_{aH} + r_{soil}} \right] \tag{67}$$

The Priestley-Taylor equation is used to calculate λE_c [see Supplementary Data S1.3, equation S18; setting $G_i = 0$ (canopy layer)]:

$$\lambda E_c = \alpha_{PT}\, f_g \frac{s}{s + \gamma} R_{n,c} \tag{68}$$

with α_{PT} the Priestley-Taylor coefficient and f_g the proportion of leaf area that is green. $R_{n,c}$, the net radiation of the canopy layer, is the sum of shortwave and longwave radiation, calculated as a function of K_{in}, α, LAI, and the clumping factor, corrected for solar angle. $R_{n,soil}$ is calculated with a similar procedure, and G_i is calculated from $R_{n,soil}$ using equation 31 with $\Gamma_i = 0.3$.

The iterative procedure to calculate λE_c and λE_{soil} goes as follows:

(a) A first estimate of λE_c is obtained with equation 68 and assuming $\alpha_{PT} = 1.3$

(b) From equation 10 (ignoring S), $R_{n,c} - \lambda E_c = H_c = \dfrac{(T_c - T_c)}{r_{aH}}$

(c) T_{soil} is estimated from T_c and equation 63.

(d) H_{soil} is estimated from T_{soil} and equation 64.

(e) λE_{soil} is calculated from $\lambda E_{soil} = R_{n,soil} - G_i - H_{soil}$

(f) If $\lambda E_{soil} \geq 0$, a solution for soil and canopy energy fluxes is reached. Else, λE_{soil} is set to 0 allowing calculating a new estimate $H_{soil} = R_{n,soil} - G_i$. Going through steps d-a backwards gives estimates of T_{soil}, T_c, H_c, and α_{PT}. Steps a–e are repeated until a solution is found for $\lambda E_{soil} \geq 0$.

Note that with this approach, T_c and T_{soil} are derived from H_c and H_{soil}; hence, they can be considered the aerodynamic temperature of the canopy and the soil layers.

This TSM generally outperformed OSMs for extreme conditions and in sparse vegetations or orchard-like ecosystems (Kustas *et al.*, 2007; Kustas and Anderson, 2009); moreover, it offers the advantage over OSMs that separate energy balances are developed for the soil and canopy compartment. However, it is clear that this TSM relies on a highly detailed knowledge of the vegetation structure; this is also the case for the more advanced OSMs. As such, in contrast with airborne and satellite thermal remote sensing, the direct estimation of λE through ground-based thermal remote sensing is in general restricted to scientific studies.

5 The future and challenges of ground-based thermal remote sensing

5.1 From scientific methods to agricultural practice

Most methods discussed in section 4 are still only used for scientific purposes. The few methods that are applied in agricultural practice (e.g. stress time, $CWSI_e$) for drought stress detection and irrigation steering use IRT sensors rather than cameras. These methods have clear limitations. Most importantly, they can only be applied in regions with very constant (semi-)arid weather conditions during the growth season and are largely limited to low, homogeneous crops.

Still, there is a strong interest for new drought stress detection or irrigation steering methods. With the increasing pressure on blue water resources, there is a growing demand for efficient irrigation methods that maximize water productivity and minimize costs and wastes. This calls for new precision irrigation techniques (Fereres and Evans, 2006; Steppe *et al.*, 2008; Fernández and Cuevas, 2010), preferably based on plant-water rather than soil-water status measurements (Jones, 2004; Naor, 2008; Steppe *et al.*, 2008; Fernández and Cuevas, 2010). With the currently available methods to measure plant-water status (e.g. sap flow and/or diameter measurements), it is impossible to assess the spatial variability. If plant-to-plant variability in plant-water status is high, this variability must be assessed for precision irrigation (Naor and Cohen, 2003; Arno *et al.*, 2009). This is particularly the case for horticultural (i.e. 'orchard-like') cash crops such as grapevine (Acevedo Opazo *et al.*, 2008).

Infrared thermography is particularly suited for these applications, because it allows the spatially explicit assessment of the water use in plants. However, several basic problems need to be overcome before thermal cameras can be used for commercial application in agriculture at this moment: (i) images of sufficiently high pixel resolution must be generated of the entire field; (ii) the acquired images must be processed automatically; and (iii) an adequate method must be developed to estimate drought stress or irrigation need at this scale.

5.2 Covering the entire field

Several methods have so far been used to increase the field area viewed by the camera.Thermal cameras are often positioned on fixed poles (e.g. Cohen *et al.*, 2005; Alchanatis *et al.*, 2010) or cranes (e.g. Möller *et al.*, 2007; Ben Gal *et al.*, 2009), but this does normally not allow viewing the entire field.

In fields equipped with a pivot irrigation system, IRT sensors (Sadler *et al.*, 2002; Peters and Evett, 2007, 2008) or thermal cameras (Colaizzi *et al.*, 2003b; El-Shikha *et al.*, 2007) can be fixed on the pivot to assess the spatial variability. Else, the entire field can be viewed with thermal cameras installed on robotic cars (Luquet *et al.*, 2003), which can be particularly suited in orchards. These truly ground-based methods allow viewing at off-nadir viewing angles but have the disadvantage that it takes considerable amount of time to cover the entire field, so that temperature correction of the images is needed sensors (Peters and Evett, 2007, 2008).

An alternative is to apply low-altitude airborne thermography. Although this is not strictly ground-based, the same methods are applied as for ground-based measurements. Application of manned flights will in most cases not be economic for agricultural practice, but in recent years, miniature unmanned aerial vehicles (UAVs), small helicopters or airplanes that are able to fly autonomously, have been developed. With relatively low capital and very low operational costs, these UAVs have the potential to become an affordable measurement tool. Moreover, they can be applied at virtually any desired moment and location, while covering areas of several hectares and providing very high resolution maps (5–25 cm, depending on flight altitude and sensor type). Their potential for assessing drought stress or estimating λE of agricultural fields has already been shown in a number of studies (e.g. Sullivan *et al.*, 2007; Berni *et al.*, 2009a,b; Gonzalez-Dugo *et al.*, 2012; Zarco-Tejada *et al.*, 2012). As such, miniature UAVs currently seem to be the most promising method for the acquisition of high-resolution drought stress maps.

5.3 Automated image processing

Image processing is still a very time-consuming step that requires expert knowledge in both software and thermography. This must be largely automated before infrared thermography can be applied as a common tool in agricultural practice. The processing is different for ground-based or low-altitude airborne measurements.

5.3.1 Ground-based measurements

Although T_l or T_c can be derived directly from the thermal images, using temperature thresholds based on T_{dry} and T_{wet} (e.g. Jones *et al.*, 2002), the acquisition of precise estimates of T_l or T_c requires the use of visual images (e.g. Leinonen and Jones, 2004; Möller *et al.*, 2007; Wang *et al.*, 2010a).

First, the visual and thermal images have to be overlaid. As the images are not taken from the exact same position and as they have a different resolution, this is often a time-consuming step that involves warping and resampling of the visual images, based on ground control points that are recognizable on visual and thermal images (Leinonen and Jones, 2004). Wang *et al.* (2010b) recently proposed an advanced method in which the image registration is performed automatically based on automatic cross-correlation algorithm of edge images generated from the visual and thermal images.

Next, pixels must be classified as canopy/leaf (preferentially separating shaded and sunlit leaves) in order to extract T_c or T_s. This is mostly done using the visual image only, through supervised classification (Leinonen and Jones, 2004; Jiménez-Bello *et al.*, 2011) or, fully automatic, through colour identification (Wang *et al.*, 2010a). As small errors in image overlap can generate significant errors in the average T_{br} estimate, it is preferable to filter out very hot or very cold pixels, as proposed by Wang *et al.* (2010a). Finally, T_{br} must be converted into T_s or T_c, through the procedure explained in section 2.2. Note that this is not strictly required if reference temperatures of leaves/surfaces with very similar emissivity are used.

If $CWSI_d$ or I_g are to be calculated, the temperatures of the reference leaves must additionally be extracted. Wang *et al.* (2010a) proposed an automatic procedure to do so. Finally, $CWSI_d$, I_g or another index can be calculated.

5.3.2 Low-altitude airborne measurements

In low-flight airborne remote sensing, a large number of images, taken within a short time span, must be mosaicked. Software is available that creates a mosaicked and geo-referenced image relatively automatically, often using the GPS location of the UAV or airplane (e.g. Berni *et al.*, 2009b). If a large amount of images is taken with great overlap, digital terrain models can be calculated, visualizing the canopy structure. More precise georeferencing can be done using ground control points. Techniques to separate soil and canopy layers are similar to those for ground-based measurements, possibly extended with information of the digital terrain model.

5.4 Adaptation of methods to field scale

It is clear that the current ground-based methods need to be adapted before they can be applied in an automated procedure at field scale. As discussed, the most promising and straightforward ground-based thermal methods for estimating drought stress are those that use T_{dry} and T_{wet} to correct T_c (e.g. $CWSI_d$, I_g). T_{wet} can be derived directly from the WARS, although the issues formulated in section 4.3.4 deserve further attention. Moreover, the required amount of reference surfaces is not clear. In theory, a reference surface should be present within each image, but this seems not feasible and even not necessary in the case of imaging with UAV systems, as all images are taken at virtually the same moment. T_{dry} can be calculated from weather data (equation 50), although it seems preferable to derive T_{dry} directly from a reference surface, which still has to be developed. Another option is to estimate T_{dry} and T_{pot} from the α–T_c or the vegetation index–T_c space, as is commonly performed for high-altitude remote sensing in, for example, the S-SEBI algorithm (Roerink *et al.*, 2000) or the empirical version of WDI (Clarke, 1997). However, this does require the presence of a sufficient amount of extreme pixels (i.e. dry and wet pixels) in the image.

A possible future alternative would be to estimate λE with OSMs or (particularly for orchards) TSMs. They could be automated provided that the information of the visual image and, if possible, the detailed digital terrain model, is used to automatically extract all required information of canopy structure.

Supplementary material

Supplementary data are available at *JXB* online.

Supplementary Data S1. Derivation of general relations between surface temperature and sensible and latent heat flux

Supplementary Data S2. Calculation of resistance to sensible and latent heat transport in air

Supplementary Data S3. Derivation of CWSI

Supplementary Data S4. Overview Table of non-water stressed baseline equations

Supplementary Data S5. Calculation of R_{ni}

Supplementary Data S6. Influence of weather conditions and leaf characteristics on $(T_{dry} - T_l)$

Acknowledgements

The authors would like to thank two anonymous reviewers for their constructive comments on an earlier version of the text. WHM is funded by the Special Research Fund (BOF) from Ghent University.

References

Acevedo Opazo C, Tisseyre B, Guillaume S, Ojeda H. 2008. The potential of high spatial resolution information to define within-vineyard zones related to vine water status. *Precision Agriculture* **9,** 285–302.

Ajayi AE, Olufayo AA. 2004. Evaluation of two temperature stress indices to estimate grain sorghum yield and evapotranspiration. *Agronomy Journal* **96,** 1282–1287.

Al-Faraj A, Meyer GE, Horst GL. 2001. A crop water stress index for tall fescue (*Festuca arundinacea* Schreb,) irrigation decision-making – a traditional method. *Computers and Electronics in Agriculture* **31,** 107–124.

Alchanatis V, Cohen Y, Cohen S, Moller M, Sprinstin M, Meron M, Tsipris J, Saranga Y, Sela E. 2010. Evaluation of different approaches for estimating and mapping crop water status in cotton with thermal imaging. *Precision Agriculture* **11,** 27–41.

Alderfasi AA, Nielsen DC. 2001. Use of crop water stress index for monitoring water status and scheduling irrigation in wheat. *Agricultural Water Management* **47,** 69–75.

Allen RG, Jensen ME, Wright JL, Burman RD. 1989. Operational estimates of reference evapotranspiration. *Agronomy Journal* **81,** 650–662.

Allen RG, Pereira LS, Raes D, Smith M. 1998. *Crop evapotranspiration – guidelines for computing crop water requirements*. Rome, Italy: Food and Agriculture Organization of the United Nations.

Alves I, Pereira LS. 2000. Non-water-stressed baselines for irrigation scheduling with infrared thermometers: a new approach. *Irrigation Science* **19,** 101–106.

Amani I, Fischer RA, Reynolds MP. 1996. Canopy temperature depression association with yield of irrigated spring wheat cultivars in a hot climate. *Journal of Agronomy and Crop Science – Zeitschrift Fur Acker Und Pflanzenbau* **176,** 119–129.

Anda A. 2009. Irrigation timing in maize by using the crop water stress index (CWSI). *Cereal Research Communications* **37,** 603–610.

Andrews PK, Chalmers DJ, Moremong M. 1992. Canopy air-temperature differences and soil-water as predictors of water stress of apple trees grown in a humid, temperate climate. *Journal of the American Society for Horticultural Science* **117,** 453–458.

Araus JL, Bort J, Steduto P, Villegas D, Royo C. 2003. Breeding cereals for Mediterranean conditions: ecophysiological clues for biotechnology application. *Annals of Applied Biology* **142,** 129–141.

Arno J, Martinez-Casasnovas JA, Ribes-Dasi M, Rosell JR. 2009. Precision viticulture: research topics, challenges and opportunities in site-specific vineyard management. *Spanish Journal of Agricultural Research* **7,** 779–790.

Aston AR, Vanbavel CH. 1972. Soil surface water depletion and leaf temperature. *Agronomy Journal* **64,** 368–373.

Ayeneh A, van Ginkel M, Reynolds MP, Ammar K. 2002. Comparison of leaf, spike, peduncle and canopy temperature depression in wheat under heat stress. *Field Crops Research* **79,** 173–184.

Bajwa SG, Vories ED. 2007. Spatial analysis of cotton (*Gossypium hirsutum* L.) canopy responses to irrigation in a moderately humid area. *Irrigation Science* **25,** 429–441.

Baker JT, Gitz DC, Payton P, Wanjura DF, Upchurch DR. 2007. Using leaf gas exchange to quantify drought in cotton irrigated based on canopy temperature measurements. *Agronomy Journal* **99,** 637–644.

Balota M, Payne WA, Evett SR, Lazar MD. 2007. Canopy temperature depression sampling to assess grain yield and genotypic differentiation in winter wheat. *Crop Science* **47,** 1518–1529.

Balota M, William AP, Evett SR, Peters TR. 2008. Morphological and physiological traits associated with canopy temperature depression in three closely related wheat lines. *Crop Science* **48,** 1897–1910.

Barnes EM, Pinter PJ, Kimball BA, Hunsaker DJ, Wall GW, LaMorte RL. 2000. Precision irrigation management using modeling and remote sensing approaches. In: RGEvans**,** BLBenham**,** TTrooien, editors, *Proceedings of the 4th Decennial National Irrigation Symposium*, 14–16 November. Phoenix, AZ: American Socity of Agricultural Engineers, pp 332–337.

Ben Gal A, Agam N, Alchanatis V, Cohen Y, Yermiyahu U, Zipori I, Presnov E, Sprintsin M, Dag A. 2009. Evaluating water stress in irrigated olives: correlation of soil water status, tree water status, and thermal imagery. *Irrigation Science* **27,** 367–376.

Berliner P, Oosterhuis DM, Green GC. 1984. Evaluation of the infrared thermometer as a crop stress detector. *Agricultural and Forest Meteorology* **31,** 219–230.

Berni JAJ, Zarco-Tejada PJ, Sepulcre-Canto G, Fereres E, Villalobos F. 2009a. Mapping canopy conductance and CWSI in olive orchards using high resolution thermal remote sensing imagery. *Remote Sensing of Environment* **113,** 2380–2388.

Berni JAJ, Zarco-Tejada PJ, Suarez L, Fereres E. 2009b. Thermal and narrowband multispectral remote sensing for vegetation monitoring from an unmanned aerial vehicle. *IEEE Transactions on Geoscience and Remote Sensing* **47,** 722–738.

Blonquist JM, Norman JM, Bugbee B. 2009. Automated measurement of canopy stomatal conductance based on infrared temperature. *Agricultural and Forest Meteorology* **149,** 2183–2197.

Blyth EM, Dolman AJ. 1995. The roughness length for heat of sparse vegetation. *Journal of Applied Meteorology* **34,** 583–585.

Boulet G, Chehbouni A, Gentine P, Duchemin B, Ezzahar J, Hadria R. 2007. Monitoring water stress using time series of observed to unstressed surface temperature difference. *Agricultural and Forest Meteorology* **146,** 159–172.

Burke JJ, Mahan JR, Hatfield JL. 1988. Crop-specific thermal kinetic windows in relation to wheat and cotton biomass production. *Agronomy Journal* **80,** 553–536.

Campbell GS. 1977. *An introduction to environmental physics*. New York: Springer.

Chaerle L, Van Caeneghem W, Messens E, Lambers H, Van Montagu M, Van Der Straeten D. 1999. Presymptomatic visualization of plant–virus interactions by thermography. *Nature Biotechnology* **17,** 813–816.

Chakravarti AK, Moitra R, Mukherjee A, Dey P, Chakraborty PK. 2010. Effect of planting methods and mulching on the thermal environment and biological productivity of groundnut. *Journal of Agrometeorology* **12,** 77–80.

Chamberlain AC. 1968. Transport of gases to and from surfaces with bluff and wave-like roughness elements. *Quarterly Journal of the Royal Meteorological Society* **94,** 318–332.

Chapin FS, Mooney HA, Chapin MC, Matson P. 2002. *Principles of terrestrial ecosystem ecology*. New York: Springer Verlag.

Chavez JL, Howell TA, Gowda PH, Copeland KS, Prueger JH. 2010. Surface aerodynamic temperature modelong over rainfed cotton. *Transactions of the ASABE* **53,** 759–767.

Chehbouni A, LoSeen D, Njoku EG, Lhomme JP, Monteny B, Kerr YH. 1997. Estimation of sensible heat flux over sparsely vegetated surfaces. *Journal of Hydrology* **189,** 855–868.

Chehbouni A, Nouvellon Y, Lhomme JP, Watts C, Boulet G, Kerr YH, Moran MS, Goodrich DC. 2001. Estimation of surface sensible heat flux using dual angle observations of radiative surface temperature. *Agricultural and Forest Meteorology* **108,** 55–65.

Chen JZ, Lin LR, Lu GA. 2010. An index of soil drought intensity and degree: an application on corn and a comparison with CWSI. *Agricultural Water Management* **97,** 865–871.

Choudhury BJ, Reginato RJ, Idso SB. 1986. An analysis of infrared temperature observations over wheat and calculation of latent heat flux. *Agricultural and Forest Meteorology* **37,** 75–88.

Clarke TR. 1997. An empirical approach for detecting crop water stress using multispectral airborne sensors. *HortTechnology* **7,** 9–16.

Clawson KL, Blad BL. 1982. Infrared thermometry for scheduling irrigation of corn. *Agronomy Journal* **74,** 311–316.

Clothier BE, Clawson KL, Pinter PJ, Moran MS, Reginato RJ, Jackson RD. 1986. Estimation of soil heat-flux from net radiation during the growth of alfalfa. *Agricultural and Forest Meteorology* **37,** 319–329.

Cohen Y, Alchanatis V, Meron M, Saranga Y, Tsipris J. 2005. Estimation of leaf water potential by thermal imagery and spatial analysis. *Journal of Experimental Botany* **56,** 1843–1852.

Colaizzi PD, Barnes EM, Clarke TR, Choi CY, Waller PM. 2003a. Estimating soil moisture under low frequency surface irrigation using crop water stress index. *Journal of Irrigation and Drainage Engineering* **129,** 27–35.

Colaizzi PD, Barnes EM, Clarke TR, Choi CY, Waller PM, Haberland J, Kostrzewski M. 2003b. Water stress detection under high frequency sprinkler irrigation with water deficit index. *Journal of Irrigation and Drainage Engineering* **129,** 36–43.

Colaizzi PD, Evett SR, Howell TA, Tolk JA. 2004. Comparison of aerodynamic and radiometric surface temperature using precision weighing lysimeters. *Remote Sensing and Modeling of Ecosystems for Sustainability* **55 44,** 215–229.

Collino DJ, Dardanelli JL, Sereno R, Racca RW. 2000. Physiological responses of argentine peanut varieties to water stress. Water uptake and water use efficiency. *Field Crops Research* **68,** 133–142.

Conaty WC. 2010. *Temperature-time thresholds for irrigation scheduling in drip and deficit furrow irrgated cotton*. PhD dissertation. Sydney: University of Sydney, 292.

da Silva BB, Ferreira JA, Rao TVR, da Silva VdPR. 2007. Crop water stress index and water-use efficiency for melon (*Cucumis melo* L.) on different irrigation regimes. *Agricultural Journal* **2,** 31–37.

da Silva BB, Rao TVR. 2005. The CWSI variations of a cotton crop in a semi-arid region of Northeast Brazil. *Journal of Arid Environments* **62,** 649–659.

Dauzat J, Rapidel B, Berger A. 2001. Simulation of leaf transpiration and sap flow in virtual plants: model description and application to a coffee plantation in Costa Rica. *Agricultural and Forest Meteorology* **109,** 143–160.

Dolman AJ. 1986. Estimates of roughness length and zero plane displacement for a foliated and non-foliated oak canopy. *Agricultural and Forest Meteorology* **36,** 241–248.

Ehrler WL. 1973. Cotton leaf temperatures as related to soil-water depletion and meteorological factors. *Agronomy Journal* **65,** 404–409.

El-Shikha DM, Waller P, Hunsaker D, Clarke T, Barnes E. 2007. Ground-based remote sensing for assessing water and nitrogen status of broccoli. *Agricultural Water Management* **92,** 183–193.

Emekli Y, Bastug R, Buyuktas D, Emekli NY. 2007. Evaluation of a crop water stress index for irrigation scheduling of bermudagrass. *Agricultural Water Management* **90,** 205–212.

Erdem Y, Arin L, Erdem T, Polat S, Deveci M, Okursoy H, Gültas HT. 2010. Crop water stress index for assessing irrigation scheduling of drip irrigated broccoli (*Brassica oleracea* L. var. *italica*). *Agricultural Water Management* **98,** 148–156.

Evett SR, Howell TA, Schneider AD, Upchurch DR, Wanjura DF. 2000. Automatic drip irrigation of corn and soybean. *National Irrigation Symposium, Proceedings*, 401–408.

Feldhake CM, Glenn DM, Edwards WM, Peterson DL. 1997. Quantifying drought for humid, temperate pastures using the Crop Water Stress Index (CWSI). *New Zealand Journal of Agricultural Research* **40,** 17–23.

Fereres E, Evans RG. 2006. Irrigation of fruit trees and vines: an introduction. *Irrigation Science* **24,** 55–57.

Fernández JE, Cuevas MV. 2010. Irrigation scheduling from stem diameter variations: a review. *Agricultural and Forest Meteorology* **150,** 135–151.

Flerchinger GN, Xaio W, Marks D, Sauer TJ, Yu Q. 2009. Comparison of algorithms for incoming atmospheric long-wave radiation. *Water Resources Research* **45**,W03423.

Fuchs M. 1990. Infrared measurement of canopy temperature and detection of plant water-stress. *Theoretical and Applied Climatology* **42,** 253–261.

Fuchs M, Tanner CB. 1966. Infrared thermometry of vegetation. *Agronomy Journal*, **58,** 597–601.

Fuentes S, Conroy JP, Kelley G, Rogers G, Collins M. 2005. Use of infrared thermography to assess spatial and temporal variability of stomatal conductance of grapevines under partial rootzone drying: an irrigation scheduling application. *Proceedings of the Seventh International Symposium on Grapevine Physiology and Biotechnology*, 309–316.

Garcia-Tejero IF, Durán-Zuazo VH, Muriel-Fernández JL, Jiménez-Bocanegra JA. 2011. Linking canopy temperature and trunk diameter fluctuations with other physiological water status tools for water stress management in citrus orchards. *Functional Plant Biology* **38,** 106–117.

Gardner BR, Blad BL, Garrity DP, Watts DG. 1981a. Relationships between crop temperature, grain-yield, evapotranspriation and phenological development in 2 hybrids of moisture stressed sorghum. *Irrigation Science* **2,** 213–224.

Gardner BR, Blad BL, Watts DG. 1981b. Plant and air temperatures in differentially-irrigated corn. *Agricultural Meteorology* **25,** 207–117.

Gardner BR, Nielsen DC, Shock CC. 1992a. Infrared thermometry and the crop water-stress index. 1. History, theory, and base-lines. *Journal of Production Agriculture* **5,** 462–466.

Gardner BR, Nielsen DC, Shock CC. 1992b. Infrared thermometry and the crop water-stress index. 2. Sampling procedures and interpretation. *Journal of Production Agriculture* **5,** 466–475.

Garrath JR, Hicks BB. 1973. Momentum, heat and water vapour transfer to and from natural and artificial surfaces. *Quarterly Journal of the Royal Meteorological Society* **99,** 680–687.

Garrot DJ, Kilby MW, Fangmeier DD, Husman SH, Ralowicz AE. 1993. Production, growth, and nut quality in pecans under water-stress based on the crop water-stress index. *Journal of the American Society for Horticultural Science* **118,** 694–698.

Garrot DJ, Ottman MJ, Fangmeier DD, Husman SH. 1994. Quantifying wheat water-stress with the crop water-stress index to schedule irrigations. *Agronomy Journal* **86,** 195–199.

Gates DM. 2003. *Biophysical ecology*. New York, Heidelberg and Berlin: Springer Verlag.

Gates DM, Keegan HJ, Schleter JC, Weidner VR. 1965. Spectral properties of plants. *Applied Optics* **4,** 11–20.

Gijzen H, Goudriaan J. 1989. A flexible and explanatory model of light-distribution and photosynthesis in row crops. *Agricultural and Forest Meteorology* **48,** 1–20.

Gontia NK, Tiwari KN. 2008. Development of crop water stress index of wheat crop for scheduling irrigation using infrared thermometry. *Agricultural Water Management* **95,** 1144–1152.

Gonzalez-Dugo MP, Moran MS, Mateos L, Bryant R. 2006. Canopy temperature variability as an indicator of crop water stress severity. *Irrigation Science* **24,** 233–240.

Gonzalez-Dugo V, Zarco-Tejada P, Berni JAJ, Suárez L, Goldhamer D, Fereres E. 2012. Almond tree canopy temperature reveals intra-crown variability that is water stress-dependent. *Agricultural and Forest Meteorology* **154–155,** 156–165.

Gowda PH, Chavez JL, Colaizzi PD, Evett SR, Howell TA, Tolk JA. 2008. ET mapping for agricultural water management: present status and challenges. *Irrigation Science* **26,** 223–237.

Grant OM, Chaves MM, Jones HG. 2006. Optimizing thermal imaging as a technique for detecting stomatal closure induced by drought stress under greenhouse conditions. *Physiologia Plantarum* **127,** 507–518.

Grant OM, Davies MJ, James CM, Johnson AW, Leinonen I, Simpson DW. 2012. Thermal imaging and carbon isotope composition indicate variation amongst strawberry (*Fragaria* × *ananassa*) cultivars in stomatal conductance and water use efficiency. *Environmental and Experimental Botany* **76,** 7–15.

Grant OM, Tronina L, Jones HG, Chaves MM. 2007. Exploring thermal imaging variables for the detection of stress responses in grapevine under different irrigation regimes. *Journal of Experimental Botany* **58,** 815–825.

Guilioni L, Jones HG, Leinonen I, Lhomme JP. 2008. On the relationships between stomatal resistance and leaf temperatures in thermography. *Agricultural and Forest Meteorology* **148,** 1908–1912.

Gutierrez M, Reynolds MP, Klatt AR. 2010. Association of water spectral indices with plant and soil water relations in contrasting wheat genotypes. *Journal of Experimental Botany* **61,** 3291–3303.

Hall FG, Huemmrich KF, Goetz SJ, Sellers PJ, Nickeson JE. 1992. Satellite remote-sensing of surface-energy balance – success, failures, and unresolved issues in FIFE. *Journal of Geophysical Research – Atmospheres* **97,** 19061–19089.

Hamidou F, Zombre G, Braconnier S. 2007. Physiological and biochemical responses of cowpea genotypes to water stress under glasshouse and field conditions. *Journal of Agronomy and Crop Science* **193,** 229–237.

Hosgood B, Jacquemoud S, Andreoli G, Verdebout J, Pedrini G, Schmuck G. 1994. *Leaf Optical Properties EXperiment 93 (LOPEX93).* Ispra: European Commission, Joint Research Centre, Institute for Remote Sensing Applications.

Howell TA, Musick JT, Tolk JA. 1986. Canopy temperature of irrigated winter wheat. *Transactions of the ASABE* **29,** 1692–1698.

Huband NDS, Monteith JL. 1986. Radiative surface-temperature and energy-balance of a wheat canopy. 1. Comparison of radiative and aerodynamic canopy temperature. *Boundary-Layer Meteorology* **36,** 1–17.

Idso SB. 1982. Non-water-stressed baselines – a key to measuring and interpreting plant water-stress. *Agricultural Meteorology* **27,** 59–70.

Idso SB, Jackson RD, Pinter PJ, Reginato RJ, Hatfield JL. 1981a. Normalizing the stress-degree-day parameter for environmental variability. *Agricultural Meteorology* **24,** 45–55.

Idso SB, Jackson RD, Reginato RJ. 1977. Remote-sensing of crop yields. *Science* **196,** 19–25.

Idso SB, Reginato RJ, Hatfield JL, Walker GK, Jackson RD, Pinter PJ. 1980. A generalization of the stress-degree-day concept of yield prediction to accomodate a diversity of crops. *Agricultural Meteorology* **21,** 205–211.

Idso SB, Reginato RJ, Jackson RD, Pinter PJ. 1981b. Measuring yield-reducing plant water potential depressions in wheat by infrared thermometry. *Irrigation Science* **2,** 205–212.

Idso SB, Reginato RJ, Reicosky DC, Hatfield JL. 1981c. Determining soil-induced plant water potential depressions in alfalfa by means of infrared thermometry. *Agronomy Journal* **73,** 826–830.

Jackson RD. 1985. Evaluating evapotranspiration at local and regional scales. *Proceedings of the IEEE* **73,** 1086–1096.

Jackson RD, Idso SB, Reginato RJ, Pinter PJ. 1981. Canopy temperature as a crop water-stress indicator. *Water Resources Research* **17,** 1133–1138.

Jackson RD, Kustas WP, Choudhury BJ. 1988. A reexamination of the crop water-stress index. *Irrigation Science* **9,** 309–317.

Jackson RD, Reginato RJ, Idso SB. 1977. Wheat canopy temperature – practical tool for evaluating water requirements. *Water Resources Research* **13,** 651–656.

Jalalifarahani HR, Slack DC, Kopec DM, Matthias AD. 1993. Crop water-stress index models for Bermudagrass turf – a comparison. *Agronomy Journal* **85,** 1210–1217.

Jarvis PG, James GB, Landsberg JJ. 1976. Coniferous forest. In: JLMonteith, editor, *Vegetation and the atmosphere*. London: Academic Press, pp 171–240.

Jensen HE, Svendsen H, Jensen SE, Mogensen VO. 1990. Canopy-air temperature of crops grown under different irrigation regimes in a temperate humid climate. *Irrigation Science* **11,** 181–188.

Jiménez-Bello MA, Ballester C, Castel JR, Intrigliolo DS. 2011. Development and validation of an automatic thermal imaging process for assessing plant water status. *Agricultural Water Management* **98,** 1497–1504.

Jones HG. 1992. *Plants and microclimate: a quantitative approach to environmental plant physiology*. Cambridge, UK: Cambridge University Press.

Jones HG. 1999a. Use of infrared thermometry for estimation of stomatal conductance as a possible aid to irrigation scheduling. *Agricultural and Forest Meteorology* **95,** 139–149.

Jones HG. 1999b. Use of thermography for quantitative studies of spatial and temporal variation of stomatal conductance over leaf surfaces. *Plant, Cell and Environment* **22,** 1043–1055.

Jones HG. 2004. Irrigation scheduling: advantages and pitfalls of plant-based methods. *Journal of Experimental Botany* **55,** 2427–2436.

Jones HG, Archer N, Rotenberg E, Casa R. 2003. Radiation measurement for plant ecophysiology. *Journal of Experimental Botany* **54,** 879–889.

Jones HG, Serraj R, Loveys BR, Xiong LZ, Wheaton A, Price AH. 2009. Thermal infrared imaging of crop canopies for the remote diagnosis and quantification of plant responses to water stress in the field. *Functional Plant Biology* **36,** 978–989.

Jones HG, Stoll M, Santos T, de Sousa C, Chaves MM, Grant OM. 2002. Use of infrared thermography for monitoring stomatal closure in the field: application to grapevine. *Journal of Experimental Botany* **53,** 2249–2260.

Jones HG, Vaughan RA. 2010. *Remote sensing of vegetation: principles, techniques and applications*. Oxford: Oxford University Press.

Kalma J, McVicar T, McCabe M. 2008. Estimating land surface evaporation: a review of methods using remotely sensed surface temperature data. *Surveys in Geophysics* **29,** 421–469.

Kar G, Kumar A. 2010. Energy balance and crop water stress in winter maize under phenology-based irrigation scheduling. *Irrigation Science* **28,** 211–220.

Katerji N, Itier B, Ferreira I. 1988. Étude de quelques critères indicateurs de l'état hydrique d'une culture de tomate en région semi-aride. *Agronomie* **8,** 425–433.

Kaukoranta T, Murto J, Takala J, Tahvonen R. 2005. Detection of water deficit in greenhouse cucumber by infrared thermography and reference surfaces. *Scientia Horticulturae* **106,** 447–463.

Keener ME, Kircher PL. 1983. The use of canopy temperature as an indicator of drought stress in humid regions. *Agricultural Meteorology* **28,** 339–349.

Khan HUR, Link W, Hocking TJ, Stoddard FL. 2007. Evaluation of physiological traits for improving drought tolerance in faba bean (*Vicia faba* L.). *Plant and Soil* **292,** 205–217.

Kirkham MB, Johnson DE, Kanemasu ET, Stone LR. 1983. Canopy temperature and growth of differentially irrigated alfalfa. *Agricultural Meteorology* **29,** 235–246.

Kirnak H, Dogan E. 2009. Effect of seasonal water stress imposed on drip irrigated second crop watermelon grown in semi-arid climatic conditions. *Irrigation Science* **27,** 155–164.

Ko J, Piccinni G. 2009. Corn yield responses under crop evapotranspiration-based irrigation management. *Agricultural Water Management* **96,** 799–808.

Koksal ES. 2008. Irrigation water management with water deficit index calculated based on oblique viewed surface temperature. *Irrigation Science* **27,** 41–56.

Kumari M, Singh VP, Tripathi R, Joshi AK. 2007. Variation for staygreen trait and its association with canopy temperature depression and yield traits under terminal heat stress in wheat. *Wheat Production in Stressed Environments* **12,** 357–363.

Kustas W, Anderson M, Norman J, Li F. 2007. Utility of radiometric–aerodynamic temperature relations for heat flux estimation. *Boundary-Layer Meteorology* **122,** 167–187.

Kustas WP, Anderson M. 2009. Advances in thermal infrared remote sensing for land surface modeling. *Agricultural and Forest Meteorology* **149,** 2071–2081.

Kustas WP, Daughtry CST. 1990. Estimation of the soil heat-flux net-radiation ratio from spectral data. *Agricultural and Forest Meteorology* **49,** 205–223.

Kustas WP, Norman JM. 1999a. Evaluation of soil and vegetation heat flux predictions using a simple two-source model with radiometric temperatures for partial canopy cover. *Agricultural and Forest Meteorology* **94,** 13–29.

Kustas WP, Norman JM. 1999b. Reply to comments about the basic equations of dual-source vegetation-atmosphere transfer models. *Agricultural and Forest Meteorology* **94,** 275–278.

Kustas WP, Norman JM. 2000. A two-source energy balance approach using directional radiometric temperature observations for sparse canopy covered surfaces. *Agronomy Journal* **92,** 847–854.

Kustas WP, Norman JM, Schmugge TJ, Anderson MC. 2004. Mapping surface energy fluxes with radiometric temperature. Chapter 7. In: DAQuattrochi**,** JCLuvall, editors, *Thermal remote sensing in land surface*. London: Taylor and Francis, pp 205–255.

Lacape MJ, Wery J, Annerose DJM. 1998. Relationships between plant and soil water status in five field-grown cotton (*Gossypium hirsutum* L.) cultivars. *Field Crops Research* **57,** 29–43.

Lebourgeois V, Chopart JL, Begue A, Le Mezo L. 2010. Towards using a thermal infrared index combined with water balance modelling to monitor sugarcane irrigation in a tropical environment. *Agricultural Water Management* **97,** 75–82.

Leinonen I, Grant OM, Tagliavia CPP, Chaves MM, Jones HG. 2006. Estimating stomatal conductance with thermal imagery. *Plant, Cell and Environment* **29,** 1508–1518.

Leinonen I, Jones HG. 2004. Combining thermal and visible imagery for estimating canopy temperature and identifying plant stress. *Journal of Experimental Botany* **55,** 1423–1431.

Lemeur R. 1973. Method for simulating direct solar-radiation regime in sunflower, Jerusalem artichoke, corn and soybean canopies using a actual stand structure data. *Agricultural Meteorology* **12,** 229–247.

Li L, Nielsen DC, Yu Q, Ma L, Ahuja LR. 2010. Evaluating the crop water stress index and its correlation with latent heat and CO2 fluxes over winter wheat and maize in the North China plain. *Agricultural Water Management* **97,** 1146–1155.

Li ZL, Tang RL, Wan ZM, Bi YY, Zhou CH, Tang BH, Yan GJ, Zhang XY. 2009. A review of current methodologies for regional evapotranspiration estimation from remotely sensed data. *Sensors* **9,** 3801–3853.

Lindenthal M, Steiner U, Dehne HW, Oerke EC. 2005. Effect of downy mildew development on transpiration of cucumber leaves visualized by digital infrared thermography. *Phytopathology* **95,** 233–240.

Lindroth A, Molder M, Lagergren F. 2010. Heat storage in forest biomass improves energy balance closure. *Biogeosciences* **7,** 301–313.

Loheide SP, Gorelick SM. 2005. A local-scale, high-resolution evapotranspiration mapping algorithm (ETMA) with hydroecological applications at riparian meadow restoration sites. *Remote Sensing of Environment* **98,** 182–200.

López A, Molina-Aiz FD, Valera DL, Peña A. 2012. Determining the emissivity of the leaves of nine horticultural crops by means of infrared thermography. *Scientia Horticulturae* **137,** 49–58.

Loveys BR, Jones HG, Theobald JC, McCarthy MG. 2008. An assessment of plant-based measures of grapevine performance as irrigation scheduling tools. *Proceedings of the Fifth International Symposium on Irrigation of Horticultural Crops* **792,** 421–427.

Luquet D, Begue A, Vidal A, Clouvel P, Dauzat J, Olioso A, Gu XF, Tao Y. 2003. Using multidirectional thermography to characterize water status of cotton. *Remote Sensing of Environment* **84,** 411–421.

Luquet D, Vidal A, Dauzat J, Begue A, Olioso A, Clouvel P. 2004. Using directional TIR measurements and 3D simulations to assess the limitations and opportunities of water stress indices. *Remote Sensing of Environment* **90,** 53–62.

Maes WH, Achten WMJ, Reubens B, Muys B. 2011. Monitoring stomatal conductance of *Jatropha curcas* seedlings under different levels of water shortage with infrared thermography. *Agricultural and Forest Meteorology* **151,** 554–564.

Mahan JR, Burke JJ, Wanjura DF, Upchurch DR. 2005. Determination of temperature and time thresholds for BIOTIC irrigation of peanut on the southern high plains of Texas. *Irrigation Science* **23,** 145–152.

Mahrt L, Vickers D. 2004. Bulk formulation of the surface heat flux. *Boundary-Layer Meteorology* **110,** 357–379.

Massai R, Remorini D, Casula F. 2000. Leaf temperature measured on peach trees growing in different climatic and soil water conditions. In: MIFerreira**,** HG**,** Jones, editors, *Proceedings of the Third International Symposium on Irrigation of Horticultural Crops*. Lisbon, Portugal: ISHS, vol 1, pp 2399–2406.

Matsushima D. 2005. Relations between aerodynamic parameters of heat transfer and thermal-infrared thermometry in the bulk surface formulation. *Journal of the Meteorological Society of Japan* **83,** 373–389.

Matsushima D, Kondo J. 1997. A proper method for estimating sensible heat flux above a horizontal-homogeneous vegetation canopy using radiometric surface observations. *Journal of Applied Meteorology* **36,** 1696–1711.

McCaughey JH. 1985. Energy balance storage terms in a mature mixed forest at Petawawa, Ontario – a case study. *Boundary-Layer Meteorology* **31,** 89–101.

Meesters A, Vugts HF. 1996. Calculation of heat storage in stems. *Agricultural and Forest Meteorology* **78,** 181–202.

Meron M, Tsipris J, Charitt D. 2003. Remote mapping of crop water status to assess spatial variability of crop stress. In: J Stafford**,** A Werner, editors, *Precision agriculture. Proceedings of the 4th European conference on precision agriculture, Berlin, Germany*. Wageningen: Academic Publishers, pp 405–410.

Meron M, Tsipris J, Orlov V, Alchanatis V, Cohen Y. 2010. Crop water stress mapping for site-specific irrigation by thermal imagery and artificial reference surfaces. *Precision Agriculture* **11,** 148–162.

Mölder M, Lindroth A. 2001. Dependence of kB^{-1} factor on roughness Reynolds number for barley and pasture. *Agricultural and Forest Meteorology* **106,** 147–152.

Möller M, Alchanatis V, Cohen Y, Meron M, Tsipris J, Naor A, Ostrovsky V, Sprintsin M, Cohen S. 2007. Use of thermal and visible imagery for estimating crop water status of irrigated grapevine. *Journal of Experimental Botany* **58,** 827–838.

Monteith JL. 1973. *Principles of environmental physics*. London: Edward Arnold.

Moran MS. 2004. Thermal infrared measurement as an indicator of plant ecosystem health. Chapter 8. In: DAQuattrochi**,** JCLuvall, editors, *Thermal remote sensing in land surface processing*. London: Taylor and Francis, pp 257–282.

Moran MS, Clarke TR, Inoue Y, Vidal A. 1994. Estimating crop water-deficit using the relation between surface-air temperature and spectral vegetation index. *Remote Sensing of Environment* **49,** 246–263.

Naor A. 2008. Water stress assessment for irrigation scheduling of deciduous trees. *Proceedings of the Fifth International Symposium on Irrigation of Horticultural Crops* **792,** 467–481.

Naor A, Cohen S. 2003. Sensitivity and variability of maximum trunk shrinkage, midday stem water potential, and transpiration rate in response to withholding irrigation from field-grown apple trees. *Hortscience* **38,** 547–551.

Nautiyal PC, Rajgopal K, Zala PV, Pujari DS, Basu M, Dhadhal BA, Nandre BM. 2008. Evaluation of wild *Arachis* species for abiotic stress tolerance: I. Thermal stress and leaf water relations. *Euphytica* **159,** 43–57.

Nielsen DC, Anderson RL. 1989. Infrared thermometry to measure single leaf temperatures for quantification of water-stress in sunflower. *Agronomy Journal* **81,** 840–842.

Norman JM, Becker F. 1995. Terminology in thermal infrared remote-sensing of natural surfaces. *Agricultural and Forest Meteorology* **77,** 153–166.

Norman JM, Kustas WP, Humes KS. 1995. Source approach for estimating soil and vegetation energy fluxes in observations of directional radiometric surface temperature. *Agricultural and Forest Meteorology* **77,** 263–293.

O'Shaughnessy K, Evett SR, Colaizzi PD, Howell TA. 2011. Using radiation thermography and thermometry to evaluate crop water stress in soybean and cotton. *Agricultural Water Management* **98,** 1523–1535.

O'Shaughnessy SA, Evett SR. 2010. Canopy temperature based system effectively schedules and controls center pivot irrigation of cotton. *Agricultural Water Management* **97,** 1310–1316.

O'Toole JC, Real JG. 1986. Estimation of aerodynamic and crop resistances from canopy temperature. *Agronomy Journal* **78,** 305–310.

Oerke EC, Froehling P, Steiner U. 2011. Thermographic assessment of scab disease on apple leaves. *Precision Agriculture* **12,** 699–715.

Oerke EC, Steiner U, Dehne HW, Lindenthal M. 2006. Thermal imaging of cucumber leaves affected by downy mildew and environmental conditions. *Journal of Experimental Botany* **57,** 2121–2132.

Olufayo A, Baldy C, Ruelle P. 1996. Sorghum yield, water use and canopy temperatures under different levels of irrigation. *Agricultural Water Management* **30,** 77–90.

Onyibe JE, Ahmed MK, Falaki AM, Ramalan AA. 2003. Canopy–air temperature differential of wheat varieties grown under different soil moisture regime on semi-arid Sudan savanna. *Discovery and Innovation* **15,** 177–185.

Orta AH, Erdem Y, Erdem T. 2003. Crop water stress index for watermelon. *Scientia Horticulturae* **98,** 121–130.

Owen PR, Thomson WR. 1963. Heat transfer across rough surfaces. *Journal of Fluid Mechanics* **15,** 321–334.

Patel NR, Mehta AN, Shekh AM. 2001. Canopy temperature and water stress quantification in rainfed pigeonpea (*Cajanus cajan* (L.) Millsp.). *Agricultural and Forest Meteorology* **109,** 223–232.

Payero JO, Irmak S. 2006. Variable upper and lower crop water stress index baselines for corn and soybean. *Irrigation Science* **25,** 21–32.

Payero JO, Neale CMU, Wright JL. 2005. Non-water-stressed baselines for calculating crop water stress index (CWSI) for alfalfa and tall fescue grass. *Transactions of the ASABE* **48,** 653–661.

Pereira LS, Perrier A, Allen RG, Alves I. 1999. Evapotranspiration: concepts and future trends. *Journal of Irrigation and Drainage Engineering* **125,** 45–51.

Peters RT, Evett SR. 2007. Spatial and temporal analysis of crop conditions using multiple canopy temperature maps created with center-pivot-mounted infrared thermometers. *Transactions of the ASABE* **50,** 919–927.

Peters RT, Evett SR. 2008. Automation of a center pivot using the temperature-time-threshold method of irrigation scheduling. *Journal of Irrigation and Drainage Engineering* **134,** 286–291.

Pettigrew WT. 2004. Physiological consequences of moisture deficit stress in cotton. *Crop Science* **44,** 1265–1272.

Qiu GY, Miyamoto K, Sase S, Gao Y, Shi PJ, Yano T. 2002. Comparison of the three-temperature model and conventional models for estimating transpiration. *Japan Agricultural Research Quarterly* **36,** 73–82.

Qiu GY, Miyamoto K, Sase S, Okushima L. 2000. Detection of crop transpiration and water stress by temperature-related approach under field and greenhouse conditions. *Japan Agricultural Research Quarterly* **34,** 29–37.

Qiu GY, Omasa K, Sase S. 2009. An infrared-based coefficient to screen plant environmental stress: concept, test and applications. *Functional Plant Biology* **36,** 990–997.

Qiu GY, Sase S, Shi P, Ding G. 2003. Theoretical analysis and experimental verification of a remotely measurable plant transpiration transfer coefficient. *Japan Agricultural Research Quarterly* **37,** 141–149.

Qiu GY, Wang LM, He XH, Zhang XY, Chen SY, Chen J, Yang YH. 2008. Water use efficiency and evapotranspiration of winter wheat and its response to irrigation regime in the North China plain. *Agricultural and Forest Meteorology* **148,** 1848–1859.

Rashid A, Stark JC, Tanveer A, Mustafa T. 1999. Use of canopy temperature measurements as a screening tool for drought tolerance in spring wheat. *Journal of Agronomy and Crop Science* **182,** 231–237.

Raupach MR. 1992. Drag and drag partition on rough surfaces. *Boundary-Layer Meteorology* **60,** 375–395.

Raupach MR. 1994. Simplified expressions for vegetation roughness length and zero-plane displacement as functions of canopy height and area index. *Boundary-Layer Meteorology* **71,** 211–216.

Reynolds M, Manes Y, Izanloo A, Langridge P. 2009. Phenotyping approaches for physiological breeding and gene discovery in wheat. *Annals of Applied Biology* **155,** 309–320.

Roerink GJ, Su Z, Menenti M. 2000. S-SEBI: a simple remote sensing algorithm to estimate the surface energy balance. *Physics and Chemistry of the Earth Part B – Hydrology Oceans and Atmosphere* **25,** 147–57.

Rubio E, Caselles V, Badenas C. 1997. Emissivity measurements of several soils and vegetation types in the 8–14, μm wave band: analysis of two field methods. *Remote Sensing of Environment* **59,** 490–521.

Sadler EJ, Bauer PJ, Busscher WJ, Millen JA. 2000. Site-specific analysis of a droughted corn crop: II. Water use and stress. *Agronomy Journal* **92,** 403–410.

Sadler EJ, Camp CR, Evans DE, Millen JA. 2002. Corn canopy temperatures measured with a moving infrared thermometer array. *Transactions of the ASAE* **45,** 581–591.

Sadras VO, Soar CJ. 2009. Shiraz vines maintain yield in response to a 2–4 degrees C increase in maximum temperature using an open-top heating system at key phenostages. *European Journal of Agronomy* **31,** 250–258.

Salisbury JW, D'Aria DM. 1992. Emissivity of terrestrial materials in the 8–14 mm atmospheric window. *Remote Sensing of Environment* **42,** 83–106.

Samson R, Lemeur R. 2001. Energy balance storage terms and big-leaf evapotranspiration in a mixed deciduous forest. *Annals of Forest Science* **58,** 529–541.

Sanchez FJ, Manzanares M, de Andres EF, Tenorio JL, Ayerbe L. 2001. Residual transpiration rate, epicuticular wax load and leaf colour of pea plants in drought conditions. Influence on harvest index and canopy temperature. *European Journal of Agronomy* **15,** 57–70.

Sánchez JM, Kustas WP, Caselles V, Anderson MC. 2008. Modelling surface energy fluxes over maize using a two-source patch model and radiometric soil and canopy temperature observations. *Remote Sensing of Environment* **112,** 1130–1143.

Sedlar J, Hock R. 2009. Testing longwave radiation parameterizations under clear and overcast skies at Storglaciären, Sweden. *The Cryosphere* **3,** 75–84.

Sepulcre-Canto G, Zarco-Tejada PJ, Jimenez-Munoz JC, Sobrino JA, De Miguel E, Villalobos FJ. 2006. Detection of water stress in an olive orchard with thermal remote sensing imagery. *Agricultural and Forest Meteorology* **136,** 31–44.

Serrano L, González-Flor C, Gorchs G. 2010. Assessing vineyard water status using the reflectance-based water index. *Agriculture, Ecosystems and Environment* **139,** 490–499.

Shae JB, Steele DD, Gregor BL. 1999. Irrigation scheduling methods for potatoes in the northern Great Plains. *Transactions of the ASABE* **42,** 351–360.

Siddique MRB, Hamid A, Islam MS. 2000. Drought stress effects on water relations of wheat. *Botanical Bulletin of Academia Sinica* **41,** 35–39.

Simsek M, Tonkaz T, Kacira M, Comlekcioglu N, Dogan Z. 2005. The effects of different irrigation regimes on cucumber (*Cucumbis sativus* L.) yield and yield characteristics under open field conditions. *Agricultural Water Management* **73,** 173–191.

Singandhupe RB, Rao GGSN, Patil NG, Brahmanand PS. 2003. Fertigation studies and irrigation scheduling in drip irrigation system in tomato crop (*Lycopersicon esculentum* L.). *European Journal of Agronomy* **19,** 327–340.

Sobrino JA, JimenezMuñoz JC, LabedNachbrand J, Nerry F. 2002. Surface emissivity retrieval from digital airborne imaging spectrometer data. *Journal of Geophysical Research – Atmospheres* **107,** 4729.

Sobrino JA, Raissouni N, Li ZL. 2001. A comparative study of land surface emissivity retrieval from NOAA data. *Remote Sensing of Environment* **75,** 256–266.

Stanhill G. 1969. A simple instrument for the field measurement of turbulent diffusion flux. *Journal of Applied Meteorology* **8,** 509–513.

Steele DD, Gregor BL, Shae JB. 1997. Irrigation scheduling methods for popcorn in the northern Great Plains. *Transactions of the ASAE* **40,** 149–155.

Steele DD, Stegman EC, Gregor BL. 1994. Field comparison of irrigation scheduling methods for corn. *Transactions of the ASABE* **37,** 1197–1203.

Steele DD, Stegman EC, Knighton RE. 2000. Irrigation management for corn in the northern Great Plains, USA. *Irrigation Science* **19,** 107–114.

Stegman EC. 1986. Efficient irrigation timing methods for corn production. *Transactions of the ASABE* **29,** 203–210.

Steppe K, De Pauw DJW, Lemeur R. 2008. A step towards new irrigation scheduling strategies using plant-based measurements and mathematical modelling. *Irrigation Science* **26,** 505–517.

Stockle CO, Dugas WA. 1992. Evaluating canopy temperature-based indexes for irrigation scheduling. *Irrigation Science* **13,** 31–37.

Stoimenov G, Kirkova Y, Kolev N, Gospodinova M. 2007. Canopy/air temperature gradient as an indication of stress in cherry trees. In: K Hrotko, editor, *Proceedings of the Eighth International Symposium on Canopy, Rootstocks and Environmental Physiology in Orchard Systems*. Leuven: International Society Horticultural Science, pp 599–603.

Stoll M, Jones HG. 2007. Thermal imaging as a viable tool for monitoring plant stress. *Journal International Des Sciences De La Vigne Et Du Vin* **41,** 77–84.

Su Z. 2002. The Surface Energy Balance System (SEBS) for estimation of turbulent heat fluxes. *Hydrology and Earth System Sciences* **6,** 85–99.

Su Z, Schmugge T, Kustas WP, Massman WJ. 2001. An evaluation of two models for estimation of the roughness height for heat transfer between the land surface and the atmosphere. *Journal of Applied Meteorology* **40,** 1933–1951.

Sullivan DG, Fulton JP, Shaw JN, Bland G. 2007. Evaluating the sensitivity of an unmanned thermal infrared aerial system to detect water stress in a cotton canopy. *Transactions of the ASABE* **50,** 1955–1962.

Testi L, Goldhamer DA, Iniesta F, Salinas M. 2008. Crop water stress index is a sensitive water stress indicator in pistachio trees. *Irrigation Science* **26,** 395–405.

Thom AS, Oliver HR. 1977. On Penman's equation for estimating regional evaporation. *Quarterly Journal of the Royal Meteorological Society* **103,** 345–357.

Tilling AK, O'Leary GJ, Ferwerda JG, Jones SD, Fitzgerald GJ, Rodriguez D, Belford R. 2007. Remote sensing of nitrogen and water stress in wheat. *Field Crops Research* **104,** 77–85.

Upchurch DR, Mahan JR. 1988. Maintenance of constant leaf temperature by plants. 2. Experimental observations in cotton. *Environmental and Experimental Botany* **28,** 359–366.

Vanderstraeten D, Chaerle L, Sharkov G, Lambers H, Vanmontagu M. 1995. Salicylic-acid enhances the activity of the alternative pathway of respiration in tobacco-leaves and induces thermogenicity. *Planta* **196,** 412–419.

Vidal A, Perrier A. 1989. Analysis of a simplified relation for estimating daily evapotranspiration from satellite thermal IR data. *International Journal of Remote Sensing* **10,** 1327–1337.

Walker GK, Hatfield JL. 1979. Test of the stress-degree-day concept using multiple planting dates of red kidney beans. *Agronomy Journal* **71,** 967–971.

Wang D, Gartung J. 2010. Infrared canopy temperature of early-ripening peach trees under postharvest deficit irrigation. *Agricultural Water Management* **97,** 1787–1794.

Wang LM, Qiu GY, Zhang XY, Chen SY. 2005. Application of a new method to evaluate crop water stress index. *Irrigation Science* **24,** 49–54.

Wang XZ, Yang WP, Wheaton A, Cooley N, Moran B. 2010a. Automated canopy temperature estimation via infrared thermography: a first step towards automated plant water stress monitoring. *Computers and Electronics in Agriculture* **73,** 74–83.

Wang XZ, Yang WP, Wheaton A, Cooley N, Moran B. 2010b. Efficient registration of optical and IR images for automatic plant water stress assessment. *Computers and Electronics in Agriculture* **74,** 230–237.

Wanjura DF, Upchurch DR. 2000. Canopy temperature characterizations of corn and cotton water status. *Transactions of the ASABE* **43,** 867–875.

Wanjura DF, Upchurch DR, Mahan JR. 1990. Evaluating decision criteria for irrigation scheduling of cotton. *Transactions of the ASABE* **33,** 512–518.

Wanjura DF, Upchurch DR, Mahan JR. 1992. Automated irrigation based on threshold canopy temperature. *Transactions of the ASABE* **35,** 153–159.

Wanjura DF, Upchurch DR, Mahan JR. 1995. Control of irrigation scheduling using temperature-time thresholds. *Transactions of the ASABE* **38,** 403–409.

Wanjura DF, Upchurch DR, Mahan JR. 2006. Behavior of temperature-based water stress indicators in BIOTIC-controlled irrigation. *Irrigation Science* **24,** 223–232.

Wanjura DF, Upchurch DR, Mahan JR, Burke JJ. 2002. Cotton yield and applied water relationships under drip irrigation. *Agricultural Water Management* **55,** 217–237.

Yazar A, Howell TA, Dusek DA, Copeland KS. 1999. Evaluation of crop water stress index for LEPA irrigated corn. *Irrigation Science* **18,** 171–180.

Yoshimoto M, Oue H, Kobayashi K. 2005. Energy balance and water use efficiency of rice canopies under free-air CO_2 enrichment. *Agricultural and Forest Meteorology* **133,** 226–246.

Yuan GF, Luo Y, Sun XM, Tang DY. 2004. Evaluation of a crop water stress index for detecting water stress in winter wheat in the North China plain. *Agricultural Water Management* **64,** 29–40.

Zarco-Tejada PJ, González-Dugo V, Berni JAJ. 2012. Fluorescence, temperature and narrow-band indices acquired from a UAV platform for water stress detection using a micro-hyperspectral imager and a thermal camera. *Remote Sensing of Environment* **117,** 322–337.

Zhang YS, Munkhtsetseg E, Kadota T, Ohata T. 2005. An observational study of ecohydrology of a sparse grassland at the edge of the Eurasian cryosphere in Mongolia. *Journal of Geophysical Research – Atmospheres* **110,** D14103.